Multi-Degree of Freedom Passive and Active Vibration Absorbers for the Control of Structural Vibration

Anthony F. Harris

Thesis submitted to the Faculty of the Virginia Polytechnic Institute and State University in partial fulfillment of the requirements for the degree of

Master of Science

In

Mechanical Engineering

APPROVED:

_____
Dr. Marty E. Johnson, Chair

_____ _____
Dr. James P. Carneal Dr. Mike R. F. Kidner

December 19, 2003
Blacksburg, Virginia

Keywords: vibration absorber, multi-degree of freedom, active control

Multi-Degree of Freedom Passive and Active Vibration Absorbers for the Control of Structural Vibration

Anthony F. Harris
Mechanical Engineering Department
Virginia Tech

Abstract

This work investigates the use of multi-degree of freedom (MDOF) passive and active vibration absorbers for the control of structural vibration as an improvement to conventional single degree of freedom (SDOF) vibration absorbers. An analytical model is first used to compare passive two degree of freedom (2DOF) absorbers to SDOF absorbers using point impedance as the performance criterion. The results show that one 2DOF absorber can provide the same impedance at two resonance frequencies as two SDOF absorbers for equal amounts of total mass. Experimental testing on a composite cylindrical shell supports the assertion that a 2DOF absorber can attenuate two resonance frequencies. Further modeling shows that MDOF absorbers can utilize the multiple mode shapes that correspond to their multiple resonance frequencies to couple into modes of a distributed primary system to improve the attenuation of structural resonance. By choosing the coupling positions of the MDOF absorber such that its mode shape mirrors that of the primary system, the mass of the absorber can be utilized at multiple resonance frequencies. For limited ranges of targeted resonance frequencies, this technique can result in MDOF absorbers providing attenuation equivalent to SDOF absorbers while using less mass. The advantage gained with the MDOF absorbers is dependent on the primary system. This work compares the advantage gained using the MDOF absorbers for three primary systems: MDOF lumped parameter systems, a pinned-pinned plate, and a cylindrical shell.

The active vibration absorber study in this work is highly motivated by the desire to reduce structural vibration in a rocket payload fairing. Since the efficiency of acoustic foam is very poor at low frequencies, the target bandwidth was 50 to 200 Hz. A 2DOF active vibration absorber was desired to exhibit broad resonance characteristics over this frequency band. An analytical model was developed to facilitate the design of the mechanical and electrical

properties of the 2DOF active vibration absorber, and is supported by experimental data. Eight active vibration absorbers were then constructed and used in a multiple-input multiple-output (MIMO) feed-forward control system on a mock payload fairing under high level acoustic excitation. The results show significant levels of global attenuation within the targeted frequency band.

Acknowledgements

I would first like to thank everyone associated with the education provided by Virginia Tech. I feel lucky and grateful to have had such an enriched learning experience at Virginia Tech. Likewise, I have a great deal of respect and gratitude for Dr. Chris Fuller and those who have helped build and sustain the Vibration and Acoustics Laboratory, which supported this research.

One of these people is Dr. Marty Johnson, the most informative, instructive, understanding, willing, and influential professor I have had the pleasure of learning from. As an undergraduate student and graduate research assistant, I can say he is always willing and eager to pass knowledge on to his students. I would also like to thank my committee, James Carneal and Mike Kidner whose oversight and recommendations are greatly appreciated. Thanks also to the many friends who been there with supported throughout the years, Simon Estève especially.

Most of all I'd like to recognize my family. Without the support of my infinitely generous parents, Richard and Michele Harris, I wouldn't have had the opportunity to attend Virginia Tech. From overseeing elementary school homework at the dinner table to encouraging conversations about finals, you have been my unwavering foundation of support in so many ways. My parents and sister Kristen have always provided encouragement, love, and support beyond the highest levels of expectation. Thank you for everything. You can't imagine your importance to me.

Finally, my fiancé Diana Dulcey deserves much of the credit for my graduate degree. She supported my decision to attend graduate school, despite the lengthening of our long distance relationship, and drove clear across the state of Virginia to see me nearly every other weekend. She sacrificed her time and money, and then waited patiently for me to finish writing. She never complained or nagged, but was patient and supportive. She is everything I could ask for. Thank you Diana. I love you.

Table of Contents

Table of Figures

Table of Tables

Acronyms

1DOF / SDOF	One Degree of Freedom
2DOF	Two Degree of Freedom
ASAC	Active Structural Acoustic Control
B&K	Bruel and Kjaer
DAQ	Data Acquisition
DAVA	Dynamic Active Vibration Absorber
dB	decibel
DVA	Dynamic Vibration Absorber
DOF	Degrees of Freedom
ELV	Expandable Launch Vehicle
HR	Helmholtz Resonator
MDOF	Multiple Degrees of Freedom
MIMO	Multiple-Input Multiple-Output
MR	Mass Ratio (of 1DOF absorber to MDOF absorber)
NdFeB	Nickel Iron Boron
PZT	Piezoelectric Material
RMS	Root Mean Square
SDOF / 1DOF	Single Degree of Freedom
SPL	Sound Pressure Level
VAL	Vibrations and Acoustics Lab (Virginia Tech)
VASci	Vibro-Acoustic Sciences, Inc.

Nomenclature

a	Acceleration of moving mass (m/s^2)
a	Air gap in actuator (m)
a_i	modal amplitude (i^{th})
B	Actuator force (N)
c	Damping value ($N/(ms^{-1})$)
C	Damping matrix
$\tilde{C}$	Mass normalized stiffness matrix
D	Dynamic stiffness matrix
F	Force (N)
I	Current (Amperes)
i	imaginary number
k	Stiffness value (N/m)
K	Stiffness matrix
$\tilde{K}$	Mass normalized stiffness matrix
L	Diagonal complex resonance matrix
L	Actuator coil inductance (mH)
l	length of actuator coil
m	Mass value (kg)
M	Mass matrix
MR	Mass ratio (of 1DOF absorber to MDOF absorber) (%)
n	Number of turns in actuator coil per total length of coil
P	Eigenvector matrix
R	Electrical resistance (Ω, Ohms)
r	Modal displacement
S	Modal coordinate system transformation matrix
v	Velocity of moving mass(m/s)
v_{nm}	Eigenvectors for mass n and mode m
w	Plate displacement (m)
x	Displacement of moving mass (m)

Z	Impedance (kg/s)
λ	Eigenvalues
$\mathbf{\Lambda}$	Diagonal eigenvalue matrix
Ψ_i	Mode shape (i^{th})
θ	Angle from zero degrees
μ	Absorber mass ratio
μ_o	Permeability of vacuum constant
ω	Frequency (rad/s)
ξ	Damping ratio

Chapter 1: Introduction

This goal of this chapter is to provide background and review existing work in the field of vibration absorbers. The first section provides a general overview of vibration absorbers and their function in an effort to familiarize the reader with the concepts and ideas that will be discussed throughout this thesis. Presented next is a discussion of previous studies and techniques that contribute to the history of vibration absorbers and how they have developed since its inception. The next section will explain the motivation of this research, how it is relevant to the existing research, and how it contributes to the progress of improving and maximizing the performance of vibration absorbers. Finally, an outline of this thesis is presented.

1.1 Background

The dynamic vibration absorber (DVA) is a device commonly used to reduce the vibration level in a variety of structures. Since its first patent in 1909[1], it has been designed to fit many applications including the reduction of ship sway, aircraft noise, vibrations in pipelines, rotating discs, tall buildings, elevators, automobiles, industrial machines, and many other vibrating structures. The most basic form of the DVA is the mass-spring-damper configuration, which consists of a small absorber mass connected by an elastic and damping element to the much larger vibrating structure. Typically, the DVA is designed to have spring and mass parameters that give it the same resonance frequency as the vibrating structure so the inertia reduces the net force on the primary structure, hence canceling the vibration at this frequency.

Much progress has been made in the optimization of vibration absorbers to improve attenuation, including the advent of tuning and optimal damping laws, and automated self tuning designs. Further advances have been made with the implementation of an active force component coupled to the vibration absorber and controlled by an active control system. A lot of successful research has been conducted in the implementation of piezoelectric materials as the active element in DAVAs. However, in situations where more powerful actuators are required, electromagnetic actuators have proven to be very effective.

Another area of investigation is the use of multi-degree of freedom vibration absorbers, or multi-mass dynamic vibration absorbers. While these devices have been investigated to a

certain extent, the research presented in this thesis introduces a technique of matching DVA modes with the modes of the primary vibrating structure. This technique will provide an advantage by requiring less mass than a single-mass DVA while achieving the same vibration attenuation. Previous work has implemented an active dual mass DAVA and shown that the amount of control necessary is reduced with the dual mass DAVA.[2] This thesis also details the design of a dual-mass DAVA for the reduction of structural vibrations in a mock payload fairing excited by high level white noise. The experimental results of the testing of this device are also presented.

1.2 Previous Work

The first U.S. patent for a vibration absorber was filed in 1909 by Hermann Frahm for the design of several devices intended to reduce unwanted vibration in a variety of structures. [1] The designs used the principal theory of counteracting the resonant vibrations of structures with smaller masses vibrating at the same resonance frequency. Frahm saw potential for the device in many applications including ships, buildings, and lathes; and he used different designs including mass-spring systems, pendulums, piston inertia, and even designed an absorber that works in two dimensions. This idea of counteracting motion with the inertia of an added mass is still in use today on many structures. The most basic form of this device is the spring-mass system, which uses an elastic and damping element to connect a small mass to the primary structure that is experiencing unwanted vibration. The small mass, known as the absorber mass, is designed to have a resonance frequency that is tuned close to either the primary structure's resonance frequency or the disturbance frequency in order to cancel the undesired vibration. The resonance frequency of the vibration absorber is a function of the size of the absorber mass and the stiffness of the elastic element, which is typically a spring.

A common example of the implementation of a spring-mass DVA is its use in the reduction of aircraft noise generated by engine and propeller excitation.[3] On the SAAB 349 and ATR 42 turbo-prop aircrafts, about 100 DVAs are tuned to attenuate fuselage response to engine noise and are attached to the frame of the aircraft. These absorbers are in the form of small masses of tungsten, weighing about a pound, and a spring element in the form of the shearing of elastomeric pads. In addition, research has been performed on how the attenuation of structural

modes with DVAs can improve the reduction of sound radiation from vibrating panels, most notably in aircraft.[4]

In addition to the reduction of aircraft noise, DVAs have been used to control many other vibration problems. In 1992, it was documented that vibration absorbers have been found to reduce vibrations in pipelines above the Arctic Circle.[5] Wind cycles result from cyclic lift forces and excite many low frequency modes of the pipelines. As many as ten of the pipeline modes are excited by the winds, all less than 5 Hz. Despite the low amplitudes of the vibration, the cyclic vibration induces fatigue on the joints of the pipelines, reducing their life span. To attenuate this vibration, 23 to 34 kg masses were hung from the pipelines and supported by a series of elastomer bands acting as springs in shear deformation. The vibration absorbers were hung from the pipelines at spans of 12 to 18 meters apart to attenuate the low frequency modes of the pipeline that were being excited by the wind cycles. And because of the high modal density of the pipelines below 5 Hz, the DVAs were able to effectively reduce the damaging vibrations in this low frequency band. The application of the DVAs lowered the RMS displacement of the pipeline by as much as a factor of seven, proving very effective.

In the case of the pipeline, the modal density of the targeted modes was high, allowing the DVA to attenuate several modes with one tuning frequency. As the DVA has developed, it has been discovered that several parameters affect the performance of the DVA. Of these parameters, it can be argued that the tuning frequency, damping level, and mass ratio are of the most critical. This had led to much research and the development of tuning laws, optimal damping level formulas, and the evaluation of effectiveness per mass ratio (mass of the absorber divided by the mass of the primary structure).[3,6] The design of the DVA mass is a parameter that largely depends on the application. For instance, it is of great importance to reduce the amount of mass used to attenuate aircraft vibration due to the proportional relationship of flight cost and weight of the aircraft. Therefore, since absorber mass is usually proportional to performance, the weight of the DVA is usually taken to the upper limit of acceptability for the particular application. Conversely, damping and tuning can usually be optimized with very few detrimental effects to the system.

First, it should be noted that depending on the excitation source, there are two techniques that are used to implement vibration absorbers; namely vibration absorption and vibration damping. In the case of vibration absorption, the absorber is tuned to a periodic disturbance or

tonal excitation of the primary structure. The optimal tuning of this type of vibration absorber is exactly the disturbance frequency, and the ideal damping of the absorber is zero. The absorber effectively adds a large impedance to the primary structure, reducing the vibration.

The other method, vibration damping, is used when there is broadband excitation or when the disturbance is unknown or likely to shift. For this method, it has been shown that the optimal tuning doesn't correspond exactly to the targeted frequency.[3] The optimal tuning frequency is dependant on the mass ratio and is always lower than the resonance frequency of the primary structure. For large mass ratios, even a slight mistuning of a DVA can result in significant loss of performance. For small mass ratios, however, this can be considered negligible and the DVA frequency can be designed to match the targeted frequency. As mentioned, the optimal damping for vibration absorption is zero, but this is not true for vibration damping. It has been shown that for this method, there is a critical damping value that optimizes attenuation and increases the effective band width of the DVA.[6,7] There are many analytical solutions to determine this value that are dependent on the mass ratio of the system and the type of excitation driving the system. It is important to note that a great deal of the effort that has gone into optimizing damping has aimed to broaden the effective bandwidth of the absorber, consequently improving attenuation.

Much research has been done to investigate different methods of expanding this effective bandwidth. One study looked at applying multiple absorbers tuned to various frequencies attached to the same point.[8] The effective impedance was said to be the sum of the individual absorber impedances, and the overall effective frequency band was broadened. The study examined different methods of determining the optimal set of tuning frequencies for the DVAs, and proved the overall technique to be effective.

The implementation of these design strategies is limited, however, if the targeted frequency changes over time. This was addressed by the development of adaptive, semi-active, and active DVAs. Adaptive DVAs use the technique of altering their design parameters automatically to control their resonance frequency to match that of the primary structure. One example tunes the DVA resonance frequency to that of the primary structure by changing the stiffness of its leaf-spring with a stepper motor.[9] Another design uses a mass at the end of coil spring. A feedback control algorithm uses a D.C. motor to adjust the effective length of the spring and tune the absorber to the desired frequency.[10] A lot of research is also performed on the tuning methods and algorithms used control these absorbers.[11,12] The use of a control system

has also been utilized to optimize damping in DVAs. Referred to as semi-active dampers, they are commonly used in automobile suspensions to minimize the amount of vibration felt by passengers.[13] Techniques known as "skyhook control" and more recently "groundhook control" use the principle of adjusting the damping values of the DVA based on the relative velocity of the primary structure and the DVA.[14]

Further improvement of the DVA design was the implementation of an active force positioned between the absorber mass and the primary structure. This device, referred to as a dynamic active vibration absorbers (DAVA) in this text, provided the capability of improved performance in some areas of vibration control. The addition of a traditionally used active control force provided the DVA with adaptability and greater performance at low frequencies, where passive DVAs become impractical due to mass and/or volume limitations. Active control has been used effectively with lightweight actuators such as piezoelectric materials (PZTs) and discrete actuators to reduce sound radiation from vibrating surfaces.[15,16] Heavier and more powerful electromagnetic actuators have also proven effective on heavier structures such as vibrating plates.[17] Along with actuator design, a lot of research in active control is the investigation of the many different control strategies used for actuation: neural networks, delayed resonator, modal feedback controller, and disturbance cancellation.[18,19] Research has also shown that using active control with a passive element (DAVA configuration) can significantly improve performance when the passive element is optimally tuned.[20]

With this improved performance, however, come limitations. For instance, providing power to the actuator can pose a problem due to the size and weight of power supplies, and the difficulties of wiring actuators. And while the power required to operate a DAVA is relatively low at or near its resonance frequency, it can increase greatly at frequencies much higher or lower.[21] Another problem with DAVAs are that they have been claimed to have poor reliability under extended operation.

An improvement to existing models of DAVAs was a design that consisted of an active mass element connected to a passive DVA.[22] The dual mass design improved performance in several ways, but mainly the power requirement was improved in comparison to the single mass design. Building on this design, a patent was granted for the design of an electromagnetic dual mass DAVA that improved control even further.[23] The new design was comprised of two masses, both coupled to the primary structure, with an active force applied in between the

masses. Research on this design showed that it required only half of the control effort to achieve the same performance as a single mass DAVA and showed less sensitivity to changes in the primary system.[2,24] The results show that the addition of a mass, and subsequently a resonance frequency, to the DAVA results in better performance under active control. This can be partially attributed to the enlarged effective bandwidth of the DAVA.

The notion of using multiple degrees of freedom (MDOF) for vibration absorption is not particularly new, as it is discussed in classic texts and regarded as more effecient.[7] The multiple resonances of multi-degree of freedom devices provide a broader bandwidth of resonance, especially when designed with optimal damping. This results in a greater force available to counteract the vibration of a structure, whether it is utilized passively or actively. This work investigates the passive and active use of MDOF devices in order to reduce structural vibration. Once developed, the implementation of this theory can be translated to parallel applications, such as Helmholtz resonators, which are acoustic equivalents to structural vibration absorbers.

1.3 Motivation and Contribution of Thesis

Due to the great expense of launching heavy launch vehicles into orbit, there has been much research in the use of lightweight materials for Expandable Launch Vehicles (ELVs) fairings. Payload fairings are now made of extremely lightweight composite materials instead of their heavier aluminum alloy predecessors. As a result, they experience greater structural vibration and transmit more noise to the expensive satellites that they house. Peak acoustic levels of 120 to 150 dB are generated from the burn of the rocket engines during launch and pose the greatest threat to these satellites. Acoustic foam has been found to be an effective treatment for high frequency noise, but there is still a great need for structural attenuation at low frequencies.

Testing was conducted on a scaled model of a composite payload fairing to demonstrate the performance of the devices researched in this work. Passive 2DOF DVAs were first modeled and then used to attenuate two structural modes of the fairing under structural excitation. This demonstrates the utilization of multiple DVA modes to attenuate multiple modes of a distributed system. Expanding on the concept of using 2DOF DVAs, computer models of a lumped mass system, a steel plate, and the cylindrical shell are used to evaluate the effectiveness of multi-degree of freedom (MDOF) DVAs greater than two degrees of freedom. The work investigates using MDOF DVAs to generate multiple absorber resonances, with corresponding mode shapes that can be coupled at positions matching the mode shapes of the primary system. Optimal coupling positioning of the DVAs to the primary structure can result in the reduction of the absorber mass compared to multiple single mass DVAs generating the same attenuation.

This thesis also presents the design and use of an electromagnetic 2DOF DAVA that is designed to attenuate the low frequency structural vibration of the payload fairing. The dual mass design, shown in Figure 1.1, couples the magnet mass of the actuator to the mass of a stiff honeycomb plate through the elastic spider plates in the actuator. An active force is generated in between the masses by the motion of the magnet when the actuator coil is supplied with power. This force is transmitted to the honeycomb plate, and then coupled to the fairing with a block of acoustic foam. The electrical and mechanical components of the DAVA are specifically designed to utilize the dual resonance of the device to maximize low frequency attenuation using active control. In addition to the design strategy, this thesis also presents the experimental

results of the DAVAs on the fairing using MIMO feed-forward control under high level excitation.

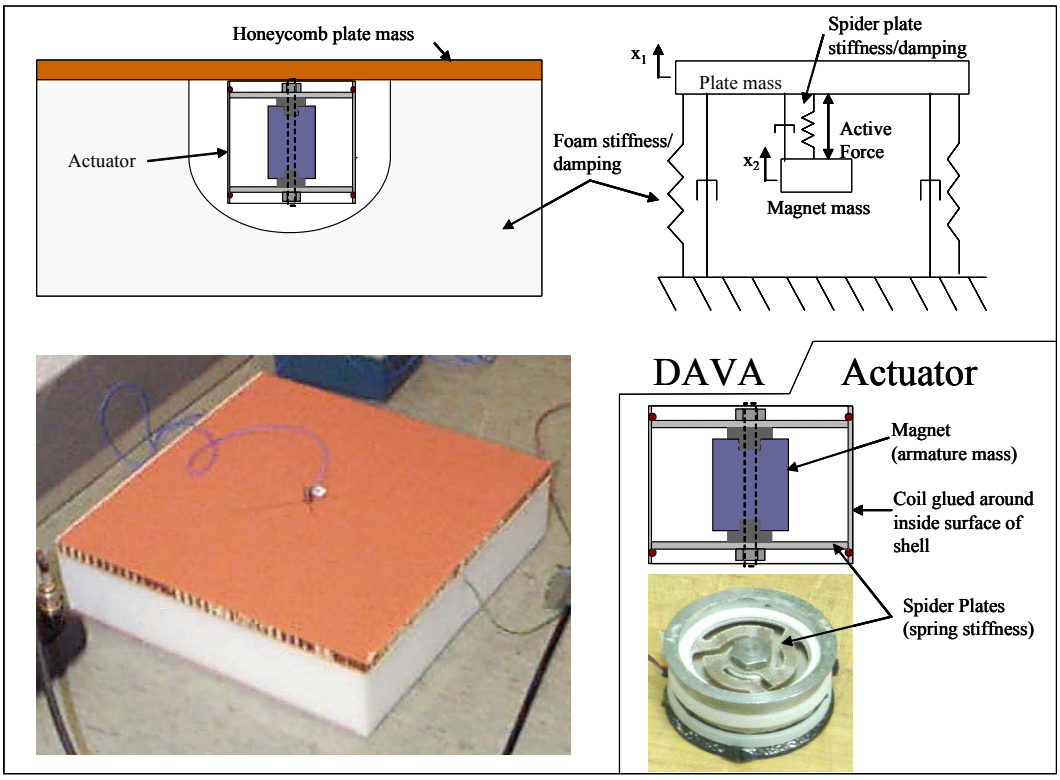

Figure 1.1 Electromagnetic actuator shown by itself and in 2DOF DAVA configuration. The honeycomb plate mass and acoustic foam stiffness provide the second degree of freedom.

1.4 Outline of Thesis

This thesis investigates the use of passive and active multi-degree of freedom vibration absorbers for structural vibration control. Chapters two and three are devoted to the passive design of MDOF DVAs, and chapters four and five concentrate on active control using a 2DOF DAVA. Chapter two will start by introducing the mathematical theory and background required for the analysis of MDOF DVAs. A comparison of the effectiveness of 1DOF DVAs and 2DOF DVAs will be made. Results from experimentation will then be presented that show the reduction of the structural vibration due to attaching 2DOF DVAs to a mock payload fairing.

Chapter three introduces the concept of "re-using" DVA mass by designing absorbers with multiple reaction points and optimizing the coupling positions. This concept will be applied to models of lumped mass systems, a steel plate, and a cylindrical shell. Methods of optimizing DVA parameters and coupling positions will be discussed and the different models compared.

The fourth chapter will begin with a theoretical description of dual mass DVAs, and then the electrical and mechanical design of a dual mass DAVA intended for low frequency active vibration control in a payload fairing will be detailed. A computer model is developed to optimize the mechanical properties of the DAVA in order to maximize the DAVA output. The results are then validated with experimental data.

Chapter five will present the results of the high level testing of the DAVAs on the mock payload fairing. Conclusions and future work will then be presented in chapter six.

Chapter 2: Two Degree of Freedom Dynamic Vibration Absorbers

The goal of this chapter is to describe the modeling, evaluation, and implementation of a passive two degree of freedom dynamic vibration absorber (2DOF DVA). This will prove to be a useful progression toward the development and analysis of MDOF DVAs, as well as 2DOF DAVAs, which will be discussed in chapter four and five. The first section of this chapter discusses the motivation for this research: why this design is being investigated and how it could improve treatment of structural vibration problems. Next, the conventional 1DOF DVA is modeled analytically, and a measure of its performance is established as its impedance at a specified frequency. This 1DOF DVA impedance will act as a baseline for comparison with the new 2DOF DVA design. Once the two designs have been modeled and evaluated, a set of stacked 2DOF DVAs were built and tested on a scaled model of the payload fairing.

2.1 MDOF DVA Motivation and Theory

As mentioned in the background, there is a great need for vibration reduction in many different structures, and DVAs have proven to be a very effective method of treatment. The specific motivation for this research is the structural vibration reduction of a payload fairing during the launch sequence of a rocket. DVAs have been used successfully for this application in the past, achieving significant reductions of targeted resonance frequencies when used in conjunction with Helmholtz resonators.[25] There is a desire to improve this performance by using one DVA to target more than one resonance frequency of the structure. This could possibly save space along the interior of the fairing wall, which is where the DVAs are attached. But more importantly, it will show that the multiple resonance frequencies of MDOF DVAs can be tuned to attenuate the multiple modes of a distributed system. This is a necessary effect for "reusing" the DVA mass in MDOF DVAs, and is discussed in Chapter 3. The principals and techniques derived in this study can be translated to parallel devices, such as Helmholtz resonators.

Since the excitation of the fairing is due to the launching of the rocket, broadband excitation with uniform energy over the frequency range of interest will be assumed. In practice, the targeted modes are generally chosen based on criteria such as magnitude, coupling with the structure, frequency, and even human perception factors. For this chapter however, in order to

eliminate the bias involved in treating a specific structure, the DVA impedance will be used as a measure of effectiveness.

The DVA impedance is defined as the ratio of force into the primary structure per velocity of the primary structure. Using an impedance matching method, a comparison is made between 1DOF and 2DOF DVAs. The method of comparison is such that the impedance at resonance of the DVAs is set to be equal, allowing a comparison of the total mass of the DVAs. This method of comparison was chosen for several reasons. First, the reduction of total DVA mass is an easily measured advantage. The advantage is based on the fundamental that DVAs improve attenuation performance as the absorber mass is increased. This leads to the second reason; if the impedance, and subsequently the attenuation of a system can be matched closely, the primary system becomes arbitrary. The only factor that can bias the comparison is the percentage of mass used in the absorber, but this can be normalized by the mass of the primary structure. In contrast, if the DVA masses are held constant, the normalization of the DVA masses is not needed, but there is now no method to normalize the vibration attenuation of the structure. Attenuation is essentially a moving scale that can be greatly biased by the mass ratio of the absorbers to the primary structure. Therefore, it was determined that holding the performance constant and comparing the required mass was a more unbiased measure of advantage.

The complications of this method arise in matching the vibration attenuation. Working under the assumption that a DVA is most effective at its resonance, the impedance of the DVAs is equated at resonance; this is discussed in greater detail in the following sections of this chapter. Unfortunately, this resonance matching technique leaves the performance of the DVA slightly variable at frequencies other than the target resonance, complicating the comparison. Overall, however, this method is a valid means for comparing the effectiveness of 1DOF and 2DOF DVAs for use in attenuating multiple modes of a structure. The following section will characterize the effects of 1DOF DVAs acting on a spring-mass-damper system, in order to establish a baseline performance.

2.2 1DOF DVA Characterization

In order to characterize the effectiveness of a DVA, a measure of its performance is needed. In this section, it will be shown that the impedance of a DVA is a valid measurement of

this effectiveness. This will be proved by showing the correlation between the impedance of a DVA and the attenuation of a host spring-mass-damper system. An investigation of optimal damping and tuning frequency for 1DOF DVAs is then described. This lays the groundwork for examining 2DOF DVAs, and eventually MDOF DVAs and DAVAs.

2.2.1 Equations of Motion for 1DOF DVAs

In order to simplify the comparison between 1DOF and 2DOF DVAs, the primary structure to which the DVAs will be applied is a lumped parameter spring-mass-damper system, as shown in Figure 2.1. Using a lumped mass system will be useful in demonstrating the effectiveness of DVAs as a function of its impedance; yet it will simplify the equations of motion and resonance characteristics of the system. The impedance of the primary structure, Z_p, is the ratio of the force applied to the structure, F_p, to the velocity of the primary mass, V_p:

$$Z_p = \frac{F_p}{V_p} \tag{2.1}$$

In terms of spring stiffness, k_p, viscous damping, c_p, and mass, m_p, of the primary system, the term is of the form

$$Z_p = c_p + i\left(\omega m_p - \frac{k_p}{\omega}\right) \tag{2.2}$$

where ω is frequency of the disturbance force in radians/second, and $i = \sqrt{-1}$.

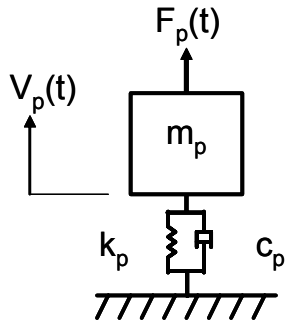

Figure 2.1 Lumped mass model of a spring-mass-damper primary structure.

The dynamic characteristics of this system are described by two parameters: the natural frequency, ω_n, and the damping ratio, ξ. These parameters are defined as

$$\omega_n = \sqrt{\frac{k_p}{m_p}} \tag{2.3}$$

and

$$\xi_p = \frac{c_p}{2\sqrt{k_p m_p}} \tag{2.4}$$

Shown in Figure 2.2 is a plot of the mobility of primary structure with a natural frequency of 100 Hz, and damping ratio of 0.02. The mobility of a structure is the inverse of the impedance, or the velocity per unit disturbance force.

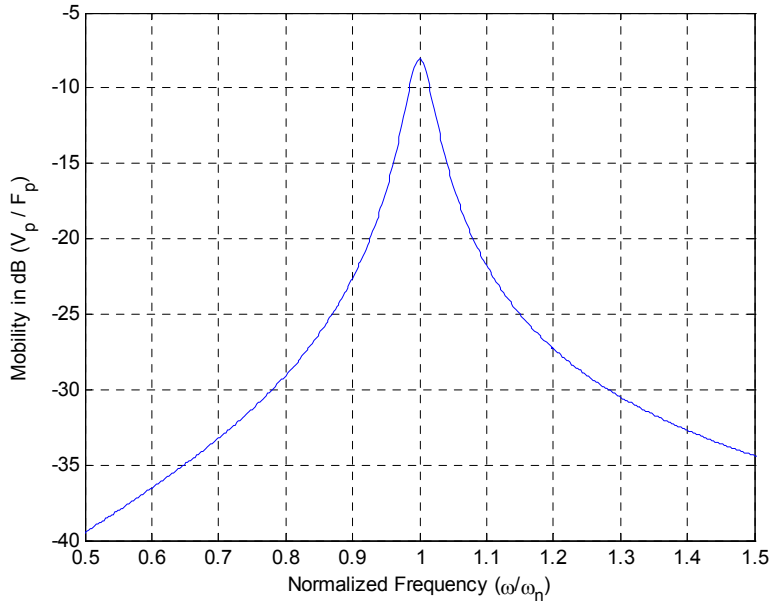

Figure 2.2 Mobility of lumped mass primary system.

The effect of a DVA can be simply modeled as an additional lumped mass attached to the primary structure via a stiffness and damping element, as shown in Figure 2.3.

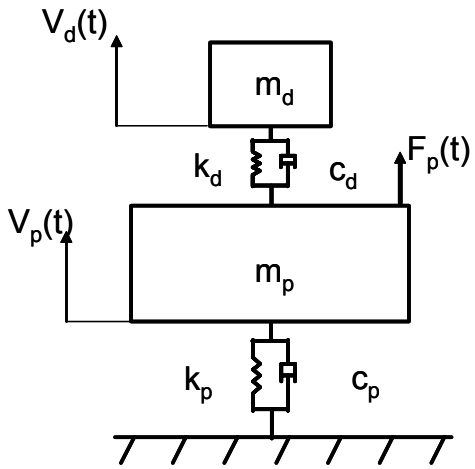

Figure 2.3 Primary structure with 1DOF DVA.

The result of adding a DVA to the system is the addition of impedance to the system. This DVA impedance can be written as

$$Z_d = \frac{m_d k_d + i\omega m_d c_d}{c_d + i\left(\omega m_d - \frac{k_d}{\omega}\right)} \tag{2.5}$$

The overall impedance of the system becomes the primary impedance, Z_p, plus the DVA impedance, Z_d:

$$Z_{sys} = Z_p + Z_d \tag{2.6}$$

Substituting equations (2.2) and (2.5) in for equation (2.6), the total impedance of the system is

$$Z_{sys} = c_p + i\left(\omega m_p - \frac{k_p}{\omega}\right) + \frac{m_d k_d + i\omega m_d c_d}{c_d + i\left(\omega m_d - \frac{k_d}{\omega}\right)} \tag{2.7}$$

This equation shows that if the DVA is tuned to the primary resonance frequency, the system impedance increases at that frequency. Equation (2.7) also indicates that the impedance is a cumulative value with respect to the primary structure. This implies that there is validity to simply examining the impedance of DVAs without taking into account the primary structure, as long as the DVA is tuned to the resonance frequency of the primary structure. Under this reasoning, this thesis will consider impedance matching to be a valid means of evaluating DVA performance. The mobility of the primary structure, shown in Figure 2.4, also shows that the system is now a second order system with two resonances, one above and one below the primary

resonance. The new response can be controlled by three different parameters: mass ratio, tuning frequency, and damping of the DVA. These techniques will be discussed in the following section.

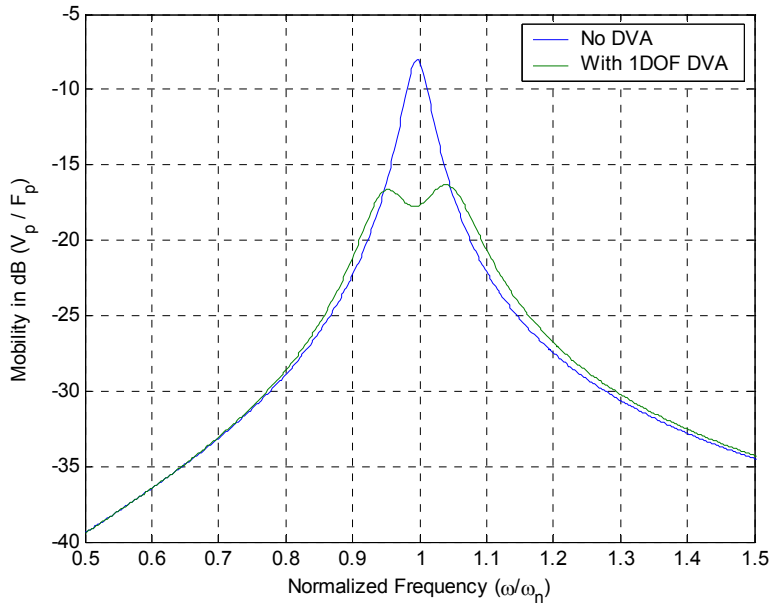

Figure 2.4 Mobility of lumped mass primary system with 1DOF DVA splitting and damping the resonance.

2.2.2 Effects of Mass Ratio, Tuning Frequency, and Damping

Three methods used to maximize the performance of DVAs are the optimization of the mass ratio, tuning frequency, and damping of the DVA. By adjusting the mass ratio of the DVA, the separation of the two new resonances can be controlled. As the mass ratio is increased, the resonances will separate, and subsequently, the response of the structure will be increasingly attenuated at the initial resonance frequency. Increasing the mass, though, is often limited due to the common constraint of minimizing added weight to the system.

The tuning frequency of the DVA can also affect the response of the system, and it is often optimized to increase performance. For a given absorber mass, the DVA stiffness, k_d, can be designed to match the DVA natural frequency with that of the primary system. The optimal tuning frequency, though, is not always the exact frequency of the primary system. When using a vibration absorber to add damping to the system, the optimal tuning frequency can be found using the following equation:

$$f_{opt} = \frac{1}{1+\mu} f_n \tag{2.8}$$

where f_n is the natural frequency of the primary structure, and

$$\mu = \frac{m_d}{m_p} \tag{2.9}$$

where μ is the absorber mass ratio of DVA mass to primary structure mass.[6] However, for very small mass ratios this can be disregarded, and the target frequency can be regarded as the primary structure natural frequency. Also, it is sometimes the case that the precision in the construction of the DVA devices is less accurate than the difference of f_n and f_{opt}, rendering the optimization ineffective. For this work, the absorber mass will be limited to less than five percent of the primary system, so the targeted system resonance frequency is used as the DVA tuning frequency.

For broadband control, it is ineffective to apply a DVA tuned to the primary structure resonance frequency, without adding damping. This approach will merely split the resonance peaks, which will remain lightly damped and highly resonant at frequencies just above and below the original resonance. If too much damping is applied, however, the impedance simply becomes proportional to the added DVA mass (see Eq. (2.7)), which is not a beneficial circumstance. Figure 2.5 shows the response of the primary mass for various levels of DVA damping, for an absorber mass ratio of 1%. Notice how the resonance is first split, then damped to an optimal response at about 6% damping. The optimal amount of damping is observed when one of the two resonance peaks is flat at the common pivot point of the curves.

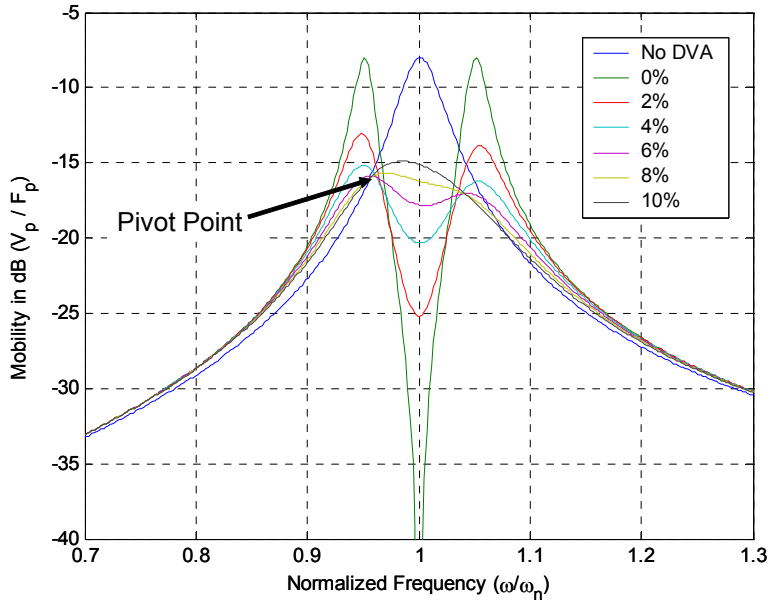

Figure 2.5 SDOF lumped parameter system with a SDOF DVA for various damping coefficients.

Many formulas have been derived to calculate this optimal damping value for various applications. Specifically, Den Hartog[6] and Korenev[7] have compiled optimal damping formulas for a variety of systems, excitations, and assumptions for a variety of responses (displacement, velocity, acceleration). For broadband random excitation, Den Hartog predicts the optimal damping ratio as

$$\xi_{opt} = \sqrt{\frac{\mu(1+0.75\mu)}{4(1+\mu)^3}} \tag{2.10}$$

It can be shown, however, that the vibration attenuation is a weak function of the damping ratio. Shown in Figure 2.6 is the attenuation achieved over all frequencies for this system as a function of damping ratio. It indicates that small deviations from the optimal damping value only result in only minor deterioration of performance. Attenuation is highly sensitive to the low damping ratios, but relatively stable for values within a broad range about ξ_{opt}. As a result, a DVA will provide comparable levels of attenuation even if the damping is not exactly optimal.

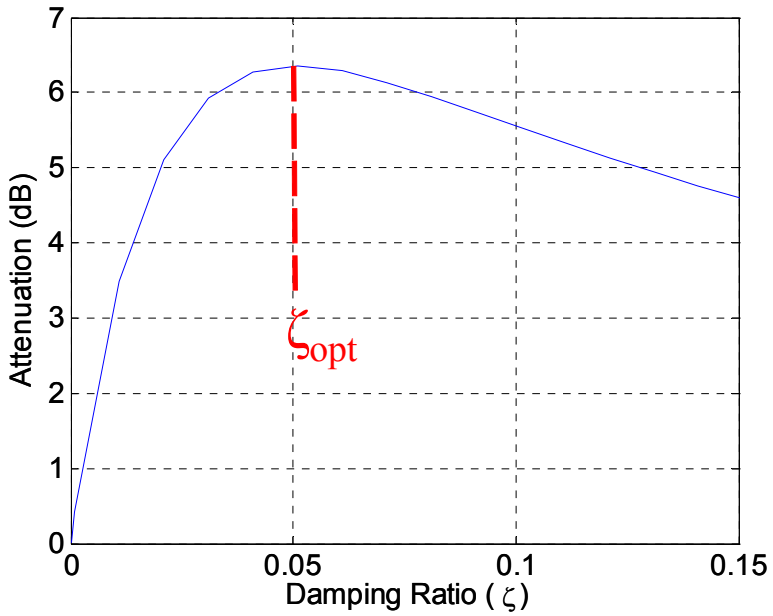

Figure 2.6 Attenuation of squared velocity response as a function of optimal damping ratio of a 1DOF DVA, for a given mass ratio of 0.01.

2.3 2DOF DVA Characterization

This section will introduce the concept of using a 2DOF DVA as a means of improving the conventional 1DOF DVAs. The notion is that since a 2DOF DVA will have two resonance frequencies, the DVA will be able to utilize its mass to provide high levels of impedance at two targeted frequencies. If the 2DOF can be designed so that both of its resonances match the resonances of a primary structure, one 2DOF DVA will provide the same performance as two 1DOF DVAs. This analysis is performed by designing a stacked 2DOF DVA and matching its impedance with two 1DOF DVAs, then evaluating the mass required to achieve this equal impedance. It will be proven that the stacked 2DOF DVA, shown in Figure 2.7(a), will provide an equal level of impedance as two 1DOF DVAs for an equal amount of total absorber mass.

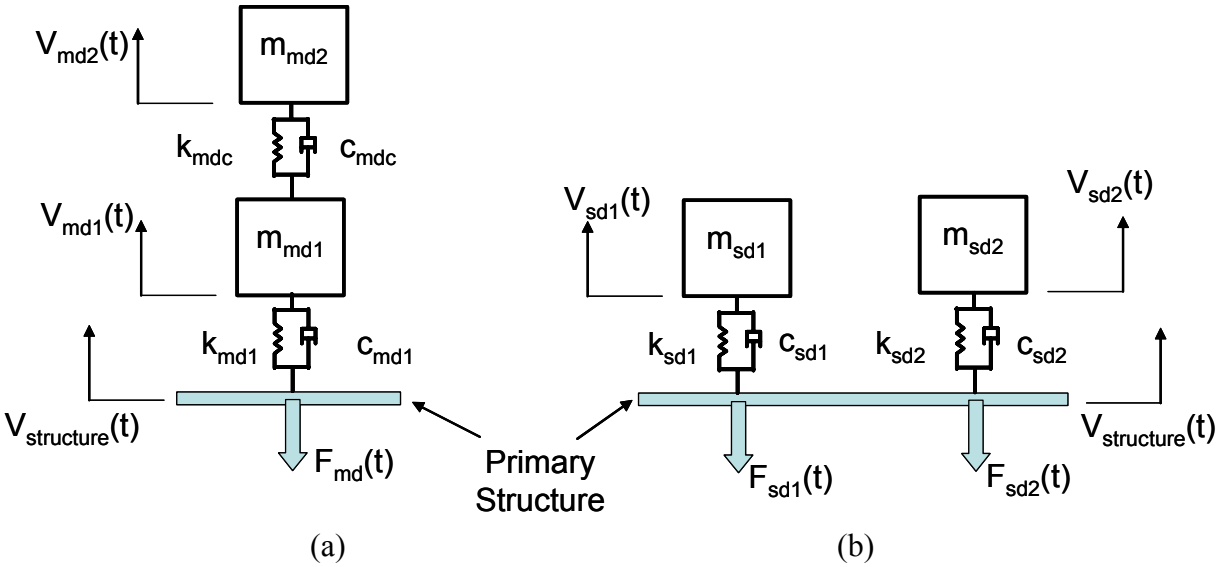

Figure 2.7 (a) 2DOF DVA acting on a vibrating structure. (b) Two 1DOF DVAs acting on a structure.

2.3.1 Equations of Motion for 2DOF DVA

In order to develop the impedance term for a 2DOF DVA as depicted in Figure 2.7(a), the equations of motion will now be written in matrix notation so as to accommodate a DVA of any order, and to make the computations more manageable and clear. Referring to Figure 2.7, the impedance can be defined in terms of modal analysis and will be defined as the force, F, input to the primary structure per velocity of the structure, $V_{structure}$. The force, F, is generated by the movement of the structure and hence the movement of the DVA. For the 2DOF case, the structure will see two occurrences of high impedance, one at each of its two resonant frequencies. And for the two 1DOF case, the base structure will also see two occurrences of high impedance, one for each of the two separate DVA resonance frequencies. For the 2DOF design, the equations of motion can be described as

$$\begin{bmatrix} m_{md1} & 0 \\ 0 & m_{md2} \end{bmatrix}\begin{bmatrix} \ddot{x}_{md1} \\ \ddot{x}_{md2} \end{bmatrix}+\begin{bmatrix} c_{md1}+c_{mdc} & -c_{mdc} \\ -c_{mdc} & c_{mdc} \end{bmatrix}\begin{bmatrix} \dot{x}_{md1} \\ \dot{x}_{md2} \end{bmatrix}+ \begin{bmatrix} k_{md1}+k_{mdc} & -k_{mdc} \\ -k_{mdc} & k_{mdc} \end{bmatrix}\begin{bmatrix} x_{md1} \\ x_{md2} \end{bmatrix}=\begin{bmatrix} k_{md1} \\ 0 \end{bmatrix}x_b+\begin{bmatrix} c_{md1} \\ 0 \end{bmatrix}\dot{x}_b \tag{2.11}$$

where x_b is the displacement of the base structure. This can be rewritten as

$$\mathbf{M}\ddot{\hat{\mathbf{x}}}+\mathbf{C}\dot{\hat{\mathbf{x}}}+\mathbf{K}\hat{\mathbf{x}}=\hat{\mathbf{k}}_{\mathbf{o}}x_b+\hat{\mathbf{c}}_{\mathbf{o}}\dot{x}_b \tag{2.12}$$

From this equation of motion, a modal analysis is performed to decouple the equation into two independent equations. With these equations decoupled, the force input to the base per velocity of the base can be calculated. The equation is first converted to a mass normalized coordinate system, *q*, where $x = \mathbf{M}^{-1/2} q$.

$$\mathbf{M}\mathbf{M}^{-1/2}\ddot{\hat{q}} + \mathbf{C}\mathbf{M}^{-1/2}\dot{\hat{q}} + \mathbf{K}\mathbf{M}^{-1/2}\hat{q} = \hat{\mathbf{k}}_{\mathbf{o}} x_b + \hat{\mathbf{c}}_{\mathbf{o}} \dot{x}_b \tag{2.13}$$

Next, the equation is pre-multiplied by $\mathbf{M}^{-1/2}$ to create a mass normalized expression.

$$\mathbf{M}^{-1/2}\mathbf{M}\mathbf{M}^{-1/2}\ddot{\hat{q}} + \mathbf{M}^{-1/2}\mathbf{C}\mathbf{M}^{-1/2}\dot{\hat{q}} + \mathbf{M}^{-1/2}\mathbf{K}\mathbf{M}^{-1/2}\hat{q} = \mathbf{M}^{-1/2}\hat{\mathbf{k}}_{\mathbf{o}} x_b + \mathbf{M}^{-1/2}\hat{\mathbf{c}}_{\mathbf{o}} \dot{x}_b \tag{2.14}$$

The equation can now be simplified into the form

$$\mathbf{I}\ddot{\hat{q}} + \tilde{\mathbf{C}}\dot{\hat{q}} + \tilde{\mathbf{K}}\hat{q} = \mathbf{M}^{-1/2}\hat{\mathbf{k}}_{\mathbf{o}} x_b + \mathbf{M}^{-1/2}\hat{\mathbf{c}}_{\mathbf{o}} \dot{x}_b \tag{2.15}$$

where

$$\tilde{\mathbf{C}} = \mathbf{M}^{-1/2}\mathbf{C}\mathbf{M}^{-1/2} \quad \text{and} \quad \tilde{\mathbf{K}} = \mathbf{M}^{-1/2}\mathbf{K}\mathbf{M}^{-1/2} \tag{2.16}$$

This results in an equation that, if not for off-diagonal damping terms, would be solvable as a symmetric eigenvalue problem. Therefore, the damping term is temporarily ignored and solved for as:

$$(\tilde{\mathbf{K}} - \lambda\mathbf{I})\mathbf{v} = 0 \tag{2.17}$$

The resulting eigenvalues, λ, and eigenvectors, $\mathbf{v}$, can be expressed in matrix form.

$$\Lambda = \begin{bmatrix} \lambda_1 & 0 \\ 0 & \lambda_2 \end{bmatrix} \quad \text{and} \quad \mathbf{P} = \begin{bmatrix} \mathbf{v}_{11} & \mathbf{v}_{12} \\ \mathbf{v}_{21} & \mathbf{v}_{22} \end{bmatrix} \tag{2.18}$$

Using the eigenvector matrix, $\mathbf{P}$, the equations of motion are converted into the modal coordinate system, *r*, where $q = \mathrm{Pr}$.

$$\mathbf{I}\mathbf{P}\ddot{\hat{\mathrm{r}}} + \tilde{\mathbf{C}}\mathbf{P}\dot{\hat{\mathrm{r}}} + \tilde{\mathbf{K}}\mathbf{P}\hat{r} = \mathbf{M}^{-1/2}\hat{\mathbf{k}}_{\mathbf{o}} x_b + \mathbf{M}^{-1/2}\hat{\mathbf{c}}_{\mathbf{o}} \dot{x}_b \tag{2.19}$$

Next, the equation is pre-multiplied by the transpose of the eigenvector matrix $\mathbf{P}^{\mathbf{T}}$.

$$\mathbf{P}^{\mathbf{T}}\mathbf{I}\mathbf{P}\ddot{\hat{\mathrm{r}}} + \mathbf{P}^{\mathbf{T}}\tilde{\mathbf{C}}\mathbf{P}\dot{\hat{\mathrm{r}}} + \mathbf{P}^{\mathbf{T}}\tilde{\mathbf{K}}\mathbf{P}\hat{r} = \mathbf{P}^{\mathbf{T}}\mathbf{M}^{-1/2}\hat{\mathbf{k}}_{\mathbf{o}} x_b + \mathbf{P}^{\mathbf{T}}\mathbf{M}^{-1/2}\hat{\mathbf{c}}_{\mathbf{o}} \dot{x}_b \tag{2.20}$$

The equation can now be simplified to the form

$$\mathbf{I}\ddot{\hat{\mathrm{r}}} + \mathrm{diag}(2\xi_n\omega_n)\dot{\hat{\mathrm{r}}} + \Lambda\hat{r} = \mathbf{P}^{\mathbf{T}}\mathbf{M}^{-1/2}\hat{\mathbf{k}}_{\mathbf{o}} x_b + \mathbf{P}^{\mathbf{T}}\mathbf{M}^{-1/2}\hat{\mathbf{c}}_{\mathbf{o}} \dot{x}_b \tag{2.21}$$

where Λ is a diagonal matrix of the eigenvalues. The damping term has been modified to a diagonal matrix so the equation of motion can be decoupled. In the modal transformation, the damping terms provide additional coupling between the equations of motion that can only be decoupled for special cases. To account for this, the fully populated damping matrix is substituted with a diagonal matrix proportional to a damping ratio and the resonance frequency. Now that the equations of motion are decoupled, they can be written independently and solved for in the modal coordinate system.

$$\ddot{r}_n + (2\xi\omega_n)\dot{r}_n + \lambda_n r = f_n \tag{2.22}$$

where

$$\mathbf{f_n} = \mathbf{P^T M}^{-½}\begin{bmatrix} k_{md1} + i\omega c_{md1} \\ 0 \end{bmatrix} x_b \tag{2.23}$$

In order to solve equation (2.22), a harmonic solution is assumed. This solution and its derivatives are

$$r_n = \mathrm{X}e^{i\omega t}, \quad \dot{r}_n = i\omega \mathrm{X}e^{i\omega t}, \quad \dot{r}_n = -\omega^2 \mathrm{X}e^{i\omega t} \tag{2.24}$$

Substituting the assumed solution into equation (2.22), the unknown value, X, can now be expressed as

$$\mathrm{X} = \frac{\mathbf{f_n}}{\left(-\omega^2 + i\omega 2\xi\omega_n + \omega_n^2\right)} \tag{2.25}$$

The solution is now written as

$$r_n = \frac{\mathbf{f_n}}{\left(-\omega^2 + i\omega 2\xi\omega_n + \omega_n^2\right)} e^{i\omega t} \tag{2.26}$$

In matrix form, the modal system of equations is

$$\begin{bmatrix} r_{md1} \\ r_{md2} \end{bmatrix} = \begin{bmatrix} \dfrac{1}{\left(\omega_1^2 - \omega^2 + i2\xi\omega_1\omega\right)} & 0 \\ 0 & \dfrac{1}{\left(\omega_2^2 - \omega^2 + i2\xi\omega_2\omega\right)} \end{bmatrix} \mathbf{P^T M}^{-½}\begin{bmatrix} k_{md1} + i\omega c_{md1} \\ 0 \end{bmatrix} x_b \tag{2.27}$$

for the stacked 2DOF system. Now that the equations of motion are decoupled, they are converted back into the physical coordinate system. This transformation is performed by

multiplying the modal equation by the transformation matrix, S, where $S = \mathbf{M}^{-1/2}\mathbf{P}$. This transformation is written as

$$x = Sr = \mathbf{M}^{-1/2}\mathbf{P}r \tag{2.28}$$

The decoupled equations of motion in the physical coordinate system are

$$\begin{bmatrix} x_{md1} \\ x_{md2} \end{bmatrix} = \mathbf{M}^{-1/2}\mathbf{P}\mathbf{L}\mathbf{P}^{\mathrm{T}}\mathbf{M}^{-1/2}\begin{bmatrix} k_{md1} + i\omega c_{md1} \\ 0 \end{bmatrix} x_b \tag{2.29}$$

where the complex resonance term has been denoted $\mathbf{L}$,

$$\mathbf{L} = \begin{bmatrix} 1/\left(\omega_1^2 - \omega^2 + i2\xi\omega_1\omega\right) & 0 \\ 0 & 1/\left(\omega_2^2 - \omega^2 + i2\xi\omega_2\omega\right) \end{bmatrix} \tag{2.30}$$

Now that the equations of motion are decoupled, the force exerted into the base structure can be calculated. The force exerted into the base is a function of the displacement and velocity of the first DVA mass, m_{md1}, relative to the base motion. This expression is written as

$$f_b = k_{md1}(x_{md1} - x_b) + c_{md1}(\dot{x}_{md1} - \dot{x}_b) = (k_{md1} + i\omega c_{md1})(x_{md1} - x_b) \tag{2.31}$$

Substituting the equation (2.29) into equation (2.31), the force exerted into the base is written as

$$f_b = \begin{bmatrix} k_{md1} + i\omega c_{md1} & 0 \end{bmatrix}\left(\mathbf{M}^{-1/2}\mathbf{P}\mathbf{L}\mathbf{P}^{\mathrm{T}}\mathbf{M}^{-1/2}\begin{bmatrix} k_{md1} + i\omega c_{md1} \\ 0 \end{bmatrix} - \begin{bmatrix} 1 \\ 1 \end{bmatrix}\right) x_b \tag{2.32}$$

This can be written as the impedance of the stacked 2DOF impedance by simply dividing both sides of the equation by the displacement of the base and dividing by a *iω* term.

$$Z_{md} = \frac{f_b}{x_b(i\omega)} = \begin{bmatrix} \left(\frac{k_{md1}}{i\omega} + c_{md1}\right) & 0 \end{bmatrix}\left(\mathbf{M}^{-1/2}\mathbf{P}\mathbf{L}\mathbf{P}^{\mathrm{T}}\mathbf{M}^{-1/2}\begin{bmatrix} k_{md1} + i\omega c_{md1} \\ 0 \end{bmatrix} - \begin{bmatrix} 1 \\ 1 \end{bmatrix}\right) \tag{2.33}$$

2.3.2 Impedance Matching

Having derived the impedance of a stacked 2DOF DVA, the next step is to match the impedance at resonance. To accomplish this, equation (2.33) needs to be broken down into terms where each resonance of the 2DOF DVA can be approximated by two SDOF DVAs. By expanding equation (2.33), we can perform the matrix multiplications to see that the impedance has two resonant terms. Expanded, the equations are

$$Z_{md} = \begin{bmatrix} (k_{md1} + i\omega c_{md1}) & 0 \\ 0 & 0 \end{bmatrix} \begin{bmatrix} m_{md1}^{-1/2} & 0 \\ 0 & m_{md2}^{-1/2} \end{bmatrix} \begin{bmatrix} v_{11} & v_{12} \\ v_{21} & v_{22} \end{bmatrix} \begin{bmatrix} \left(\omega_1^2 - \omega^2 + i2\xi\omega_1\omega\right)^{-1} & 0 \\ 0 & \left(\omega_2^2 - \omega^2 + i2\xi\omega_2\omega +\right)^{-1} \end{bmatrix} \begin{bmatrix} v_{11} & v_{21} \\ v_{12} & v_{22} \end{bmatrix} \begin{bmatrix} m_{md1}^{-1/2} & 0 \\ 0 & m_{md2}^{-1/2} \end{bmatrix} \begin{bmatrix} (k_{md1} + i\omega c_{md1}) \\ 0 \end{bmatrix} - \begin{bmatrix} (k_{md1} + i\omega c_{md1}) \\ 0 \end{bmatrix} \quad (2.34)$$

After matrix multiplication, we find that there are two resonance terms corresponding to the two natural frequencies of the stacked 2DOF DVA.

$$Z_{md} = \frac{v_{11}^2 (k_{md1} + i\omega c_{md1})^2}{m_{md1}\left(\omega_1^2 - \omega^2 + i2\xi\omega_1\omega\right)} + \frac{v_{12}^2 (k_{md1} + i\omega c_{md1})^2}{m_{md1}\left(\omega_2^2 - \omega^2 + i2\xi\omega_2\omega +\right)} - (k_{md1} + i\omega c_{md1}) \quad (2.35)$$

In order to match two 1DOF DVAs with the stacked 2DOF DVA, equation (2.35) must be broken down into two terms based on their values at each resonance. The first term in equation (2.35) is the dominant term when $\omega = \omega_1$; so the first 1DOF DVA will be designed to have an impedance of equal value to this first term. Likewise, the second term will be used to assign the parameters for the second 1DOF DVA. The third term in equation (2.35) is negligible at both resonances and can be ignored during the process of matching impedance. If equation (2.35) is written for a 1DOF DVA, the eigenvector v_{11} is unity and v_{12} is zero. Ignoring the third term, the impedances can be equated as,

$$\frac{(k_{sd1} + i\omega c_{sd1})^2}{m_{sd1}\left(\omega_1^2 - \omega^2 + i2\xi\omega_1\omega\right)} \cong \frac{v_{11}^2 (k_{md1} + i\omega c_{md1})^2}{m_{md1}\left(\omega_1^2 - \omega^2 + i2\xi\omega_1\omega\right)} \quad (2.36)$$

The left term is the impedance for a SDOF DVA, and the right term is the impedance for one mode of a MDOF DVA, specifically a stacked 2DOF DVA. From this equation, the complex resonance term is equivalent and can be cancelled. The damping term can also be ignored due to its low magnitude relative to the stiffness value:

$$\frac{(k_{sd1} + \cancel{i\omega c_{sd1}})^2}{m_{sd1}\cancel{\left(\omega_1^2 - \omega^2 + i2\xi\omega_1\omega\right)}} \cong \frac{v_{11}^2 (k_{md1} + \cancel{i\omega c_{md1}})^2}{m_{md1}\cancel{\left(\omega_1^2 - \omega^2 + i2\xi\omega_1\omega\right)}} \quad (2.37)$$

This results in an equation that relates the 1DOF parameters to the MDOF impedance at resonance,

$$k_{sd1}\frac{k_{sd1}}{m_{sd1}} \cong \frac{v_{11}^2 k_{md1}^{\ 2}}{m_{md1}} \quad (2.38)$$

Since $\omega_1^2 = k_{sd1} / m_{md1}$, the equation simplifies to the 1DOF DVA stiffness as a function of the resonance frequency and the 2DOF parameters:

$$k_{sd1} = \frac{v_{11}^2 (k_{md1})^2}{\omega_1^2 m_{md1}} \tag{2.39}$$

With the first resonance frequency and the MDOF stiffness and mass known, the 1DOF DVA stiffness can be calculated to match the impedance at the first resonance of the stacked 2DOF DVA. Now, the mass to be used for the 1DOF DVA is simply a function of the resonance frequency and the stiffness, as shown by

$$m_{sd1} = \frac{k_{sd1}}{\omega_1^2} \tag{2.40}$$

This process is repeated for the second resonance term of equation (2.35) to generate the two 1DOF DVAs equivalent to a stacked 2DOF DVA. Once the values are found for the 1DOF equivalent, the two impedance functions are calculated using the process leading up to equation (2.35), and compared over the frequency range of interest.

Using the impedance matching process, two 1DOF DVAs are designed and plotted in Figure 2.8 against the 2DOF design. It can be seen from the figure that the impedance matching is accurate to within a few tenths of a decibel, dB. This matching technique will suffice given that the precision of tuning DVAs is often less accurate. Figure 2.8 can be better understood by looking at the eigenvectors of the 2DOF DVA, which describe the modal direction of each mass.

$$P_{md} = \begin{bmatrix} 0.28 & 0.96 \\ 0.96 & -0.28 \end{bmatrix} \tag{2.41}$$

These values are normalized and indicate direction only, not magnitude. The 2DOF DVA utilizes both of its masses to impede movement in its first mode; the first mode of the DVA is both masses moving in phase. This is indicated by the equivalent sign of the two elements in the first column of equation (2.41). In the second mode of the 2DOF DVA, the masses move with a phase of 180^o. In comparison to the 1DOF DVA, the 2DOF DVA uses both masses to impede motion at the first mode, and therefore requires the 1DOF equivalent to have a large mass. It is the second mode that is less effective for the 2DOF DVA, though, as the motion of the masses oppose each other and compromise each other's performance. For this resonance, the 1DOF DVA requires significantly less mass to accomplish the same performance. Overall, the

performance of the two 1DOF DVAs and one 2DOF DVA is identical for this, and all cases. The underlying principle is that there is no advantage gained by using a stacked 2DOF DVA in place of a set of SDOF DVAs.

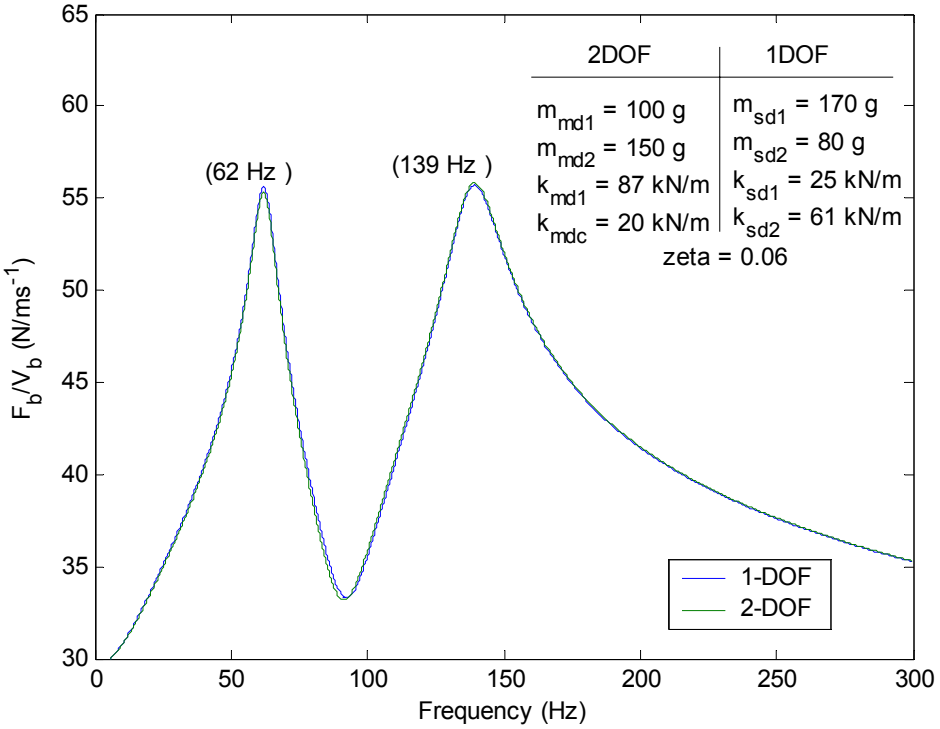

Figure 2.8 Impedance comparison of a stacked 2DOF DVA and two 1DOF DVAs.

2.4 Stacked 2DOF DVA on Cylinder

This section will detail the modeling, design, implementation, and testing of 15 stacked 2DOF DVAs on a mock payload cylinder. This will experimentally prove that a 2DOF DVA can utilize its multiple modes to attenuate vibration at multiple targeted resonance frequencies.

2.4.1 Mock Payload Fairing

As mentioned in the motivation of this research, the mock payload fairing, shown in Figure 2.9, is a scaled cylindrical model of a payload fairing. Made of composite materials, it has a diameter of 2.5 meters, a height of 2.8 meters, and weighs only 80 kg. The cylinder is transported on the maroon dolly shown in Figure 2.9(a), but otherwise sits on the ground during testing. The end caps of the cylinder are made of plywood and compress the cylinder with tightened threaded rods that circle the cylinder. Prior tests using DVAs in the cylinder have

proven that they are an effective means of reducing structural vibration at specific resonance frequencies.[26] The targeted frequencies were chosen based on this existing frequency response data of the cylinder, shown in Figure 2.9(b). Observing that the first several structural resonances are around 60 Hz, the (1,7) mode at 62 Hz was chosen to be the first target frequency. Due to the relatively high damping of the foam used for the DVAs, a fairly large separation between the two target frequencies was desired so the target frequency bands did not overlap each other. The second target frequency was chosen to be 139 Hz, due to the large modal amplitudes observed in the (2,4), (1,11), (3,9), and (3,8) modes in this region.

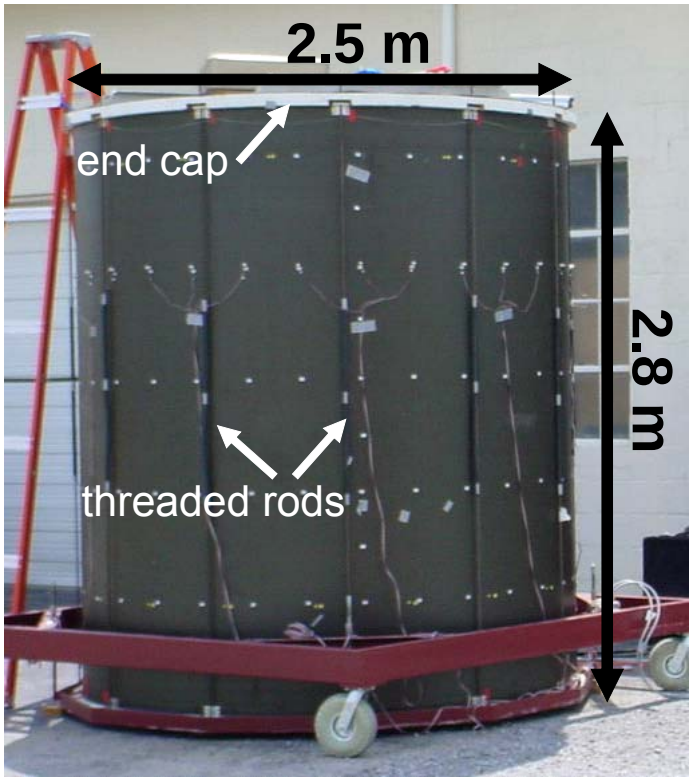

(a)

Axial Order	Circum. Order	Experimental Frequency (Hz)
1	5	47.5
1	6	49.5
1	4	56.5
1	7	61.8
1	3	76.5
1	8	76.9
2	7	92.2
1	9	96.3
2	8	98.0
2	6	100.5
2	9	109.5
2	5	114.0
1	10	117.5
2	10	128.0
2	4	139.0
1	11	141.2
3	9	141.4
3	8	141.5
1	2	145.0
3	7	147.5
2	11	150.0

(b)

Figure 2.9 (a) Photograph of mock payload fairing on dolly. (b) Experimental results of cylinder resonance frequencies from structural excitation.

2.4.2 Impedance Model of Stacked 2DOF DVA

Before production of the stacked 2DOF DVAs, an analytical model was developed using the aforementioned impedance equations to determine the proper design parameters. Along with the targeted resonance frequencies of 62 and 139 Hz, a mass limitation was imposed restricting the total DVA mass to under 250 grams. Another criterion was that the stiffness elements, which are blocks of foam, had to be the same value for both springs. This is due to the difficulty in

cutting the foam to have repeatable stiffness properties. The foam used in the production of the DVAs is supplied in a large 2" thick sheet. While cutting blocks of 2" thickness from the blanket does not affect the stiffness, cutting the blocks along a surface that interfaces the mass or the primary structure greatly affects the stiffness of the foam, and makes tuning the DVAs extremely difficult. Because of this, there was no way to adjust the stiffness of the foam blocks. Thus, both stiffness values were restricted to be equivalent. The remaining parameters are the two lumped masses of the DVA. Shown in Figure 2.10 is the impedance of a 2DOF DVA with resonance frequencies of 58 and 139 Hz. Given the restriction on equal stiffness, this is the closest match attainable to the target frequencies. Notice from the figure that the 1DOF DVAs have a total impedance very near that of the 2DOF DVA. In this case, the lower resonance has an impedance nearly 20 dB greater than the higher resonance. This is due to the high stiffness connecting the two masses. Referring to the eigenvectors,

$$P = \begin{bmatrix} 0.70 & 0.72 \\ 0.72 & -0.70 \end{bmatrix} \tag{2.42}$$

this system should perform very well in the first mode. Both masses are in phase, and act in unison to impede motion. In contrast, the masses have near equal eigenvalues for the second mode, and have a phase of 180^{o}. The masses effectively cancel each other's performance in impeding motion. Subsequently, the equivalent mass required to copy this impedance for the 1DOF case is only six grams. Given the constraints, however, this system is used to develop the prototype stacked 2DOF DVAs.

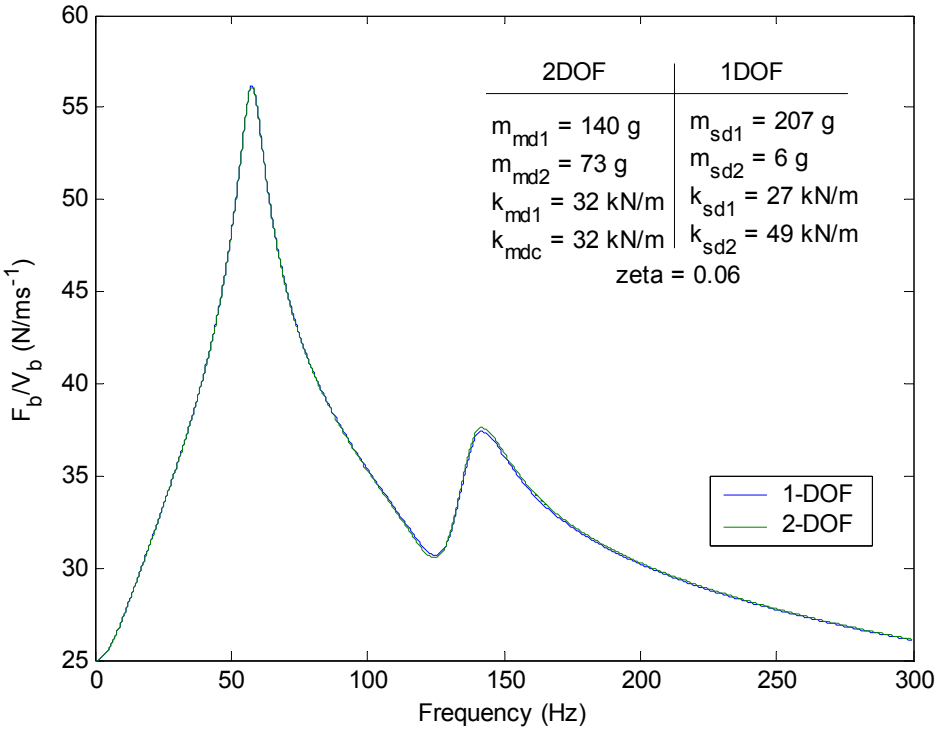

Figure 2.10 Impedance comparison of a stacked 2DOF DVA and two 1DOF DVAs.

2.4.3 Stacked 2DOF DVA Design

The design used to build the stacked 2DOF DVAs was based on existing research that concluded that DVAs with broad footprints are able to attenuate a broader frequency band of resonances. This is in contrast to conventional point absorbers that only attenuate one frequency.[27] Figure 2.11 shows a photograph and free body diagram of the stacked 2DOF DVA. As seen in the photographs, the DVA consists of two 3" x 5" x 2" foam blocks that act as spring-dampers, and two 3 x 5 inch steel plates that act as plate masses. Because the stiffness and damping of the foam are not exactly reproducible, small masses are added to the top plate in order to tune the DVA to resonant frequencies to within two or three Hz of the targeted frequencies. The overall mass of a stacked 2DOF DVA is less than 250 grams.

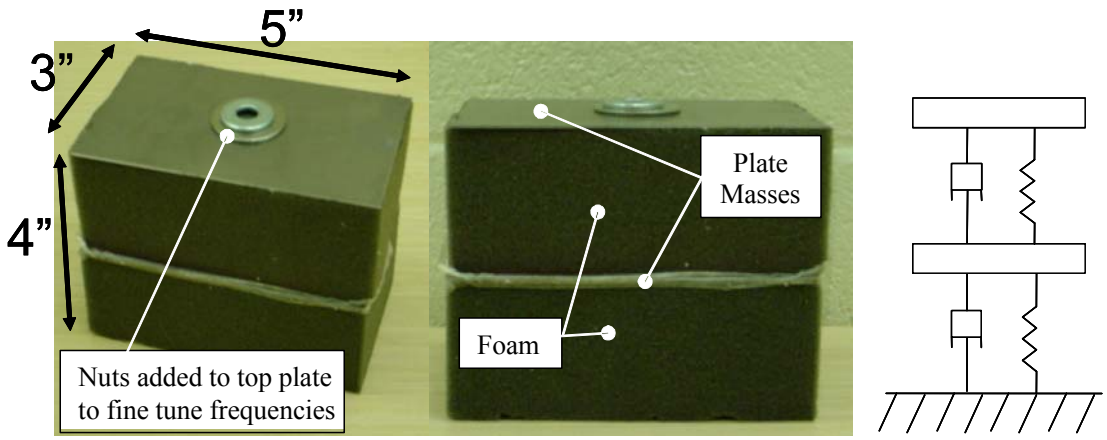

(a) (b) (c)

Figure 2.11 (a,b) Photographs of stacked 2DOF DVA. (c) Free body diagram of stacked 2DOF DVA.

In order to tune the DVAs, each 2DOF DVA was glued to a shaker plate, and the transfer function between the input voltage and the top plate acceleration was measured. The masses of the two plates are approximately 140 and 70 grams as dictated by the model described in the previous section. By gluing nuts to the top plate, the DVAs were tuned very accurately to within two or three Hz of the target frequencies. Figure 2.12 shows a frequency response of one of the 2-DOF DVAs.

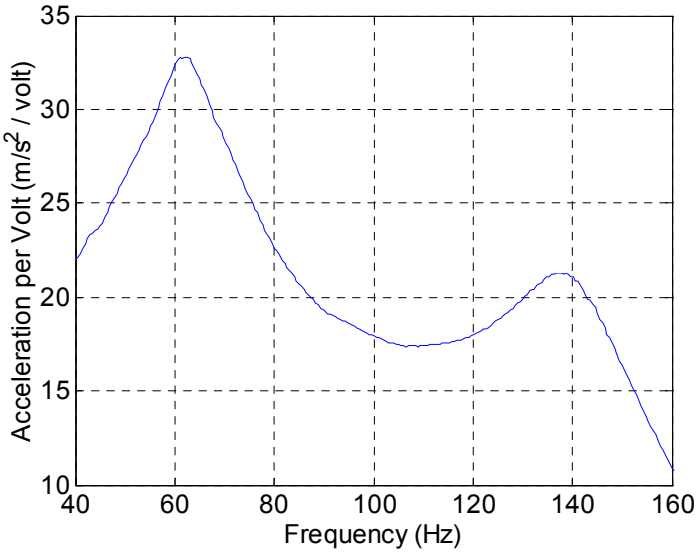

Figure 2.12 Acceleration of top plate of stacked 2DOF DVA for shaker input.

2.4.4 Experimental Results of Stacked 2DOF DVA on Cylinder

Once 15 DVAs were tuned to the target frequencies, they were taped to the interior of the cylinder, as shown in Figure 2.13(b). The 15 DVAs were positioned in a ring at a height of 27" from the base, each 24° apart from each other. In total, less than 4 kg were added to the cylinder in DVA material, compared to the 80kg mass of the cylinder. To measure the structural vibrations of the cylinder, a 50 lb shaker was hung from bungee cord and attached through a stinger and a force transducer to a female coupling already mounted to the cylinder approximately 25" from the base. A ring of 30 accelerometers, placed 30" from the top of the cylinder, simultaneously measured the acceleration of the cylinder at these 30 points.

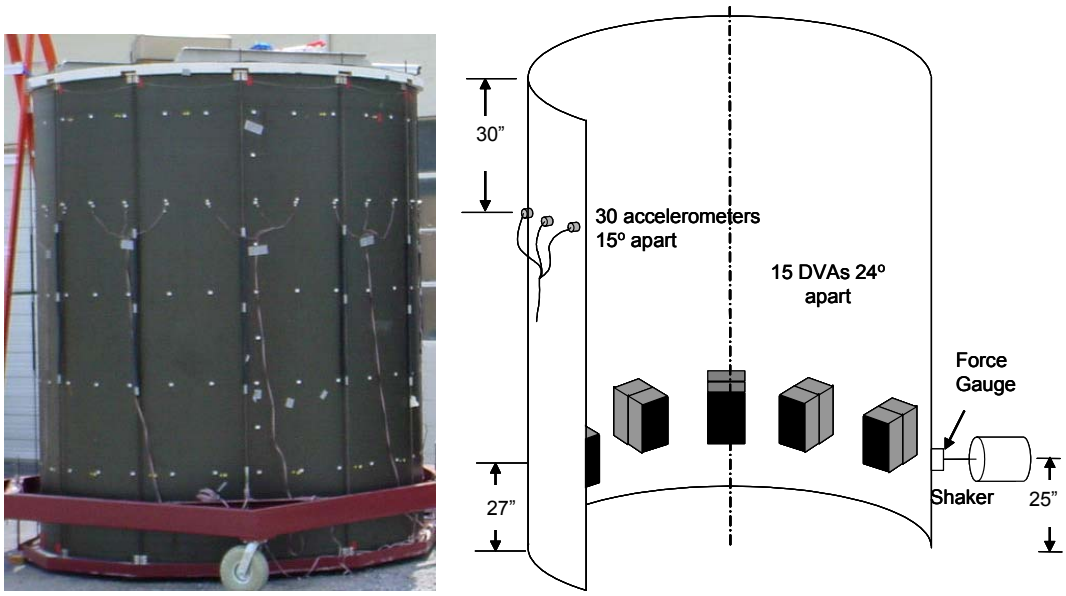

Figure 2.13 (a) Photograph of cylinder with accelerometers attached to outside surface. (b) Cut away schematic of cylinder with 2-DOF DVAs mounted inside cylinder, and accelerometers and shaker attached to the outside of the cylinder.

The results shown in Figure 2.14 are the average of the squared transfer functions of all 30 accelerometer measurements in velocity per input force to the cylinder. This conversion to velocity per force was done to provide the best estimate of the kinetic energy, which is proportional to the velocity squared. The omission of the 0 to 40 Hz frequency band is due to high pass filtering of the random noise used to power the shaker. These results indicate that the 2DOF DVAs are very effective in attenuating the structural vibration over two bands of frequencies. From the figure, it can be seen that the first targeted frequency range attenuated the

50 and 62 Hz modes by 19 and 11 dB respectively. Likewise, the second targeted frequency range attenuated the 128, 140, and 150 Hz modes by 9, 8, and 8 dB, respectively. The overall attenuations in the 40 to 70 Hz, and 120 to 160 Hz frequency bands were 5.6 and 4.3 dB respectively.

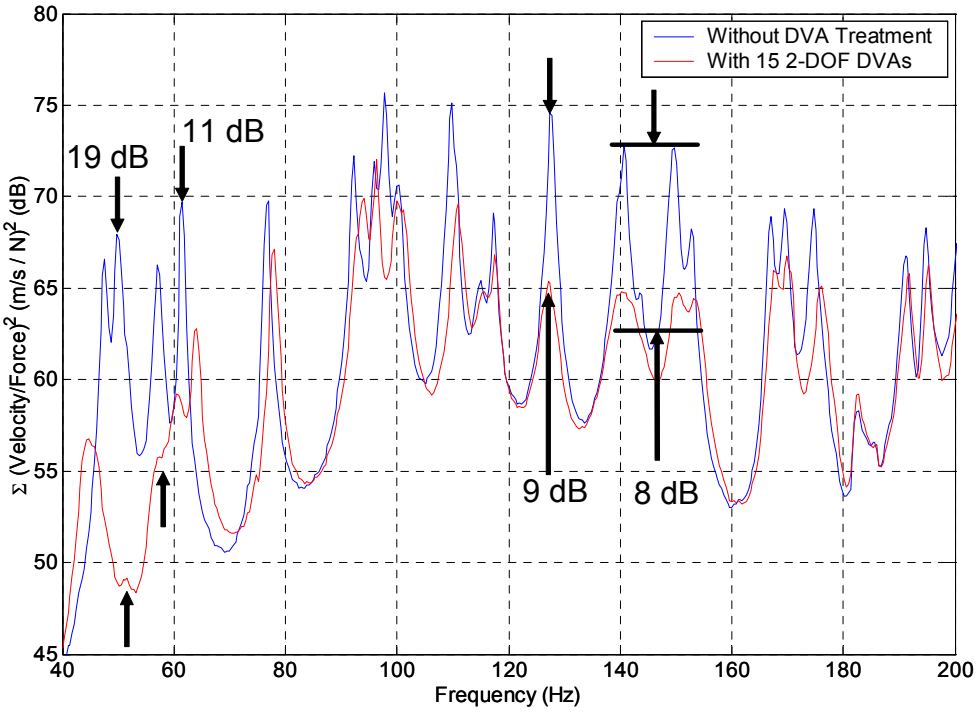

Figure 2.14 Kinetic energy of payload cylinder with and without ring of 15 stacked 2DOF DVAs. Attenuations in the 40 to 70 Hz, and 120 to 160 Hz frequency bands were 5.6 and 4.3 dB respectively.

Another indicator of effectiveness is the circumferential mode order plot, which is shown in Figure 2.15. The circumferential mode order plot is obtained by first collecting the 30 transfer functions of acceleration per force input into the cylinder. These transfer functions are filtered by multiplying each one by a series of cosine functions corresponding to the first 15 circumferential modes of the cylinder. By plotting these filtered functions, we can essentially see the frequency response of each circumferential mode separately. This enables us to see exactly which modes are being affected by the DVAs, and which are not. This plot shows the reduction of modal amplitudes in the same frequency regions as Figure 2.14, the targeted frequencies of 60 and 140 Hz.

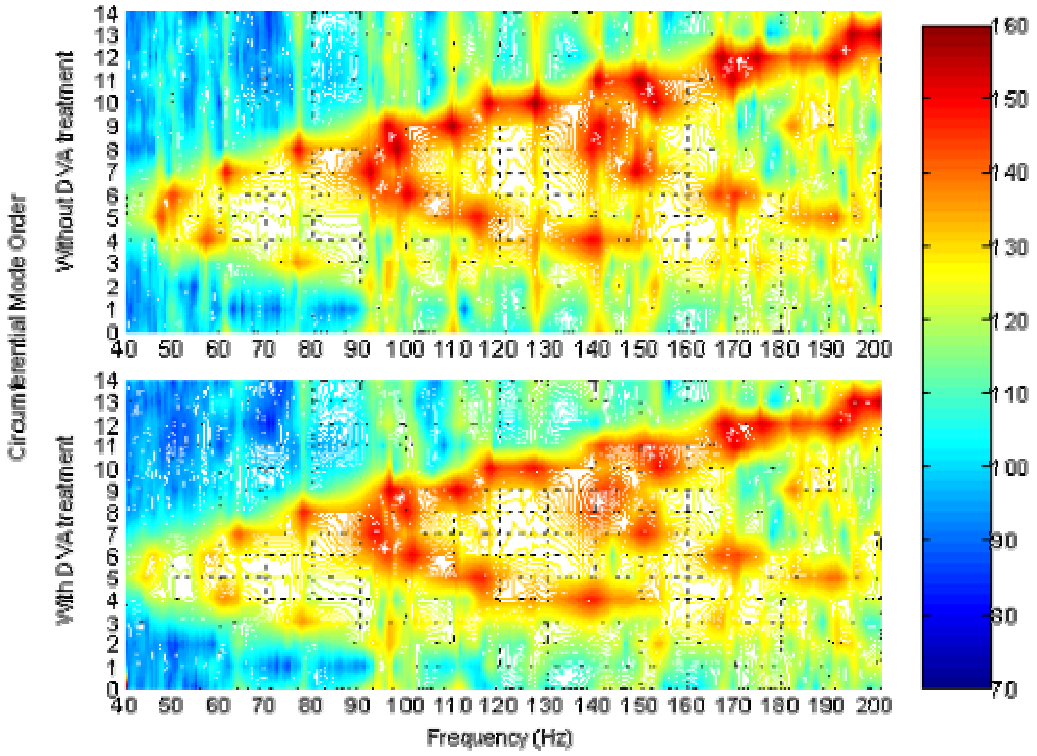

Figure 2.15 Circumferential mode order plot, which indicates the reduction of modal amplitudes with the addition of DVAs.

2.5 Conclusions

The goal of this chapter was to first establish a method of comparing 2DOF DVAs to the conventional 1DOF DVAs. This was accomplished by designing 1DOF DVAs to have an impedance equivalent to a 2DOF DVA at resonance, and comparing the total absorber masses. It was shown that for equal impedance, both systems use an equal amount of total mass, and therefore stacked DVAs do not provide any advantage in terms of used mass. This principle is true for all cases comparing stacked 2DOF DVAs to a set of 1DOF DVAs. However, it was proven that while 2DOF DVAs were unable to generate a mass advantage, they are able to attenuate multiple frequencies of a distributed system. This was proven with the design of 15 stacked 2DOF DVAs that were applied to a cylindrical shell in order to target two resonance frequencies. The experimental results showed that the DVAs attenuated both of the targeted frequencies by as much as 19dB. These results indicate that the multiple resonance frequencies of the MDOF DVAs can be utilized to gain an advantage if implemented with multiple reaction points; a premise explored in chapter three.

Chapter 3: Multi-Degree of Freedom Dynamic Vibration Absorbers Acting at Multiple Reaction Points

The performance of multi-degree of freedom dynamic vibration absorbers (MDOF DVAs) acting at multiple reaction points compared to conventional 1DOF DVAs is discussed in this chapter. By matching the resonance frequencies and mode shapes of the MDOF DVA with those of the primary structure, the DVA mass can be used more effectively at each structural resonance and thus gain an advantage. The advantage gained in terms of absorber mass required for a given level of attenuation with a MDOF DVA is demonstrated in this chapter. The design techniques used to optimize the performance of the absorber on this system will be discussed. The lumped parameter system is a simple, if unrealistic, way to evaluate the MDOF DVA potential. The MDOF DVA is most effective on a lumped parameter system because the mode shapes of the two systems can be coupled perfectly. To demonstrate the MDOF DVAs on a distributed system, the response of a pinned-pinned plate coupled to a MDOF DVA is modeled. The position of the DVA is an integral factor in performance; the DVA design and positioning algorithm will be discussed. Next, the MDOF DVA will be investigated for use on a cylindrical shell, such as the payload cylinder discussed in the preceding chapter. This application introduces significant limitations due to the high modal density and the symmetrical modes exhibited by cylindrical shells. Finally, the chapter will end with a discussion of the overall advantages and disadvantages of MDOF DVAs.

3.1 Theory of MDOF DVAs Acting at Multiple Reaction Points

The preceding chapter demonstrated theoretically and experimentally that a MDOF DVA could be designed and constructed to have two resonances that passively reduce vibration in a multiple resonance structure. Through analytical modeling, it was shown that the stacked 2DOF design was equivalent to two 1DOF DVAs, but not more effective. In order to gain an advantage, the mode shapes of the DVA need to be coupled to the primary system such that the DVA uses both of its masses to impede both resonances. This is accomplished by positioning the DVA reaction points at locations that correspond to the mode shapes of the structure. It will be demonstrated first on a simple 2DOF lumped parameter system, shown in Figure 3.1.

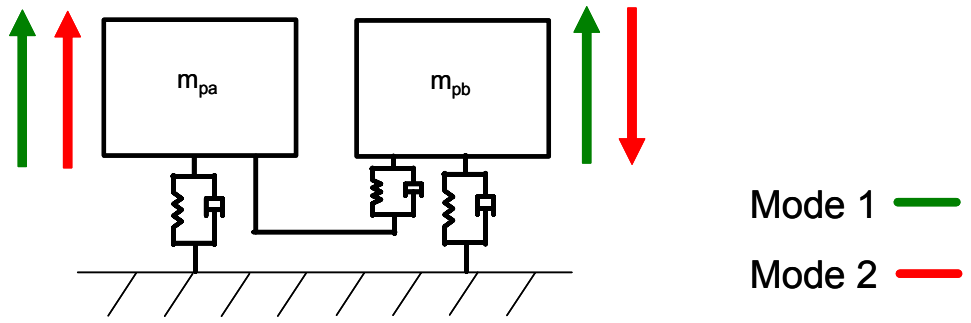

Figure 3.1 2DOF spring-mass-damper system exhibiting two modes. The masses are in phase for mode 1, and have a phase of 180° for mode 2.

The lumped parameter system shown in Figure 3.1 exhibits two resonance frequencies, corresponding to each degree of freedom. At the first resonance of the system, the masses are in phase as indicated by the green arrows. At the second resonance, the masses are 180° out of phase as indicated by the red arrows. If two 1DOF DVAs are used to impede both resonances of this system, each of the DVAs would be tuned to a resonance frequency of the system as shown in Figure 3.2(a). Each of the DVAs would have one resonance, and thus, each mass would only be utilized for one mode of the system. This is assuming the resonance frequencies are well spaced.

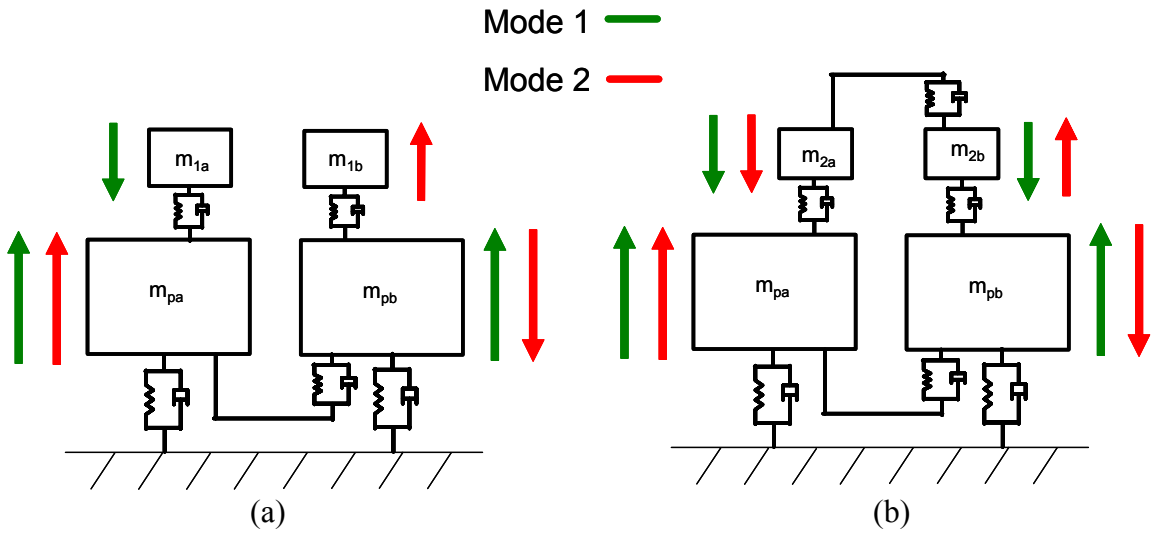

Figure 3.2 (a) First two modes of a 2DOF lumped parameter system with two SDOF DVAs. (b) First two modes of a 2DOF lumped parameter system with a 2DOF DVA.

For the 2DOF system, the 2DOF DVA is designed such that the resonance frequencies and the mode shapes match the primary system exactly. For the lumped parameter system shown, each mass and spring stiffness is scaled to a percentage of the primary system. The result

is such that the 2DOF DVA has equivalent resonance frequencies and mode shapes to the primary system. Both DVAs have two resonance frequencies that correspond to two frequency bands of high impedance that inhibit the motion of the primary system at its resonance frequencies. The advantage of the 2DOF DVA is generated by the utilization of both masses at both resonance frequencies. For the first mode (green), both mass m_{pa} and m_{pb} are moving in phase with each other. For the 2DOF case, both m_{2a} and m_{2b} are moving in phase to impede the motion of the primary system. In contrast, the 1DOF case only utilizes m_{1a} for the first mode. The second mode (red) exhibits similar behavior. The primary masses, m_{pa} and m_{pb} are moving with a phase of 180^{o} relative to each other. The 1DOF DVA impedes the motion of m_{pb} with the mass of m_{1b}. But the 2DOF DVA uses both masses, again, to impede both m_{pa} and m_{pb}.

For a lumped parameter primary system, the coupling for both the SDOF and MDOF DVAs is unity because the DVAs are also modeled as lumped parameter systems. This means the absorbers can be designed to have equivalent mode shapes that can impede the motion of the primary system. For a distributed system, such as a beam, plate, or cylinder, the mode shapes are more complex functions such as sines and cosines. The optimal location is at the peak of the mode shape that corresponds to the targeted frequency. For a MDOF DVA to target two resonances, however, the reaction points need to be in locations that have high coupling coefficients at both resonance frequencies. This is the why the stacked 2DOF DVA did not provide an advantage over the 1DOF DVAs; there needs to be another reaction point for the stacked DVA. Referring to Figure 3.3, the stacked 2DOF DVA is shown in comparison to two 1DOF DVAs on a pinned-pinned beam. Notice that the coupling coefficient, ψ, is unity for both 1DOF DVAs, but is less than unity for both modes of the stacked 2DOF DVA. This is because the stacked 2DOF DVA can only be positioned to have one of the modes coupled perfectly. Shown in the figure, the reaction point is such that neither of the modes are coupled perfectly, but neither are at a node. This compromise in coupling, however, severely deteriorates the performance since the modal forcing of the beam is a function of the coupling squared. The motion of the beam is first coupled through the reaction point to generate the motion of the DVA mass. Then the motion of the DVA mass is coupled through the reaction point again in the form of a force back onto the beam. So, it is critical that the coupling coefficient remain as close to unity as possible.

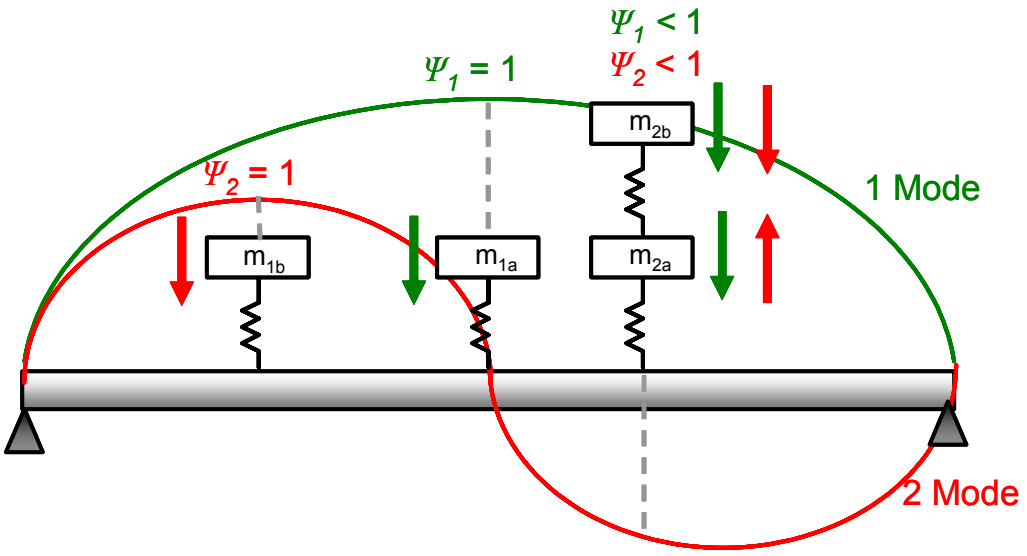

Figure 3.3 Comparison of coupling coefficients for two 1DOF DVAs and one stacked 2DOF DVA acting on a pinned-pinned beam. The stacked 2DOF DVA can not be coupled well into both modes due to its single reaction point.

Shown in Figure 3.4 is a comparison of two 1DOF DVAs and a 2DOF DVA with two reaction points. The third and fourth modes of the beam are targeted, and the corresponding mode shapes are shown in green and red respectively. The 1DOF DVAs maintain their performance with coupling coefficients equal to unity. However, the 2DOF DVA is now able to utilize both masses at both resonance frequencies. The first resonance of the 2DOF DVA is designed to have the same resonance as the third mode of the beam. For this frequency, the DVA masses are in phase, and are positioned such that the reaction points on the beam are in phase. Therefore both masses will be impeding the motion of the beam at this resonance. The coupling factor for the third beam mode at this location is not unity, but very close. The second resonance of the 2DOF DVA is tuned to match the fourth mode of the beam. At this frequency, the 2DOF DVA masses will move with a phase of 180^{o} relative to each other. This corresponds to the two reaction points on the beam, which are also moving with a phase of about 180^{o} at this frequency. So, both 2DOF DVA masses are also utilized at the fourth beam mode, but also have a coupling coefficient less than unity.

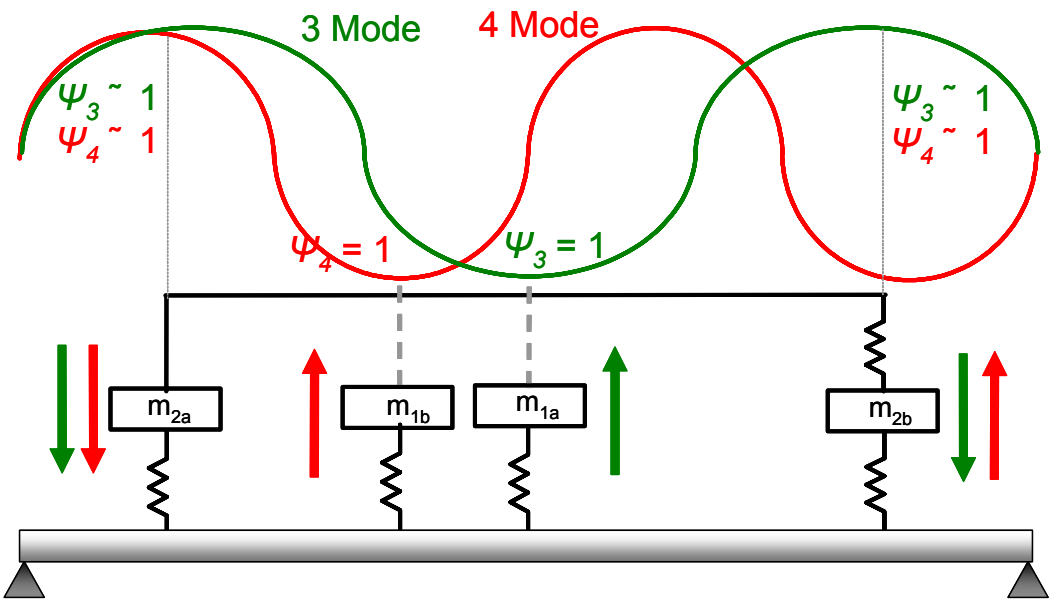

Figure 3.4 Comparison of coupling coefficients for two 1DOF DVAs and one 2DOF DVA with two reaction points on a beam. The two reaction points of the 2DOF DVA provide it with the ability to couple well into both modes.

In general, there is a design strategy that is required in order to gain an advantage from the MDOF DVAs. As mentioned, the mode shapes of the DVAs must be designed such that they mirror the primary system, or are positioned such that the locations are optimal for the given mode shapes of the DVA. This is given that the resonance frequencies of the DVA match with the primary system resonance frequencies corresponding to the targeted mode shapes. Despite this design strategy, there are limitations to using MDOF DVAs. For instance, it is possible for the detrimental effect of poor coupling to outweigh the positive effect of utilizing both DVA modes to impede a primary system. This is often the case when the targeted frequencies correspond to mode shapes that do not provide advantageous coupling coefficients. An example would be the first and second modes of a beam, as shown in Figure 3.3, where the coupling coefficient greatly deteriorates the performance. Another situation that limits the potential is when the targeted frequencies are far apart; this is discussed in section 3.2.3 . Obtaining separated MDOF DVA resonance frequencies requires large coupling stiffness values, which essentially lock the masses together, transforming the absorber masses into a larger 1DOF DVA. This restricts the separation of the targeted frequencies to a limited bandwidth. Conversely, if the targeted modes are too close together, the 1DOF DVAs essentially act on both resonance frequencies and outperform the MDOF DVAs, which are restricted by the coupling coefficient.

The opportunity of an advantage gained by using MDOF DVAs is therefore reduced as the complexity of the system increases. This will be shown in the following sections as the performance of the MDOF DVAs deteriorate as they are applied to first, a lumped mass system, then a pinned-pinned plate, and then a cylindrical shell.

3.2 MDOF DVAs Acting on a Lumped Parameter System

It has been established that the advantage of MDOF DVAs is not that they have greater impedance, but that they can be designed and positioned to mirror the mode shapes of a primary system and apply impedance at optimal positions at multiple resonance frequencies. Because of this, it is necessary to evaluate the DVA performance as the change in the energy of the primary system at specific frequencies or over a specified frequency band. For this section, the measure of *advantage* will remain the reduction of the required mass, but the overall measure of *performance* will be the squared velocity of the primary system at the targeted resonance frequencies. The primary system analyzed in this section is an 'n' degree of freedom lumped parameter system, as shown in Figure 3.5. The system will be forced from each of the masses and averaged so as not to bias the response of the system. This will be discussed further in the following sections. For an 'n' degree of freedom lumped parameter system, a scaled 'n' degree of freedom DVA will be applied to the system. Since each parameter of the DVA is simply a scaled down version of the primary system, its mode shapes and resonance frequencies are equivalent to the primary system. Using the impedance matching method discussed in chapter two, 'n' 1DOF DVAs will be applied to the same primary system to evaluate the difference between it and the MDOF DVA performance. The squared velocity of the primary system will be similar for both cases, but the absorber mass should be lower for the MDOF DVA in certain cases, indicating an advantage. The following section details the equations of motion for developing this comparison.

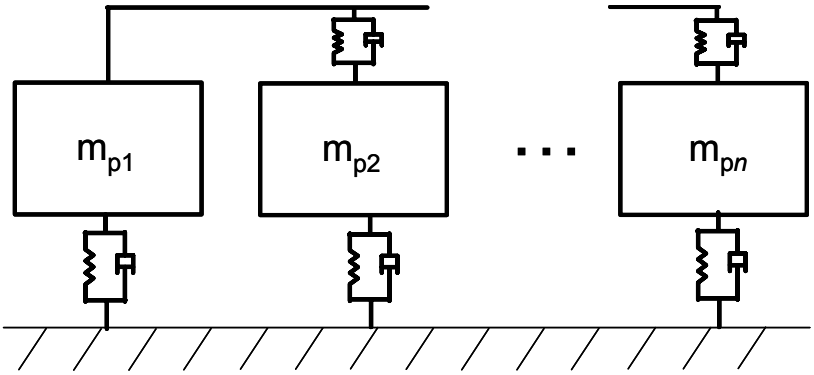

Figure 3.5 Lumped parameter system of 'n' degree of freedom as a primary system.

3.2.1 Equations of Motion for MDOF DVAs Acting on a Lumped Parameter System

The equations of motion for an 'n' degree of freedom DVA are simple to form from the equations of motions defined in chapter two. By using the modal analysis technique, the equations can be rewritten for an 'n' order DVA system. These equations will be used with a modal analysis of the primary system to develop an approximation of the energy of the system with and without the DVAs. A diagram depicting an 'n' order system is shown in Figure 3.6.

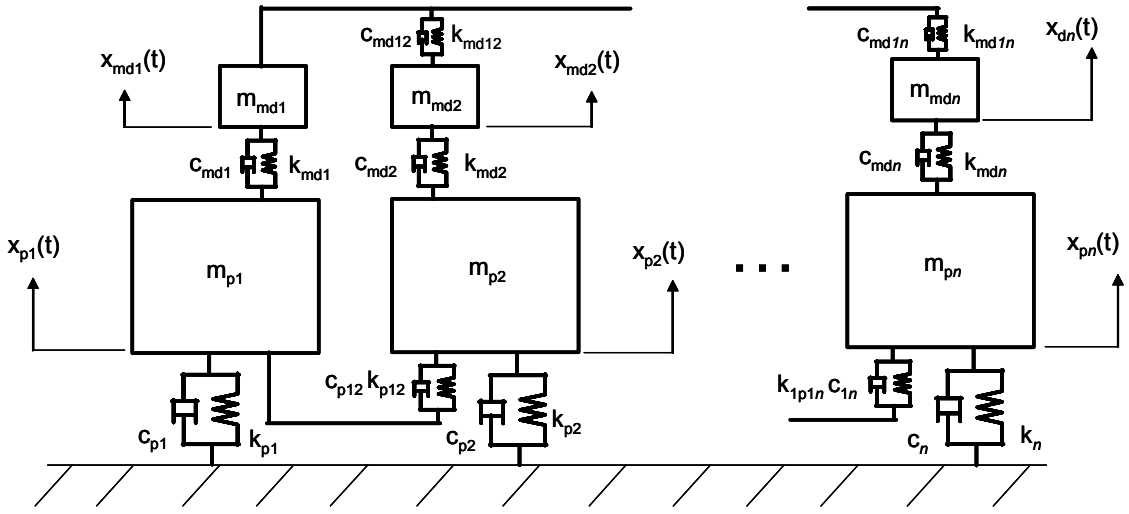

Figure 3.6 Free-body diagram of an 'n^{th}' order MDOF lumped parameter system and MDOF DVA.

The equations of motion for this system are of the form,

$$\begin{bmatrix} m_{p1} & 0 & 0 & 0 \\ 0 & m_{p2} & 0 & 0 \\ 0 & 0 & \ddots & 0 \\ 0 & 0 & 0 & m_{pn} \end{bmatrix}\begin{bmatrix} \ddot{x}_{p1} \\ \ddot{x}_{p2} \\ \vdots \\ \ddot{x}_{pn} \end{bmatrix}+\begin{bmatrix} \left(c_{p1}+c_{p12}+\ldots c_{p1n}\right) & -c_{p12} & \cdots & -c_{p1n} \\ -c_{p12} & \left(c_{p2}+c_{p12}+\ldots c_{p2n}\right) & & \vdots \\ \vdots & & \ddots & \vdots \\ -c_{pn1} & \cdots & \cdots & \left(c_{pn}+c_{p1n}+\ldots c_{p(n-1)n}\right) \end{bmatrix}\begin{bmatrix} \dot{x}_{p1} \\ \dot{x}_{p2} \\ \vdots \\ \dot{x}_{pn} \end{bmatrix}+$$
$$\begin{bmatrix} \left(k_{p1}+k_{p12}+\ldots k_{p1n}\right) & -k_{p12} & \cdots & -k_{p1n} \\ -k_{p12} & \left(k_{p2}+k_{p12}+\ldots k_{p2n}\right) & & \vdots \\ \vdots & & \ddots & \vdots \\ -k_{pn1} & \cdots & \cdots & \left(k_{pn}+k_{p1n}\ldots k_{p(n-1)n}\right) \end{bmatrix}\begin{bmatrix} x_{p1} \\ x_{p2} \\ \vdots \\ x_{pn} \end{bmatrix}=\begin{bmatrix} F_{D1} \\ F_{D2} \\ \vdots \\ F_{Dn} \end{bmatrix}+\begin{bmatrix} F_{P1} \\ F_{P2} \\ \vdots \\ F_{Pn} \end{bmatrix} \tag{3.1}$$

where F_P is the primary force on each mass (not shown in figure), and F_D is the reaction force inputted back into the system by the DVA. This system of equations can be simplified into matrix form as,

$$\mathbf{M}_S\hat{\ddot{\mathbf{x}}}+\mathbf{C}_S\hat{\dot{\mathbf{x}}}+\mathbf{K}_S\hat{\mathbf{x}}=\hat{F}_D+\hat{F}_P \tag{3.2}$$

where the subscript, *S*, denotes the properties of the primary system. By performing the same modal analysis calculations as in chapter two, the equations can be solved for in the modal domain as functions of the primary and DVA forces. The modal amplitudes, r_p, are of the form

$$\hat{r}_p=\mathbf{L}_S\mathbf{P}_S{}^{\mathrm{T}}\mathbf{M}_S{}^{-1/2}\hat{F}_D+\mathbf{L}_S\mathbf{P}_S{}^{\mathrm{T}}\mathbf{M}_S{}^{-1/2}\hat{F}_P \tag{3.3}$$

where

$$\mathbf{L}_S=\begin{bmatrix} \dfrac{1}{\left(\omega_1^2-\omega^2+i2\xi\omega_1\omega\right)} & 0 & 0 & 0 \\ 0 & \dfrac{1}{\left(\omega_2^2-\omega^2+i2\xi\omega_2\omega\right)} & 0 & 0 \\ 0 & 0 & \ddots & 0 \\ 0 & 0 & 0 & \dfrac{1}{\left(\omega_n^2-\omega^2+i2\xi\omega_n\omega\right)} \end{bmatrix} \tag{3.4}$$

and represents the complex resonance of the primary system. The DVA force F_D, however, is a function of the primary system modal amplitudes. Expanding the DVA force, the modal amplitude is written as

$$\hat{r}_p=\mathbf{L}_S\mathbf{P}_S{}^{\mathrm{T}}\mathbf{M}_S{}^{-1/2}\underbrace{\mathbf{D}\overbrace{\mathbf{M}_S{}^{-1/2}\mathbf{P}_S\hat{r}_p}^{\text{DVA displacement}}}_{\text{DVA Force, } F_D}+\mathbf{L}_S\mathbf{P}_S{}^{\mathrm{T}}\mathbf{M}_S{}^{-1/2}F_P \tag{3.5}$$

The equation can be solved for the modal amplitude, r_p, and rewritten as

$$\hat{r}_p = \left(\mathbf{I} - \mathbf{L}_S \mathbf{P}_S{}^{\mathrm{T}} \mathbf{M}_S{}^{-½} \mathbf{D} \mathbf{M}_S{}^{-½} \mathbf{P}_S\right)^{-1} \left(\mathbf{L}_S \mathbf{P}_S{}^{\mathrm{T}} \mathbf{M}_S{}^{-½} \hat{F}_P\right) \tag{3.6}$$

The dynamic stiffness matrix, D, is generated from the properties of the 'n' degree of freedom DVA system, and is of the same form as equation (2.33),

$$\mathbf{D} = \mathbf{K}_{0D}\left(\mathbf{M}_D{}^{-½} \mathbf{P}_D \mathbf{L}_D \mathbf{P}_D{}^{\mathrm{T}} \mathbf{M}_D{}^{-½} \mathbf{K}_{0D} - \mathbf{I}\right) \tag{3.7}$$

where K_{0D} is the diagonal stiffness matrix,

$$\mathbf{K}_{0D} = \begin{bmatrix} k_{md1} & 0 & 0 & 0 \\ 0 & k_{md2} & 0 & 0 \\ 0 & 0 & \ddots & 0 \\ 0 & 0 & 0 & k_{mdn} \end{bmatrix} \tag{3.8}$$

and all of the matrices are developed from the same procedure as chapter two. Each element in the dynamic stiffness matrix translates the displacement of that reaction point to a force input to the primary system. Each matrix in D, equation (3.7), is based solely on the DVA parameters and contains the complex resonance term, L, which is developed through the same procedure as chapter two. The resulting equation of motion for the primary system is

$$\hat{r}_p = \left(\mathbf{I} - \mathbf{L}_S \mathbf{P}_S{}^{\mathrm{T}} \mathbf{M}_S{}^{-½} \left\{\mathbf{K}_{0D} \mathbf{M}_D{}^{-½} \mathbf{P}_D \mathbf{L}_D \mathbf{P}_D{}^{\mathrm{T}} \mathbf{M}_D{}^{-½} \mathbf{K}_{0D} - \mathbf{K}_{0D}\right\}_{DVA} \mathbf{M}_S{}^{-½} \mathbf{P}_S\right)^{-1} \left(\mathbf{L}_S \mathbf{P}_S{}^{\mathrm{T}} \mathbf{M}_S{}^{-½} \hat{F}_P\right) \tag{3.9}$$

where the length of the modal amplitudes vector is equal to the number of degrees of freedom, and subsequently, the number of modes of the system. These modal amplitudes are multiplied by $i\omega$ to translate the term into units of velocity, then squared and summed to represent the kinetic energy of the system at each frequency.

3.2.2 Modal Force Matching for a Lumped Parameter System

The matching technique used for this chapter is similar to the method used in chapter two; except the primary system is taken into account, and there is more than one reaction point. Because of this, the new technique will match the modal force at each of the system's resonance frequencies. This technique requires the examination of equation (3.9). Simplifying this equation by ignoring the K_{0D} element, which is negligible at any of the resonance frequencies, the equation reduces to

$$\hat{r}_p = \left(\mathbf{I} - \underbrace{\mathbf{L}_S \mathbf{P}_S{}^{\mathrm{T}} \mathbf{M}_S{}^{-1/2} \mathbf{K}_{0D} \mathbf{M}_D{}^{-1/2} \mathbf{P}_D \mathbf{L}_D \mathbf{P}_D{}^{\mathrm{T}} \mathbf{M}_D{}^{-1/2} \mathbf{K}_{0D} \mathbf{M}_S{}^{-1/2} \mathbf{P}_S}_{\text{term of interest}} \right)^{-1} \left(\mathbf{L}_S \mathbf{P}_S{}^{\mathrm{T}} \mathbf{M}_S{}^{-1/2} \hat{F}_P \right) \quad (3.10)$$

where, *S*, denotes properties of the system and, *D*, denotes properties of the DVA. The first complex resonance matrix, L_S, can be ignored as it is the same for both DVA designs (i.e. the DVAs are designed to have the same natural frequencies as the structure). The terms of interest are then simplified to

$$\underbrace{\mathbf{P}_S{}^{\mathrm{T}} \mathbf{M}_S{}^{-1/2} \mathbf{K}_{0D} \mathbf{M}_D{}^{-1/2} \mathbf{P}_D}_{R} \mathbf{L}_D \underbrace{\mathbf{P}_D{}^{\mathrm{T}} \mathbf{M}_D{}^{-1/2} \mathbf{K}_{0D} \mathbf{M}_S{}^{-1/2} \mathbf{P}_S}_{R^T} \quad (3.11)$$

where the term labeled *R* on each side of the DVA complex resonance term is related by the transpose of the other. From this, if the 1DOF DVA *R* term can be equated to the MDOF DVA *R* term, then the DVA performances at resonance will be near equal. Expanded, the *R* term is written as

$$\begin{bmatrix} R_{11} & \cdots & \cdots & R_{1n} \\ \vdots & R_{22} & & \vdots \\ \vdots & & \ddots & \vdots \\ R_{n1} & \cdots & \cdots & R_{nn} \end{bmatrix} = \begin{bmatrix} v_{11} & \cdots & \cdots & v_{n1} \\ \vdots & v_{22} & & \vdots \\ \vdots & & \ddots & \vdots \\ v_{1n} & \cdots & \cdots & v_{nn} \end{bmatrix}_S \begin{bmatrix} m_{p1} & 0 & 0 & 0 \\ 0 & m_{p2} & 0 & 0 \\ 0 & 0 & \ddots & 0 \\ 0 & 0 & 0 & m_{pn} \end{bmatrix}_S^{-1/2} \cdots$$
$$\begin{bmatrix} k_{md1} & 0 & 0 & 0 \\ 0 & k_{md2} & 0 & 0 \\ 0 & 0 & \ddots & 0 \\ 0 & 0 & 0 & k_{mdn} \end{bmatrix}_D \begin{bmatrix} m_{md1} & 0 & 0 & 0 \\ 0 & m_{md2} & 0 & 0 \\ 0 & 0 & \ddots & 0 \\ 0 & 0 & 0 & m_{mdn} \end{bmatrix}^{-1/2} \begin{bmatrix} v_{11} & \cdots & \cdots & v_{1n} \\ \vdots & v_{22} & & \vdots \\ \vdots & & \ddots & \vdots \\ v_{n1} & \cdots & \cdots & v_{nn} \end{bmatrix}_D \quad (3.12)$$

Because the equations become cumbersome very quickly, consider the system to have two degrees of freedom. The *R* matrix will then look like

$$R = \begin{bmatrix} \left\{ \left(\frac{v_{11}}{\sqrt{m_{p1}}} \right)_S \left(\frac{v_{11}}{\sqrt{m_{md1}}} k_{md1} \right)_D + \left(\frac{v_{21}}{\sqrt{m_{p2}}} \right)_S \left(\frac{v_{21}}{\sqrt{m_{md2}}} k_{md2} \right)_D \right\} & \left\{ \left(\frac{v_{11}}{\sqrt{m_{p1}}} \right)_S \left(\frac{v_{12}}{\sqrt{m_{md1}}} k_{md1} \right)_D + \left(\frac{v_{21}}{\sqrt{m_{p2}}} \right)_S \left(\frac{v_{22}}{\sqrt{m_{md2}}} k_{md2} \right)_D \right\} \\ \left\{ \left(\frac{v_{12}}{\sqrt{m_{p1}}} \right)_S \left(\frac{v_{11}}{\sqrt{m_{md1}}} k_{md1} \right)_D + \left(\frac{v_{22}}{\sqrt{m_{p2}}} \right)_S \left(\frac{v_{21}}{\sqrt{m_{md2}}} k_{md2} \right)_D \right\} & \left\{ \left(\frac{v_{12}}{\sqrt{m_{p1}}} \right)_S \left(\frac{v_{12}}{\sqrt{m_{md1}}} k_{md1} \right)_D + \left(\frac{v_{22}}{\sqrt{m_{p2}}} \right)_S \left(\frac{v_{22}}{\sqrt{m_{md2}}} k_{md2} \right)_D \right\} \end{bmatrix} \quad (3.13)$$

The resulting term of interest, from equation (3.11), will look like

$$\begin{bmatrix} R_{11} & \cdots & \cdots & R_{1n} \\ \vdots & R_{22} & & \vdots \\ \vdots & & \ddots & \vdots \\ R_{n1} & \cdots & \cdots & R_{nn} \end{bmatrix} \mathrm{L} \begin{bmatrix} R_{11} & \cdots & \cdots & R_{n1} \\ \vdots & R_{22} & & \vdots \\ \vdots & & \ddots & \vdots \\ R_{1n} & \cdots & \cdots & R_{nn} \end{bmatrix} \tag{3.14}$$

The result is an *n* by *n* matrix of terms containing *n* resonances.

$$\begin{bmatrix} \left(\frac{R_{11}^2}{\omega_1^2-\omega^2+i2\zeta\omega\omega_1}+\frac{R_{12}^2}{\omega_2^2-\omega^2+i2\zeta\omega\omega_2}\right) & \left(\frac{R_{11}R_{21}}{\omega_1^2-\omega^2+i2\zeta\omega\omega_1}+\frac{R_{12}R_{22}}{\omega_2^2-\omega^2+i2\zeta\omega\omega_2}\right) \\ \left(\frac{R_{11}R_{21}}{\omega_1^2-\omega^2+i2\zeta\omega\omega_1}+\frac{R_{12}R_{22}}{\omega_2^2-\omega^2+i2\zeta\omega\omega_2}\right) & \left(\frac{R_{21}^2}{\omega_1^2-\omega^2+i2\zeta\omega\omega_1}+\frac{R_{22}^2}{\omega_2^2-\omega^2+i2\zeta\omega\omega_2}\right) \end{bmatrix} \tag{3.15}$$

This matrix can be thought of as a conversion of modal amplitude to modal forcing. To understand each term, it will help to substitute this matrix into the first term of equation (3.5), ignoring the primary forcing.

$$\begin{bmatrix} r_{p1} \\ r_{p2} \end{bmatrix}_{DVA} = \mathbf{L}_S \begin{bmatrix} \left(\frac{R_{11}^2}{\omega_1^2-\omega^2+i2\zeta\omega\omega_1}+\frac{R_{12}^2}{\omega_2^2-\omega^2+i2\zeta\omega\omega_2}\right) & \left(\frac{R_{11}R_{21}}{\omega_1^2-\omega^2+i2\zeta\omega\omega_1}+\frac{R_{12}R_{22}}{\omega_2^2-\omega^2+i2\zeta\omega\omega_2}\right) \\ \left(\frac{R_{11}R_{21}}{\omega_1^2-\omega^2+i2\zeta\omega\omega_1}+\frac{R_{12}R_{22}}{\omega_2^2-\omega^2+i2\zeta\omega\omega_2}\right) & \left(\frac{R_{21}^2}{\omega_1^2-\omega^2+i2\zeta\omega\omega_1}+\frac{R_{22}^2}{\omega_2^2-\omega^2+i2\zeta\omega\omega_2}\right) \end{bmatrix} \begin{bmatrix} r_{p1} \\ r_{p2} \end{bmatrix} \tag{3.16}$$

To obtain the modal amplitude of the first mode, the top row is matrix multiplied with the modal amplitude vectors, r_{p1} and r_{p2}. The result is the modal force generated from the first modal amplitude plus the modal force generated from the second modal amplitude. Likewise, the second modal force is the matrix multiplication of the bottom row with the modal amplitude vectors. The resulting modal forces are the source of the DVA impedance at each particular mode. The greater the modal force, the higher the impedance at that mode. It is this term that will be used to design 1DOF DVAs of equivalent performance to MDOF DVAs.

The first modal amplitude of the system can be written from equation (3.16)

$$\left[r_{p1}\right]_{DVA} = \left(\frac{1}{\left(\omega_1^2-\omega^2+i2\xi\omega_1\omega\right)}\right)_S \left\{\left(\frac{R_{11}^2}{\omega_1^2-\omega^2+i2\zeta\omega\omega_1}+\frac{R_{12}^2}{\omega_2^2-\omega^2+i2\zeta\omega\omega_2}\right)r_{p1}+\left(\frac{R_{11}R_{21}}{\omega_1^2-\omega^2+i2\zeta\omega\omega_1}+\frac{R_{12}R_{22}}{\omega_2^2-\omega^2+i2\zeta\omega\omega_2}\right)r_{p2}\right\} \tag{3.17}$$

This equation represents the first modal amplitude caused by the DVA as a function of both the first and the second modal amplitudes, r_{p1} and r_{p2}. In order to match the modal forcing, some assumptions must be made. The first assumption is that the dominant contributor to the modal amplitude $r_{p1,DVA}$ is r_{p1}. In this case, it means that the second modal amplitude r_{p2} doesn't contribute to the modal force generated by the DVAs because we are concerned with the

behavior at ω_1 and the second modal amplitude r_{p2} is away from its resonance frequency and is likely to be small.

$$\left[r_{p1}\right]_{DVA} = \left(\frac{1}{\left(\omega_1^2 - \omega^2 + i2\xi\omega_1\omega\right)}\right)_S \left\{\left(\frac{R_{11}^2}{\omega_1^2 - \omega^2 + i2\zeta\omega\omega_1} + \frac{R_{12}^2}{\omega_2^2 - \omega^2 + i2\zeta\omega\omega_2}\right) r_{p1} + \left(\frac{R_{11}R_{21}}{\omega_1^2 - \omega^2 + i2\zeta\omega\omega_1} + \frac{R_{12}R_{22}}{\omega_2^2 - \omega^2 + i2\zeta\omega\omega_2}\right) r_{p2}\right\} \quad (3.18)$$

The second assumption is that the dominant term from equation (3.18) is the term that resonates at the first natural frequency.

$$\left[r_{p1}\right]_{DVA} = \left(\frac{1}{\left(\omega_1^2 - \omega^2 + i2\xi\omega_1\omega\right)}\right)_S \left\{\left(\frac{R_{11}^2}{\omega_1^2 - \omega^2 + i2\zeta\omega\omega_1} + \frac{R_{12}^2}{\omega_2^2 - \omega^2 + i2\zeta\omega\omega_2}\right) r_{p1}\right\} \quad (3.19)$$

This simplifies the equation to

$$\left[r_{p1}\right]_{DVA} = \left(\frac{1}{\left(\omega_1^2 - \omega^2 + i2\xi\omega_1\omega\right)}\right)_S \left\{\frac{R_{11}^2}{\omega_1^2 - \omega^2 + i2\zeta\omega\omega_1} r_{p1}\right\} \quad (3.20)$$

Substituting in R_{11} from equation (3.13), the equation is

$$\left[r_{p1}\right]_{DVA} = \left(\frac{1}{\left(\omega_1^2 - \omega^2 + i2\xi\omega_1\omega\right)}\right)_S \left\{\frac{\left\{\left(\frac{v_{11}}{\sqrt{m_{p1}}}\right)_S \left(\frac{v_{11}}{\sqrt{m_{md1}}} k_{md1}\right)_D + \left(\frac{v_{21}}{\sqrt{m_{p2}}}\right)_S \left(\frac{v_{21}}{\sqrt{m_{md2}}} k_{md2}\right)_D\right\}^2}{\omega_1^2 - \omega^2 + i2\zeta\omega\omega_1}\right\} r_{p1} \quad (3.21)$$

Since the complex resonance terms are equal for both MDOF and 1DOF DVA designs, they can be ignored during the modal force matching procedure. Now, the two designs can be compared. For the 1DOF DVA design, the off-diagonal eigenvectors are zero since there is no coupling between the masses.

$$\left\{\left(\frac{v_{11}}{\sqrt{m_{p1}}}\right)_S \left(\frac{v_{11}}{\sqrt{m_{md1}}} k_{md1}\right)_D + \left(\frac{v_{21}}{\sqrt{m_{p2}}}\right)_S \left(\frac{v_{21}}{\sqrt{m_{md2}}} k_{md2}\right)_D\right\}^2_{\text{MDOF}} = \left\{\left(\frac{v_{11}}{\sqrt{m_{p1}}}\right)_S \left(\frac{v_{11}}{\sqrt{m_{sd1}}} k_{sd1}\right)_D + \left(\frac{v_{21}}{\sqrt{m_{p2}}}\right)_S \left(\frac{v_{21}}{\sqrt{m_{sd2}}} k_{sd2}\right)_D\right\}^2_{\text{1DOF}} \quad (3.22)$$

This leaves the modal force matching equation as simply the R_{11} term.

$$\left\{\left(\frac{v_{11}}{\sqrt{m_{p1}}}\right)_S \left(\frac{v_{11}}{\sqrt{m_{md1}}} k_{md1}\right)_D + \left(\frac{v_{21}}{\sqrt{m_{p2}}}\right)_S \left(\frac{v_{21}}{\sqrt{m_{md2}}} k_{md2}\right)_D\right\}^2_{\text{MDOF}} = \left\{\left(\frac{v_{11}}{\sqrt{m_{p1}}}\right)_S \left(\frac{v_{11}}{\sqrt{m_{ms1}}} k_{ms1}\right)_D\right\}^2_{\text{1DOF}} \quad (3.23)$$

This is where the benefit of the MDOF DVA is evident. Assuming a system of uniform mass and stiffness, the eigenvectors of the primary system, the MDOF DVA, and the 1DOF DVA will respectively be

$$\Lambda_S = \begin{bmatrix} 0.707 & 0.707 \\ 0.707 & -0.707 \end{bmatrix}; \qquad \Lambda_{\text{MDOF}} = \begin{bmatrix} 0.707 & 0.707 \\ 0.707 & -0.707 \end{bmatrix}; \quad \Lambda_{\text{1DOF}} = \begin{bmatrix} 1 & 0 \\ 0 & 1 \end{bmatrix} \tag{3.24}$$

Plugging these values into equation (3.23), the MDOF is twice as effective. The stiffness and masses will not be equal, and will depend on the primary system. But it can be seen through these equations that there exists potential for the MDOF DVA to have an advantage for some primary systems.

To solve for the equivalent performing 1DOF stiffness and mass, equation (3.23) is used in the same way as chapter two.

$$\left(R_{11}\right)^2_{\text{MDOF}} = \left\{ \left(\frac{v_{11}}{\sqrt{m_{p1}}} \right)_S \left(\frac{v_{11}}{\sqrt{m_{md1}}} k_{md1} \right)_D + \left(\frac{v_{21}}{\sqrt{m_{p2}}} \right)_S \left(\frac{v_{21}}{\sqrt{m_{md2}}} k_{md2} \right)_D \right\}^2_{\text{MDOF}} \tag{3.25}$$

Setting the 1DOF parameters equal to this known term, and substituting 1 in for v_{11D},

$$\left(R_{11}\right)^2_{\text{MDOF}} = \left\{ \left(\frac{v_{11}}{\sqrt{m_{p1}}} \right)^2_S \left(\sqrt{\frac{k_{sd1}}{m_{sd1}}} \sqrt{k_{sd1}} \right)^2_D \right\}_{\text{1DOF}} \tag{3.26}$$

Knowing that $\omega_1 = \sqrt{k_{sd1} / m_{sd1}}$, the equation can be solved for k_{sd1}

$$k_{sd1} = \frac{\left(\left(R_{11}\right)^2_{\text{MDOF}} \right) \left(m_{p1} \right)}{\left(v_{11} \right)^2_S \left(\omega_1^{\,2} \right)} \tag{3.27}$$

And knowing the 1DOF stiffness, the 1DOF mass can then be found through the natural frequency relationship

$$m_{sd1} = \frac{k_{sd1}}{\omega_1^2} \tag{3.28}$$

This procedure is carried out for each degree of freedom for the system.

3.2.3 Performance: Mass Ratio as a function of Frequency Separation

As previously stated, the measure of advantage of a MDOF DVA over a system of 1DOF DVAs will be the total absorber mass used by the DVA. For a given performance, measured by the attenuation of energy over a targeted frequency band, there will be a factor, *MR*, which is the measure of total mass difference between the 1DOF DVAs and the MDOF DVA.

$$\mathrm{MR} = \left(\frac{m_{1\mathrm{DOF}} - m_{\mathrm{MDOF}}}{m_{1\mathrm{DOF}}} \right)\% \tag{3.29}$$

This factor is defined such that, for a 1DOF system of DVAs that requires twice the mass of a MDOF design, the *MR* will be equal to 50% signifying half of the mass can be saved. If the 1DOF design was initially six grams, for instance, and the MDOF design uses three grams, there is a savings of three grams, or 50% of the conventional design. For a comparison of DVA designs that results in no advantage, where the MDOF total mass equals that of the 1DOF system, the *MR* is equal to zero. If the MDOF absorber requires more mass than the SDOF, the *MR* will be a negative value, indicating there is no advantage. The *MR* will always have a value less than one.

Several factors affect the *MR* for absorbers applied to a lumped parameter system. But, the most important factor is the frequency band separation between the targeted modes of the system. This frequency separation reduces the *MR* greatly when the modes are very close together and very far apart. For an optimal primary system, however, where the resonance frequencies are well spaced, the advantage of using a MDOF DVA can be significant. The variable, σ, will be used as a measure of frequency band separation that accounts for the increasing density of resonances for increasing frequencies. The frequency separation factor is defined as

$$\sigma = \frac{f_b - f_a}{f_{mean}} \tag{3.30}$$

where the variables are indicated in Figure 3.7. The system in Figure 3.7 would have a frequency separation value equal to 0.29. For high and low σ values, the *MR* approaches zero. But for a limited bandwidth of σ, there is a distinct advantage in using MDOF DVAs over SDOF DVAs. This will now be demonstrated with a few examples.

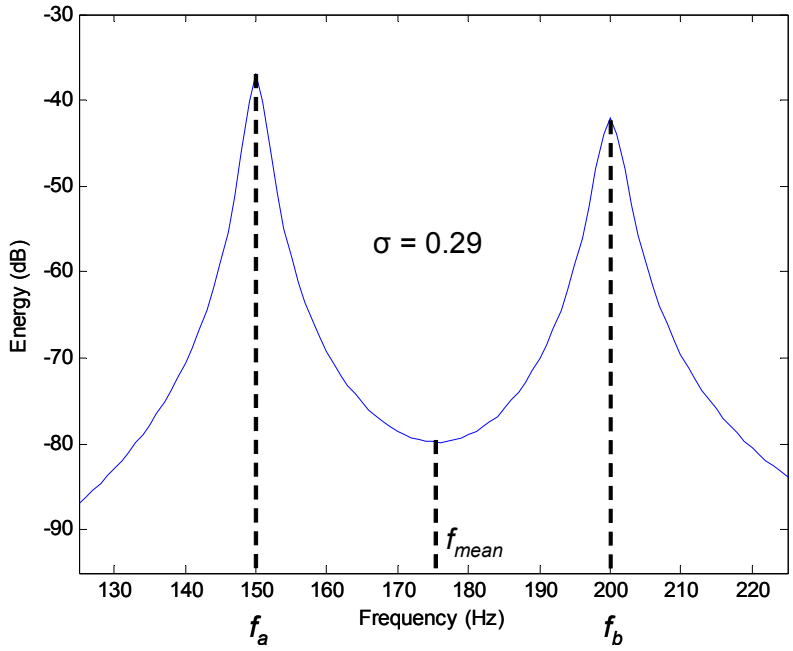

Figure 3.7 Example of frequency separation for a 2DOF system. The frequency separation, σ, has a significant influence on the performance of MDOF DVAs.

Consider the 2DOF primary system,and a 2DOF DVA or two 1DOF DVAs for passive attenuation, shown in Figure 3.2. In order to minimize the variable parameters in an attempt to simplify the system, both masses and non-coupling spring stiffness values are kept uniform. The primary masses are each 100g and both have 100 kN spring stiffness. The MDOF DVA masses are designed to each have masses of one percent of the primary system, 1 gram each. The 1DOF DVA mass and spring are designed, as mentioned in section 3.2.2 , to provide attenuation near equal that of the MDOF DVA. In order to account for a bias in the forcing location, the response is taken as the average response of unit forcing on both masses. This system, with a coupling stiffness of 21 kN, has a frequency separation value, sigma, of 0.17.

Referring to Figure 3.8, it can be seen that the attenuation of the 2DOF system is nearly equal over the targeted frequency bands for both the 1DOF DVA system and the 2DOF DVA. The total energy attenuation over the frequency bands 150 to 170 Hz and 180 to 200 Hz, is 11.6dB for the two 1DOF DVAs, and 11.2 dB for the MDOF DVA. The 1DOF masses are 2 and 1 grams, whereas the MDOF DVA masses are 1 gram each, resulting in 33% of the total mass saved. Incorporating the tuning and damping laws discussed in chapter two, both treatments use 6% damping and are tuned using equation (2.8). This system is ideal for a MDOF DVA treatment because the assumptions made in the simplification of equations (3.18) and (3.19) are

proven valid. These equations assume that the motion at a resonance frequency is dominated by the term that resonates at that frequency. When the resonance frequencies are not well separated, this assumption in inaccurate. The 2DOF resonances are far enough apart, in this case, not to impact each other, yet not so far that the coupling stiffness hinders their advantage. As the primary system resonances shift closer or farther to each other, the advantage of using a MDOF DVA will decay.

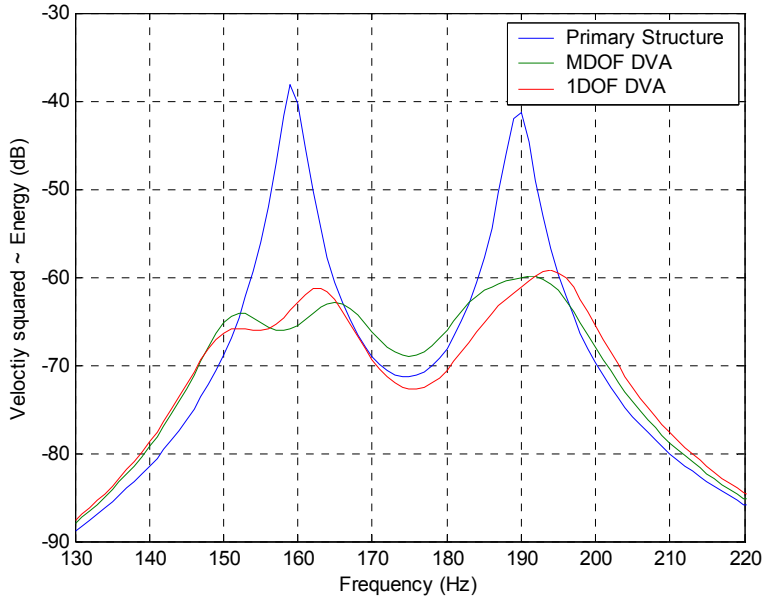

Figure 3.8 Energy of a 2DOF system, with a sigma value of 0.17, shown with 2DOF and 1DOF DVAs treatments applied. With equal performance, 33% of the mass can be saved by using an MDOF DVA.

If the primary system modes are brought closer together, the advantage decreases rapidly. For the case shown in Figure 3.9 where the sigma value is 0.05, the *MR* is 2.2%. The MDOF DVAs perform equally in this case is because the 1DOF DVAs are effective at both resonances. Because the resonant frequencies are so close together, both 1DOF DVAs are effective at each resonance, and thus utilize all of their available mass at both resonance frequencies. Conversely, the MDOF masses are unable to act in an advantageous way. The advantage of the 2DOF DVA is generated by utilizing both DVA masses at both resonance frequencies of the system. But because both modes are so close together, the rigid body motion of first mode of the system is at the same frequency as the second mode where the masses are at a phase of 180^{o}. Because both modes are counteracting each other at the same frequency, the advantage that could be generated by the use of the MDOF DVA is nullified.

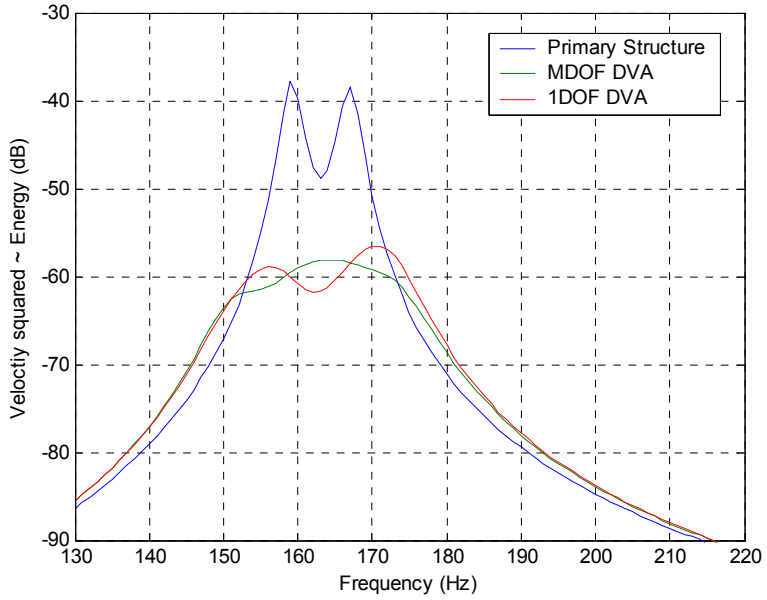

Figure 3.9 Energy of a 2DOF lumped parameter system, having a sigma value of 0.05 (k_{12}=5kN), shown with 2DOF and 1DOF DVA treatments applied. The comparison results in an MR of 2.2%.

It is also important to note that the matching technique starts to break down when the targeted modes get close together. This is because the matching technique accounts for each mass as an absorber for only one mode. When the targeted modes start to get close together, the matching technique must be facilitated with a compensator, which simply reduces the 1DOF absorber masses by increments of one percent until the integration of the kinetic energy over the targeted frequency band is to within a specified tolerance.

For a primary system with a large coupling stiffness, and subsequently resonance frequencies that are well separated, MDOF DVAs are unable to generate an advantage over 1DOF systems. In this case, the resonance frequencies of the primary system are too far apart for the MDOF DVA to be effective. When the frequency separation is high, the MDOF DVA coupling stiffness (i.e. the stiffness between the DVA masses) must be increased to attain the frequency separation needed to match the primary system. This increases the stiffness between the masses, and essentially locks the masses together. For the first rigid body resonance, the locked masses both act to attenuate the motion. But for the second, out of phase, resonance there is very little attenuation because the dynamic forces are transferred between the DVA masses and not between the DVA and primary structure. So, in order to match this small attenuation of

the second mode, the 1DOF DVA is only required to use a small mass, which makes the total 1DOF DVA mass small as well.

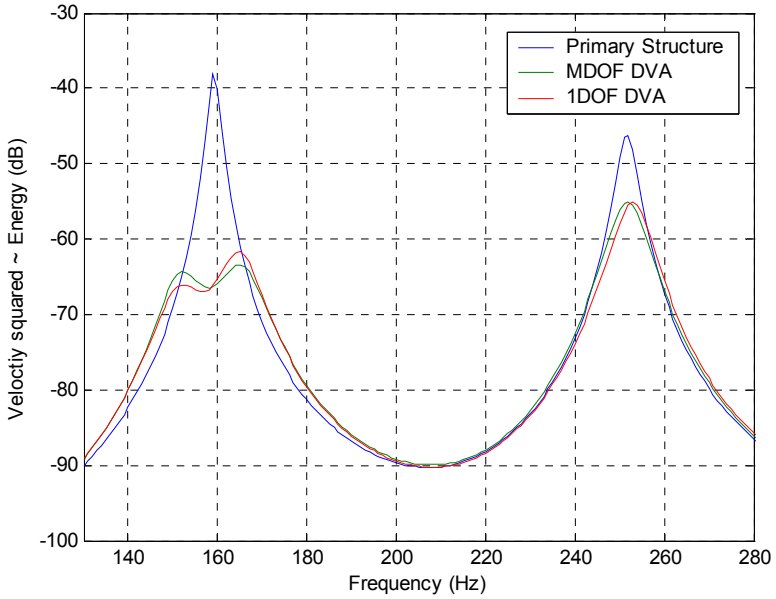

Figure 3.10 Energy of a 2DOF lumped parameter system with a sigma of 0.45(k_{12}=75kN), shown with 2DOF and 1DOF DVA treatment. The MR is 12.9%.

The three cases that have been examined have demonstrated how the frequency separation affects the *MR* comparison of the two DVA designs. Figure 3.11shows a plot of *MR* versus σ. The figure shows that there is a sharp increase in advantage as the resonance frequencies of the primary system are first separated. This happens until the optimal system is achieved at a sigma value of 0.17, where the advantage starts to decrease.

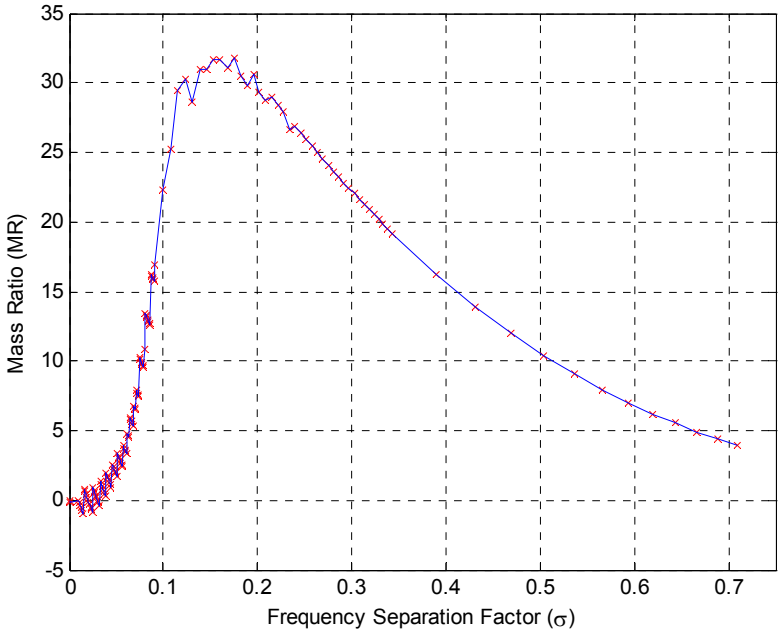

Figure 3.11 Mass ratio versus frequency separation value for a 2DOF lumped mass primary system for a comparison of a 2DOF and two 1DOF DVAs applied.

3.3 MDOF DVAs Acting on a Plate

This section will address the application of MDOF DVAs on a pinned-pinned plate. The primary difference in the application will be the addition of a new variable, the location of the DVA reaction point on the plate. Since the DVA mode shapes no longer match the primary system mode shapes exactly, the optimal position providing the greatest attenuation over the targeted frequency band needs to be found. In order to find the optimal DVA positions, a genetic algorithm finds the optimal coupling coefficient for 'n' degree of freedom DVAs. This coupling will only hurt the performance of the MDOF DVAs in comparison to 1DOF DVAs, because 1DOF DVAs can always be positioned optimally as long as the mode shape characteristics of the primary system are known. The following sections will discuss the design strategies used to optimize the positioning of the DVAs, the performance and advantage gained by using MDOF DVAs on the plate, and conclude with specific cases.

3.3.1 Equations of Motion for MDOF DVAs Acting on a Plate

This section will examine the effectiveness of MDOF DVAs on a pinned-pinned plate, as shown in Figure 3.12. A plate is a good system to evaluate the potential of MDOF DVAs

because there is a high density of low frequency modes to couple with. The response of the plate is taken as an average of multiple random unit forces in the frequency domain. The average response is taken for the same reasons as the lumped mass case. Even though the primary force is random, it is still biased to one particular primary forcing location. The goal of this analysis is to measure the advantage of MDOF DVAs to SDOF DVAs in a general sense. By spatially averaging random primary forces, the system eventually converges to a non-specific case.

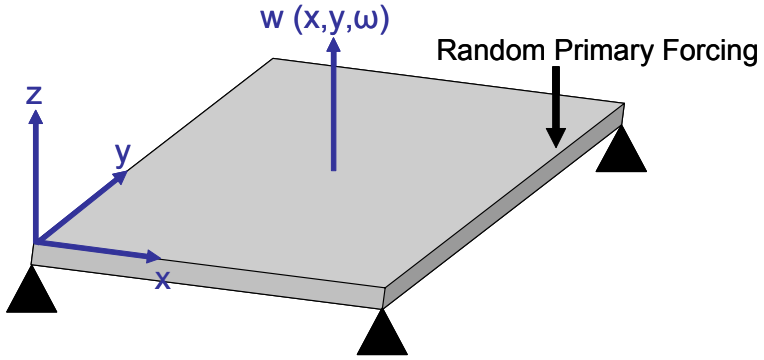

Figure 3.12 Pinned-pinned plate shown with primary force applied at a random position.

The vibration response of a plate is described by the variable, *w*, and it measures the displacement in the *z* direction as a function of *x* and *y* positions on the plate, and frequency, ω. The displacement of the plate, *w*, is the sum of the product of mode shapes, Ψ, and the modal amplitudes, *a*, at each frequency.

$$w = \sum_{i=1}^{N} \Psi_i(x,y) a_i(\omega) \tag{3.31}$$

where the i^{th} mode shape is,

$$\psi_i = \sin\left(n\pi\frac{x}{l_x}\right)\sin\left(m\pi\frac{y}{l_y}\right) \tag{3.32}$$

where *n* and *m* are the mode orders for the i^{th} mode. The modal amplitude

$$a_i = \left(\frac{4}{m_p\left(\omega_i^2 - \omega^2 + i2\xi\omega_i\omega\right)}\right)\psi_i f^{\mathrm{P}} \tag{3.33}$$

where m_p is the plate mass, and f^P is the magnitude of the primary force. The measure of performance will be the kinetic energy of the plate defined as,

$$E_k = \frac{1}{2} m_p \sum_{i=1}^{N} \left[\frac{\partial w(x,y,\omega)}{\partial t} \right]^2 \tag{3.34}$$

For a comparison of DVA treatments, the significant component of this equation is the modal amplitude. The modal amplitude describes the response due to the primary and DVA forces applied to the plate. The modal amplitude of the plate with DVA treatment is,

$$a_i = \left[\frac{4}{m_p \left(\omega_i^2 - \omega^2 + i2\xi\omega_i\omega \right)} \right] \left[\underbrace{\boldsymbol{\psi}_i^{\mathbf{D}}}_{1 \text{ x } n_d} \underbrace{\mathbf{f}^{\mathbf{D}}}_{n_d \text{x } 1} + \psi_i^{\mathbf{P}} f^{\mathbf{P}} \right] \tag{3.35}$$

where the modal amplitude is a function of the coupled DVA force, f^D, and the coupled primary force, f^P. The force generated by the DVA is a function of the displacement of the plate, which can also be written in terms of modal displacement.

$$a_i = \left[\frac{4}{m_p \left(\omega_i^2 - \omega^2 + i2\xi\omega_i\omega \right)} \right] \left[\underbrace{\boldsymbol{\psi}_i^{\mathbf{D}}}_{1 \text{ x } n_d} \overbrace{\left(\underbrace{\mathbf{D}}_{n_d \text{ x } n_d} \underbrace{\Psi^{\mathbf{D}}}_{n_d \text{ x } N} \underbrace{\mathbf{a}_i}_{N \text{ x } 1} \right)}^{\mathbf{f^D}} + \psi_i^{\mathbf{P}} f^{\mathbf{P}} \right] \tag{3.36}$$

where D is the same dynamic stiffness matrix as equation (3.7), and is defined the same way. It is a square matrix, of size n_d by n_d, where n_d is equal to the number of degrees of freedom of the DVA. The modal amplitude vector is as a function of the primary force vector and the DVA force vector, which is a function of the modal amplitude.

$$\underbrace{[\mathbf{a}]}_{(N \text{ x } 1)} = \underbrace{[\mathbf{L}_S]}_{\substack{(N \text{ x } N) \text{ diagonal} \\ \text{complex resonance}}} \left\{ \underbrace{\left[\left(\Psi_{\mathbf{N}}^{\mathbf{D}} \right)^T \right]}_{(N \text{ x } n_d)} \underbrace{[\mathbf{D}]}_{(n_d \text{ x } n_d)} \underbrace{\left[\Psi_{\mathbf{N}}^{\mathbf{D}} \right]}_{(n_d \text{ x } N)} \underbrace{[\mathbf{a}]}_{(N \text{ x } 1)} + \underbrace{[\boldsymbol{\psi}^{\mathbf{P}}]}_{(N \text{ x } 1)} f^{\mathbf{P}} \right\} \tag{3.37}$$

Solving for the modal amplitude, the resulting term is

$$[\mathbf{a}] = \left\{ [\mathbf{I}] - [\mathbf{L}_S] \left[\left(\Psi_{\mathbf{N}}^{\mathbf{D}} \right)^T \right] [\mathbf{D}] \left[\Psi_{\mathbf{N}}^{\mathbf{D}} \right] \right\}^{-1} \left\{ [\mathbf{L}_S] [\boldsymbol{\psi}^{\mathbf{P}}] f^{\mathbf{P}} \right\} \tag{3.38}$$

3.3.2 Coupled Modal Force Matching for a Plate

To match the performance of a MDOF DVA with multiple SDOF DVAs, the same technique used in section 3.2.2 is employed. Referring to that section, equation (3.10) can be equated to the plate modal amplitude of equation (3.37) by simply substituting the lumped parameter mode shape *P*, with the plate mode shape, Ψ. And since every term is equivalent for the MDOF and SDOF case except for the *D* matrix and the coupling coefficients at the DVA positions, $\Psi_{D,}$ the resulting terms of interest become simply that,

$$\Psi_D \mathbf{D} \Psi_D \Rightarrow \Psi_D \mathbf{K}_{0D} \mathbf{M}_D^{-1/2} \mathbf{P}_D \mathbf{L}_D \mathbf{P}_D^{\mathrm{T}} \mathbf{M}_D^{-1/2} \mathbf{K}_{0D} \Psi_D \tag{3.39}$$

Expanded, the terms of interest look very similar to those of the lumped parameter system, except they require the inclusion of the plate mode shapes at the DVA position, Ψ_D.

$$\underbrace{\Psi_D \mathbf{K}_{0D} \mathbf{M}_D^{-1/2} \mathbf{P}_D}_{R} \mathbf{L}_D \underbrace{\mathbf{P}_D^{\mathrm{T}} \mathbf{M}_D^{-1/2} \mathbf{K}_{0D} \Psi_D}_{R^T} \tag{3.40}$$

This *R* term is the equivalent to the lumped parameter *R* value defined by equation (3.12) except for the mass term, which is factored out. The resulting *R* term is

$$\begin{bmatrix} R_{11} & \cdots & \cdots & R_{1n} \\ \vdots & R_{22} & & \vdots \\ \vdots & & \ddots & \vdots \\ R_{n1} & \cdots & \cdots & R_{nn} \end{bmatrix} = \begin{bmatrix} \Psi_{11} & \cdots & \cdots & \Psi_{n1} \\ \vdots & \Psi_{22} & & \vdots \\ \vdots & & \ddots & \vdots \\ \Psi_{1n} & \cdots & \cdots & \Psi_{nn} \end{bmatrix}_D \begin{bmatrix} k_{md1} & 0 & 0 & 0 \\ 0 & k_{md2} & 0 & 0 \\ 0 & 0 & \ddots & 0 \\ 0 & 0 & 0 & k_{mdn} \end{bmatrix}_D \cdots \begin{bmatrix} m_{md1} & 0 & 0 & 0 \\ 0 & m_{md2} & 0 & 0 \\ 0 & 0 & \ddots & 0 \\ 0 & 0 & 0 & m_{mdn} \end{bmatrix}^{-1/2} \begin{bmatrix} P_{11} & \cdots & \cdots & P_{1n} \\ \vdots & P_{22} & & \vdots \\ \vdots & & \ddots & \vdots \\ P_{n1} & \cdots & \cdots & P_{nn} \end{bmatrix}_D \tag{3.41}$$

which, when expanded, looks like

$$R = \begin{bmatrix} \left\{ \left(\frac{\Psi_{11} v_{11} k_{md1}}{\sqrt{m_{md1}}} \right) + \left(\frac{\Psi_{12} v_{21}}{\sqrt{m_{md2}}} k_{md2} \right) \right\} & \left\{ \left(\frac{\Psi_{11} v_{12} k_{md1}}{\sqrt{m_{md1}}} \right) + \left(\frac{\Psi_{12} v_{22}}{\sqrt{m_{md2}}} k_{md2} \right) \right\} \\ \left\{ \left(\frac{\Psi_{21} v_{11} k_{md1}}{\sqrt{m_{md1}}} \right) + \left(\frac{\Psi_{22} v_{21}}{\sqrt{m_{md2}}} k_{md2} \right) \right\} & \left\{ \left(\frac{\Psi_{21} v_{11} k_{md1}}{\sqrt{m_{md1}}} \right) + \left(\frac{\Psi_{22} v_{22}}{\sqrt{m_{md2}}} k_{md2} \right) \right\} \end{bmatrix} \tag{3.42}$$

With the same methodology as section 3.2.2 , a series of SDOF DVAs can be designed from the dominant *R* terms of the MDOF DVA. The dominant terms are the on-diagonal terms

for each mode. For instance, the dominant term for the first mode is *R(1,1)*; the second mode, *R(2,2)*, etc. These terms are dominant because they represent the magnitude of the modal forces that are applied to that mode, from the motion of that mode. This makes sense because the system is essentially a feedback loop where the DVA force comes from the motion of the primary system. The *R(1,2)* term is the modal force put into mode one, from mode two. The *R(2,1)* term is the modal force put into mode two from the motion of mode one. These terms do not significantly affect the vibration because the first and second modes do not facilitate each other's movement. The dominant terms are the diagonal *R* terms because the DVA force input corresponds exactly with the movement. This assumption simplifies the equations to

$$\left\{\left(\frac{\Psi_{11}v_{11}k_{md1}}{\sqrt{m_{md1}}}\right)+\left(\frac{\Psi_{12}v_{21}}{\sqrt{m_{md2}}}k_{md2}\right)\right\}^2_{\text{MDOF}}=\left\{\frac{\Psi_{11}v_{11}k_{sd1}}{\sqrt{m_{sd1}}}\right\}^2_{\text{SDOF}} \tag{3.43}$$

Since the SDOF DVA can be positioned anywhere on the plate, the SDOF coupling coefficient and the DVA mode shape v_{11} are unity. This reduces the equation to

$$\{R_{11}\}^2_{\text{MDOF}}=\left\{\sqrt{k_{md1}}\sqrt{\frac{k_{md1}}{m_{sd1}}}\right\}^2_{\text{SDOF}} \tag{3.44}$$

And because the resonance frequency of the DVA is known to be $\omega_1=\sqrt{k_{sd1}/m_{sd1}}$, the equation simplifies to

$$\{R_{11}\}^2_{\text{MDOF}}=\left\{\sqrt{k_{sd1}}\omega_1\right\}^2_{\text{SDOF}} \tag{3.45}$$

Now the stiffness for the SDOF DVA corresponding to the first DVA resonance can be solved for.

$$k_{md1}=\frac{\{R_{11}\}^2_{\text{MDOF}}}{\omega_1^2} \tag{3.46}$$

From this, the SDOF absorber mass can be found,

$$m_{sd1}=\frac{k_{sd1}}{\omega_1^2} \tag{3.47}$$

This procedure is repeated for the number of degrees of freedom of the MDOF DVA.

3.3.3 Design: Generating a Stiffness Matrix for MDOF DVAs Acting on a Plate

The preceding section designs a SDOF DVA for each mass of the MDOF DVA. This assumes the MDOF DVA is designed most appropriately to attenuate the plate vibration in the targeted frequency band. But in order to accomplish this optimal MDOF design, two factors must be considered, the DVA parameters and the DVA positioning. The three DVA parameters that affect performance are the absorber mass, the stiffness, and the damping. As the damping is relatively easy to control without significantly affecting the DVA characteristics, it is held at 6% for both MDOF and SDOF designs. Since the DVA mass is an adjustable parameter that greatly affects performance, each MDOF DVA mass is held at a 0.1% of the plate mass. By keeping the absorber masses small, the plate's resonance characteristics remain relatively constant with the addition of absorber masses.

The remaining design parameter is the DVA stiffness values. The requirements of the stiffness values are first that they have to result in DVA resonance frequencies that correspond to the plate frequencies that are to be attenuated. And second, they must have mode shapes that are not representative of SDOF DVAs; they must have significant coupling stiffness values. Both of these criteria can be met by using a search algorithm in MATLAB called 'fgoalattain'. By inputting the desired natural frequency and mode shapes, the command will output a stiffness matrix that closely correspond to the criteria. The natural frequencies are known because they are the resonance frequencies in the targeted frequency band. However, the optimal mode shapes are not always known.

It is known that the SDOF DVA case is a subset of the many possible mode shapes a DVA can have. Likewise, if a DVA is designed with symmetric mass and stiffness properties, the resulting mode shapes are symmetric. For example, the following mode shapes are the result of DVA designs that have equal masses and equal non-coupling stiffness values.

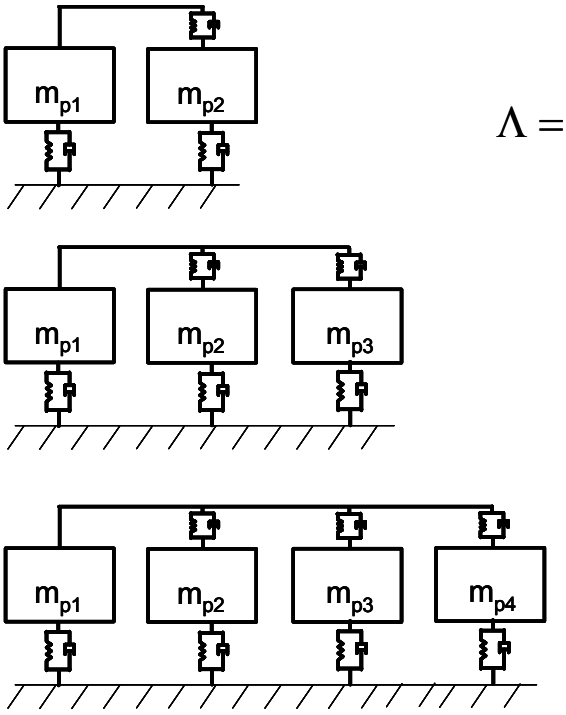

$$\Lambda = \begin{array}{c} \begin{matrix} \text{Mode 1} & \text{Mode 2} \end{matrix} \\ \begin{bmatrix} 0.707 & 0.707 \\ 0.707 & -0.707 \end{bmatrix} \end{array} \begin{matrix} \\ \text{Mass 1} \\ \text{Mass 2} \end{matrix}$$

$$\Lambda = \begin{bmatrix} 0.577 & 0.408 & 0.707 \\ 0.577 & -0.816 & 0 \\ 0.577 & 0.408 & -0.707 \end{bmatrix}$$

$$\Lambda = \begin{bmatrix} 0.5 & 0.653 & 0.5 & 0.271 \\ 0.5 & 0.271 & -0.5 & -0.653 \\ 0.5 & -0.271 & -0.5 & 0.653 \\ 0.5 & -0.653 & 0.5 & -0.271 \end{bmatrix}$$

Figure 3.13 Free body diagrams and symmetric mode shapes of two, three, and four degree of freedom systems.

These mode shapes exhibit a distributive characteristic, and while they do not correspond exactly to any specific structure or boundary condition, there is clearly no dominance of one mass in any mode. These symmetric mode shapes can be considered a subset of the infinite set of possible DVA mode shapes.

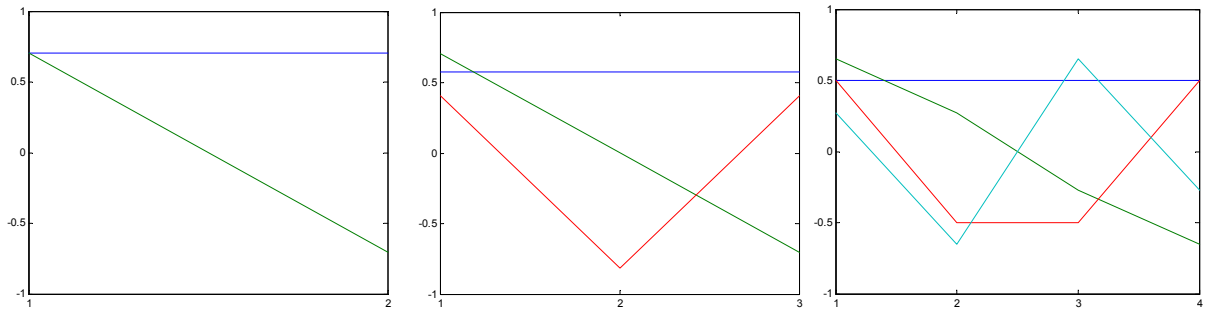

Figure 3.14 Symmetric mode shapes of two, three, and four DOF DVAs.

It is contended that the symmetric mode shapes represent the extreme opposite of the diagonally dominant SDOF mode shapes. For instance, the normalized 2DOF system modes shapes can range from the symmetric form to the 1DOF form,

$$\Lambda_{MDOF} = \begin{bmatrix} 0.707 & 0.707 \\ 0.707 & -0.707 \end{bmatrix}; \quad \Lambda_{1DOF} = \begin{bmatrix} 1 & 0 \\ 0 & 1 \end{bmatrix} \tag{3.48}$$

By plotting these mode shapes and their 180° alternative forms in Figure 3.15, it can be seen that the angle of separation between the 2DOF and 1DOF is at its extreme, 45°. This is also true for the opposite forms of the mode shapes, which are simply 180° phase shifts. The implication here is that the symmetrical mode shapes are as un-1DOF as possible, and suited well for MDOF DVAs that aim to utilize each of their masses at each resonance. Therefore, for this research, the symmetric mode shape form is specified as the desired mode shapes in the 'fgoalattain' algorithm that provides a matrix of stiffness values for the MDOF DVAs.

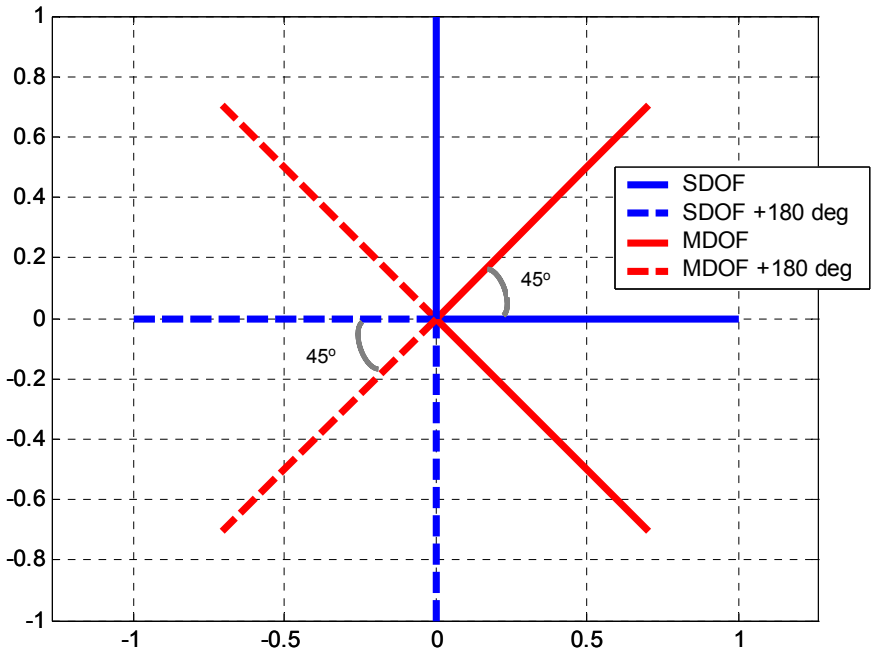

Figure 3.15 Mode shapes of symmetrical 2DOF and 1DOF DVAs.

3.3.4 Design: Finding the Optimal Position for a MDOF DVA on a Plate

The other factor to consider in designing an optimal MDOF DVA is the positioning of the DVA reaction points on the plate. For the lumped mass system, this was not a concern because the DVA mode shapes matched the system perfectly, and therefore needed no optimization. For a MDOF DVA on a plate, though, there is a great stake in the positioning of the DVA. The process is sometimes intuitive, but as the number of degrees of freedom increases, so does the complexity of optimal positioning. For this reason, a genetic algorithm

written in MATLAB, is used to search for the optimal position on the plate.[28] The cost function is derived directly from the equations of motion described in section 3.3.2 . The genetic algorithm uses the trial positions to find the coupling coefficient for that position, and from that, the *R* matrix can be calculated for the targeted modes.

$$R = \Psi_D \mathbf{K}_{0D} \mathbf{M}_D^{-1/2} \mathbf{P}_D \tag{3.49}$$

Under the same assumptions made throughout the modal force matching process, the cost function only uses the diagonal terms in the *R* matrix. This reasoning is discussed in greater detail in section 3.2.2 . These diagonal terms are squared, summed, and used as the cost function for the genetic algorithm.

$$\text{cost function} = \sum \text{diag}(\mathbf{R}^2) \tag{3.50}$$

This particular genetic algorithm was, "tested on a series of non-linear, multi-modal, non-convex test problems," and was found to be, "superior to both a binary genetic algorithm and simulated annealing in terms of efficiency and quality of solution."[28] The converged solution consistently leads to the optimal DVA positions on the plate, which is necessary for MDOF DVAs to achieve an advantage over SDOF DVAs. The significance of this positioning will be discussed in the following sections.

3.3.5 Performance: Mass Ratio as a Function of Targeted Modes, Positioning, and Degrees of Freedom

The mass ratio advantage, *MR*, of MDOF DVAs over SDOF DVAs is a function of three major variables. The frequency separation, σ, has been shown to influence the *MR*. The second factor, positioning, is affected by the targeted mode shapes. High spatial coupling coefficients are crucial to achieving an *MR* advantage. For instance, if a (1,1) mode and a (2,1) mode were being targeted, there is an optimal position that can be found on the plate to maximize the performance of the MDOF DVA. But the overall performance is limited greatly by the fact that the targeted modes are not conducive to the use of an MDOF DVA (i.e. the optimal position for the (1,1) mode is a node of the (2,1) mode). The third factor is the number of degrees of freedom of the DVA. The complexity of the system increases with the number of degrees of freedom. This means the chances of finding a situation in which the MDOF DVA will be advantageous is significantly reduced as the number of DOF is increased.

In this section, an optimal situation will be examined, where the MDOF DVA has a distinct advantage over the SDOF DVA. The primary system is a 48"x 50"x ¼" pinned-pinned steel plate, with a damping ratio of 0.005. A 2DOF DVA is designed to target the (5,1) and the (2,5) modes of the plate, which respectively correspond to 266 and 277 Hz. The absorber masses are 100 grams each, about 0.1% mass of the 77 kilogram plate. The stiffness matrix is developed through the 'fgoalattain' MATLAB function with the goal of producing symmetric mode shapes, and then run through the genetic algorithm to find the optimal reaction point locations on the plate. For this case, the DVAs are able to match the mode shapes of the plate very well by counteracting the plate motion at the chosen positions with the motion of the DVA modes shapes. Figure 3.16 shows the DVA positioned at the genetic algorithm solution. The (x,y) locations are

$$\begin{aligned} \underline{\text{2DOF}} \quad & mass_1 = (0.500, 0.707) \\ & mass_2 = (0.693, 0.709) \end{aligned} \tag{3.51}$$

As a result of the good coupling, the plate's in-phase motion at those positions, at the (5,1) resonance frequency of 266 Hz, corresponds exactly with the DVA motion at its first mode. Likewise, the motion of the plate at the DVA positions are matched at the (2,5) resonance frequency of 277 Hz by the second mode of the DVA. Also shown in Figure 3.16 is the positioning for the SDOF DVAs,

$$\begin{aligned} \underline{\text{SDOF}} \quad & mass_1 = (0.50, 0.10) \\ & mass_2 = (0.90, 0.25) \end{aligned} \tag{3.52}$$

which result in unity coupling coefficients for their intended target resonance frequencies. As mentioned, the SDOF DVAs are able to attenuate modes that are close to their tuned frequency, even if it is not the intended target. Its effectiveness in this capacity is proportional to the frequency separation and its coupling coefficient for the targeted mode shape. In this case, the SDOF DVAs are only effective at their initially targeted modes; so the 2DOF DVA gains a mass advantage.

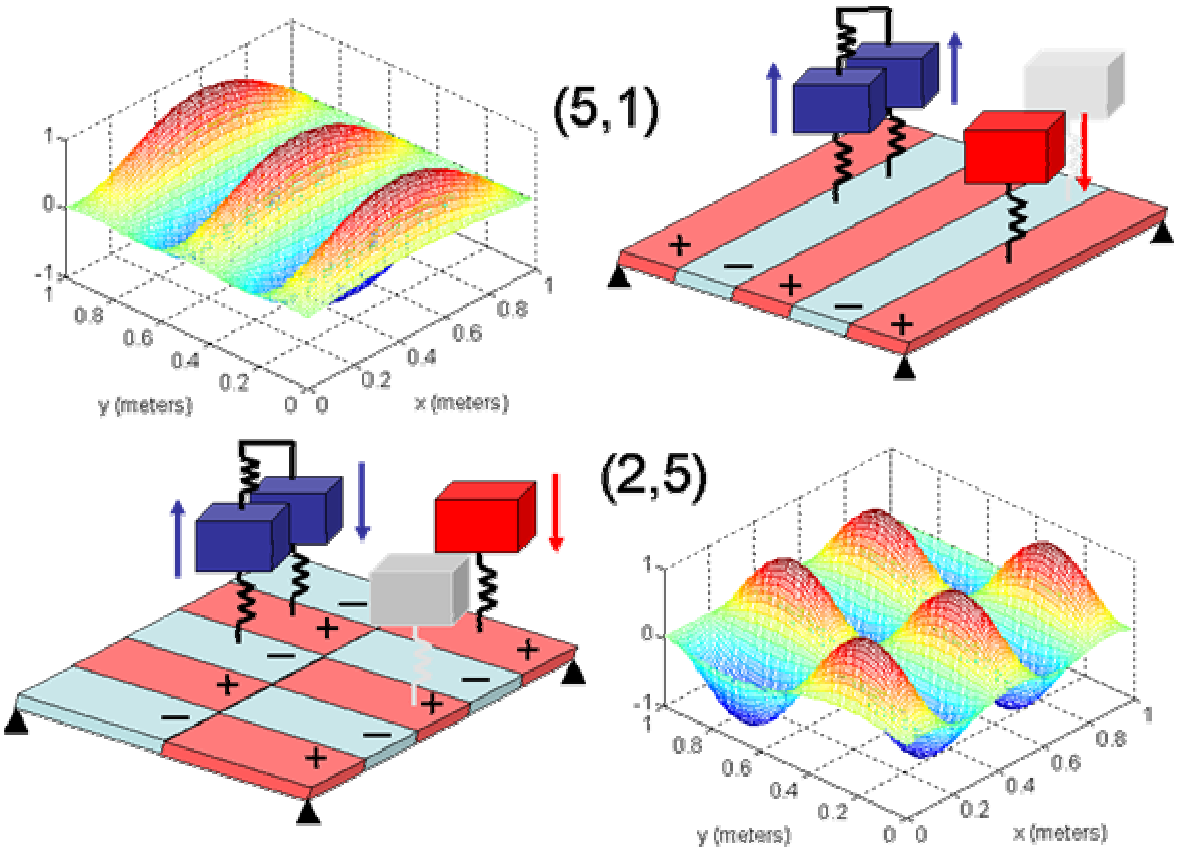

Figure 3.16 2DOF and SDOF DVA positioning for (5,1) and (2,5) plate modes. The 2DOF DVAs utilize both masses at each resonance, while the SDOF DVAs can not be positioned to couple well into both modes.

Targeting this pair of modes is effective because of the large 2DOF DVA coupling coefficients. The 2DOF DVA is positioned such that the coupling coefficients, Ψ_D, all have the same sign as the 2DOF DVA mode shapes, Λ_{2DOF}.

$$\Psi_D = \begin{bmatrix} 0.994 & 0.964 \\ 0.815 & -0.960 \end{bmatrix} \tag{3.53}$$

$$\Lambda_{2DOF} = \begin{bmatrix} 0.707 & 0.707 \\ 0.707 & -0.707 \end{bmatrix} \tag{3.54}$$

Shown in Figure 3.17, the treated response is nearly 20dB less than the initial vibration level. Over the 170 to 180 Hz frequency band, there is a difference of less than 0.3 dB between the 2DOF and SDOF designs. The resulting *MR* for this case is 37.5%, meaning that over 37% of the mass could be saved if a properly designed and positioned 2DOF DVA was used in place of two SDOF DVAs.

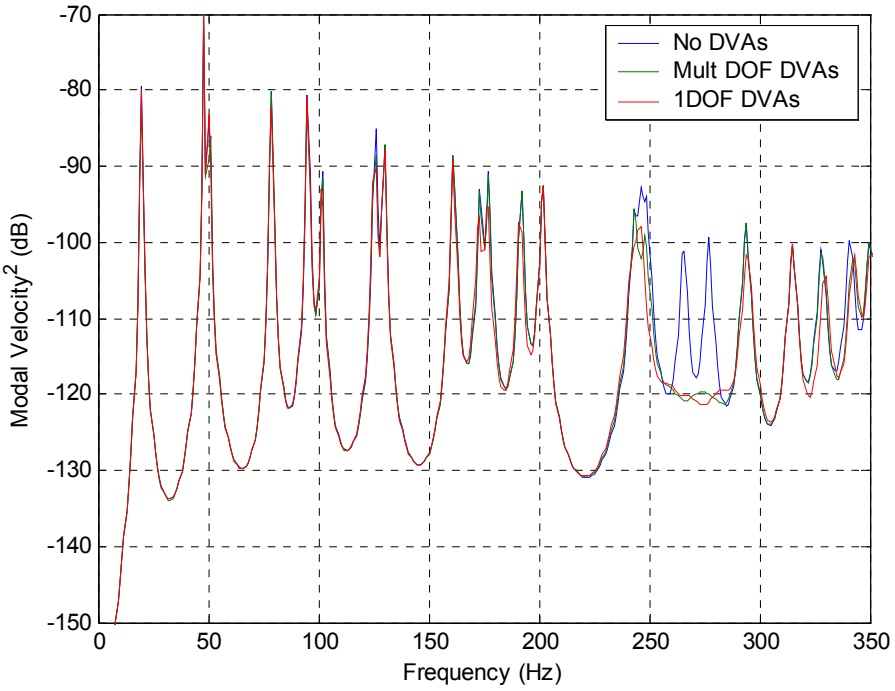

Figure 3.17 Frequency response of Figure 3.16: kinetic energy of plate without treatment, with one 2DOF DVA, and with two SDOF DVAs.

In an enlarged view of the targeted frequency band, Figure 3.18, shows that the difference in designs is negligible, despite the reduced mass of the 2DOF DVA.

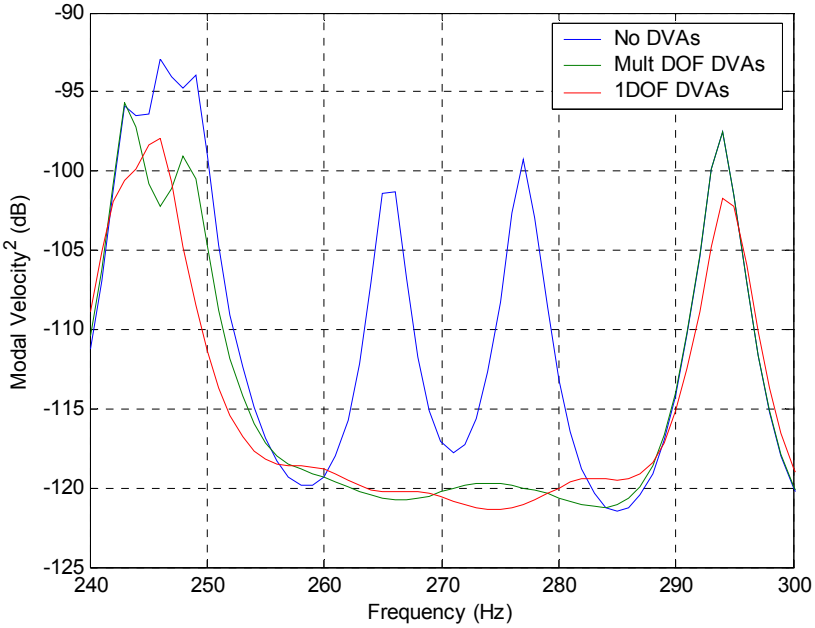

Figure 3.18 Enlarged view of frequency response. The kinetic energy of the two systems is matched very well.

As mentioned in section 3.3.1 , the kinetic energy of the plate is best described by a spatial average of random primary forces. Figure 3.19 shows the change in response for increasing summations of primary forces. Because the magnitude of the modal amplitude is unity for each summation, the sum is equivalent to an average of random forcing positions and gives a more generalized representation of the primary system. Notice that after five randomly located forces are applied to the plate, the response starts to converge to a generalized frequency spectrum. The convergence can be noticed by closely observing the modes resonating at 161 and 192 Hz. Both resonance frequencies only start to show magnitudes equal to the 173 and 177 Hz modes after the fifth additional primary force.

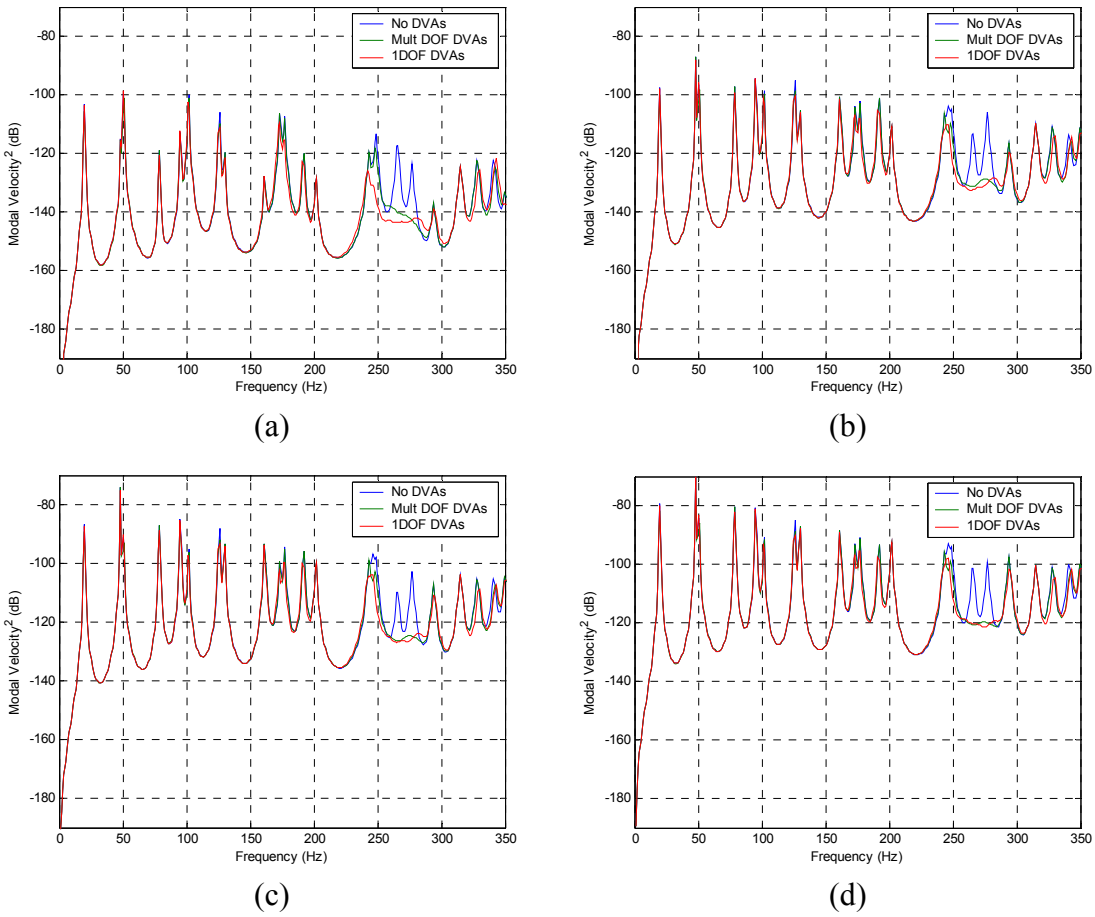

Figure 3.19 Progression of response as number of random primary forces is increased: (a) first primary force, (b) fifth primary forces, (c) tenth primary forces, (d) twentieth primary forces.

So, for this case, the targeted modes work in favor of the 2DOF DVA and against the SDOF DVA, in terms of the *MR*. To further illustrate the importance of the targeted modes, an

analysis was performed to evaluate the optimal coupling coefficient for every possible pair of targeted modes using a 2DOF DVA. Figure 3.20 shows the sum of the optimal DVA coupling coefficients for a 2DOF DVA on a pinned-pinned plate versus the pair of modes targeted. The *x* and *y* axis are the incremental mode order of the plate listed in order of increasing natural frequency, which is shown in Table 3.1, with their corresponding mode orders up to the (7,7) mode at 964 Hz. Therefore, there are 2,401 possible pairings of targeted modes, including repeated pairings. The *z-axis* value corresponds to the coupling coefficient of each position at each mode, *K*. The formula used is,

$$\mathrm{K} = \left[\left(\psi_{11} + \psi_{21} \right)^2 + \left(\psi_{12} - \psi_{22} \right)^2 \right] \tag{3.55}$$

The resulting value, *K*, has no units, and is simply a quantitative measure of coupling coefficient of each reaction point while accounting for the 180^{o} phase difference of the 2DOF DVA's second mode.

Table 3.1. Listing of natural frequencies of plate and their mode order.

#	Natural Frequency (Hz)	'n' order	'm' order
1	19.7	1	1
2	48.0	1	2
3	50.4	2	1
4	78.7	2	2
5	95.2	1	3
6	101.6	3	1
7	125.9	2	3
8	129.9	3	2
9	161.3	1	4
10	173.3	4	1
11	177.2	3	3
12	192.0	2	4
13	201.7	4	2
14	243.2	3	4
15	246.2	1	5
16	248.9	4	3
17	265.5	5	1
18	277.0	2	5
19	293.8	5	2
20	314.9	4	4
21	328.2	3	5
22	341.0	5	3
23	350.1	1	6
24	378.2	6	1
25	380.8	2	6
26	399.9	4	5
27	406.5	6	2
28	407.1	5	4
29	432.0	3	6
30	453.7	6	3
31	472.8	1	7
32	492.1	5	5
33	503.5	2	7
34	503.7	4	6
35	511.4	7	1
36	519.8	6	4
37	539.7	7	2
38	554.8	3	7
39	586.9	7	3
40	595.9	5	6
41	604.8	6	5
42	626.5	4	7
43	653.0	7	4
44	708.6	6	6
45	718.6	5	7
46	737.9	7	5
47	831.3	6	7
48	841.8	7	6
49	964.5	7	7

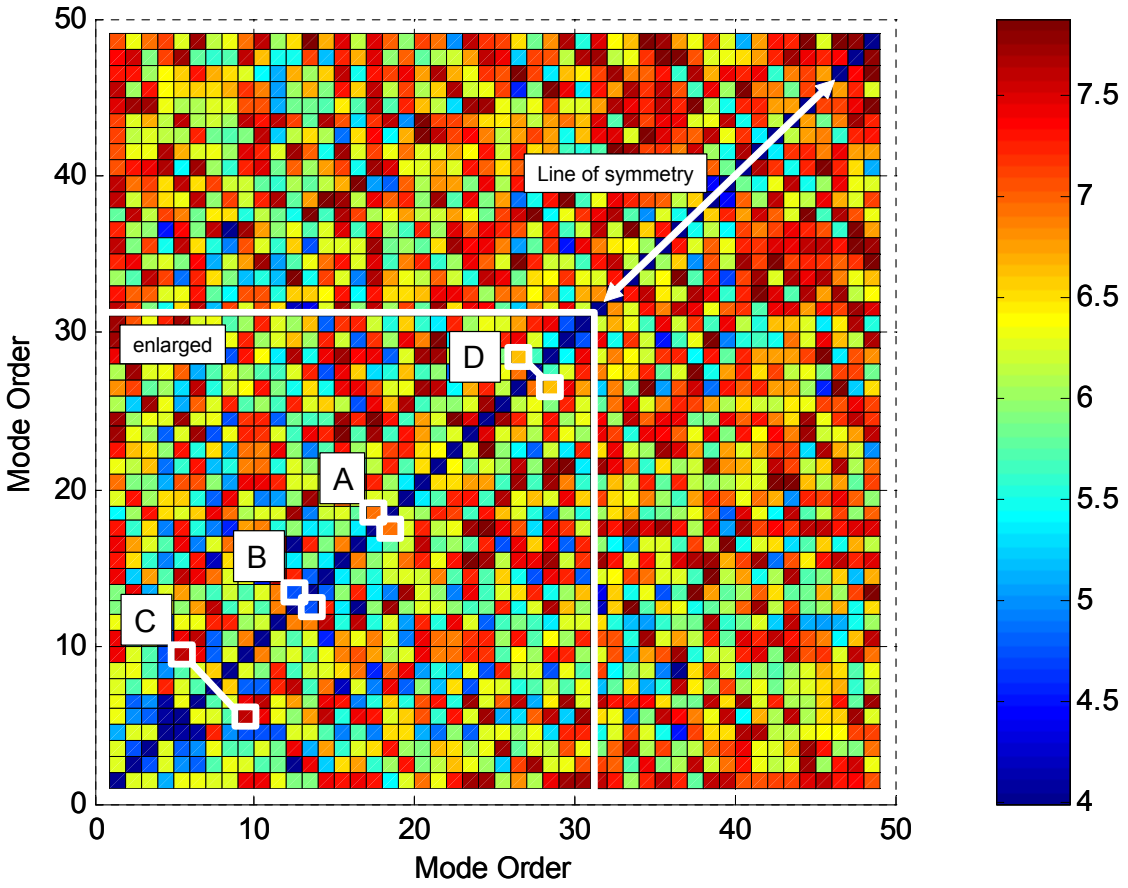

Figure 3.20 Countour plot measuring 2DOF DVA optimal coupling for all combinations of two targeted modes on a pinned-pinned plate.

The data from Figure 3.20 was generated by evaluating, with the genetic algorithm, the best summation of coupling coefficients for each pair of modes. This figure will be used as a map to provide some examples of good and bad performances of 2DOF DVAs, with respect to SDOF DVAs, as a function of the modes targeted. And while this figure is specific to the plate used in the analysis, the attributes of the figure can be interpreted in a way that is universal. First, the 45^{o} centerline of symmetry splits the graph into two equivalent pieces of data due to the repeating of mode pairs. The data along this centerline represent the targeting of one mode with both resonances of the 2DOF DVA. As it has been established, this is not advantageous for the 2DOF DVA because the motion of the first and second modes of the DVA are counterproductive to each other, and therefore result in poor coupling coefficients.

Another characteristic of the data is that the higher the frequency of the targeted mode, the greater the chance for good coupling. This is seen in the high density of good coupling in the

upper-right hand corner of Figure 3.20. This characteristic is intuitive because, when higher frequency modes are targeted, each of the plate's modes has more anti-node positions, and is thus more likely to pair well with an anti-node of the other targeted mode. What this figure doesn't account for is that a SDOF DVA can attenuate more than one mode with its single tuning frequency if the targeted modes are close together. This circumstance diminishes the possible advantage of the 2DOF DVA because both SDOF DVA masses are being utilized; which is the principle advantage of MDOF DVAs. And while the coupling coefficients are shown as favorable in this region of the figure, the high frequency modes tend to be closer together, which leads to this inefficiency. This situation occurs along the centerline, too, where the targeted modes are also close together in resonance frequency.

The only circumstance in which closely spaced modes are not both attenuated very well is when the SDOF DVAs can not be positioned to couple well with both targeted modes. This is shown in the previous example where the optimal SDOF positions for the (4, 1) mode were on nodes of the (3,3) mode, and vice versa. So, to illustrate some of the advantages and limitations of 2DOF DVAs, several examples will be discussed. These examples are labeled "A" through "D" in Figure 3.20 and Figure 3.21, with the case examined earlier in this section labeled "A": Figure 3.17 and Figure 3.18.

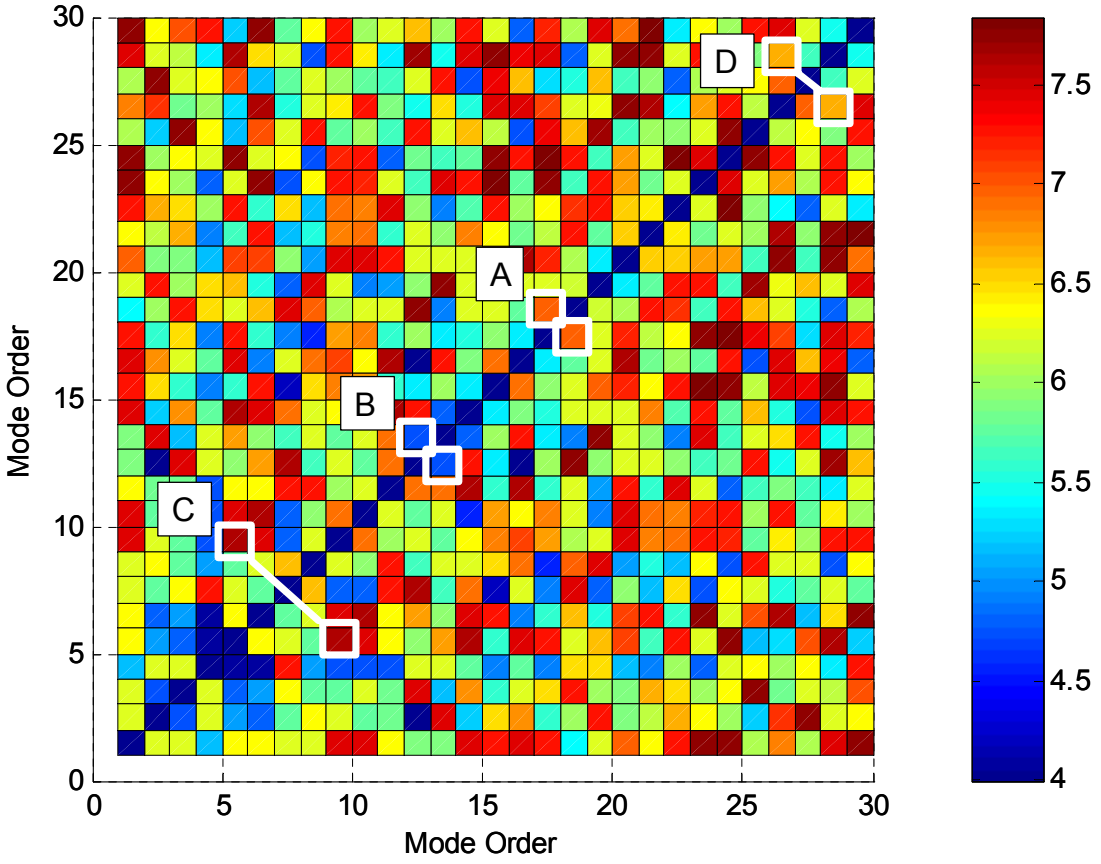

Figure 3.21 Enlarged Figure 3.20. Countour plot measuring 2DOF DVA optimal coupling for all combinations of two targeted modes on a pinned-pinned plate. Labels indicate specific cases examined.

Referring to the square labeled "B" in Figure 3.21, the targeted modes correspond to the twelfth and thirteenth modes, when listed in order of increasing natural frequency. This corresponds to the (2,4) and (4,2) modes, which have small coupling coefficients. As indicated by Figure 3.22, the best coupling position for the (4,2) mode falls directly on a nodal line of the (2,4) mode. This results in a poor coupling coefficient, which deteriorates the performance of the 2DOF DVA, despite the relatively close frequency separation of less than 10 Hz. The resulting coupling value, *K*, is a low 4.7.

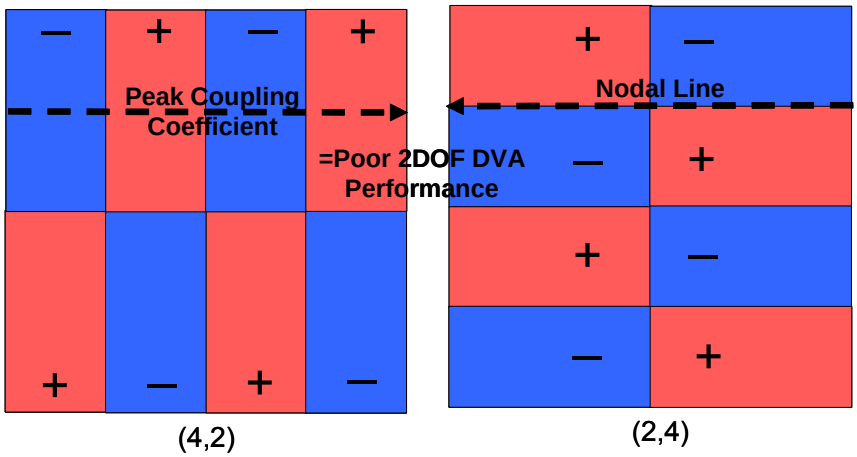

Figure 3.22 Mode shape diagram of the (4,2) and (2,4) modes of a pinned-pinned plate. The peak coupling position for the (4,2) mode is at a nodal line of the (2,4) mode, resulting in poor overall coupling.

Shown in Figure 3.23 is the comparison of kinetic energy of the plate for both treatments. As a result of the poor coupling, the *MR* is 7.3, with the 1DOF mass being 216 grams and the 2DOF mass 200 grams. While the 2DOF DVA is lighter, it does not demonstrate a significant advantage over the SDOF DVA.

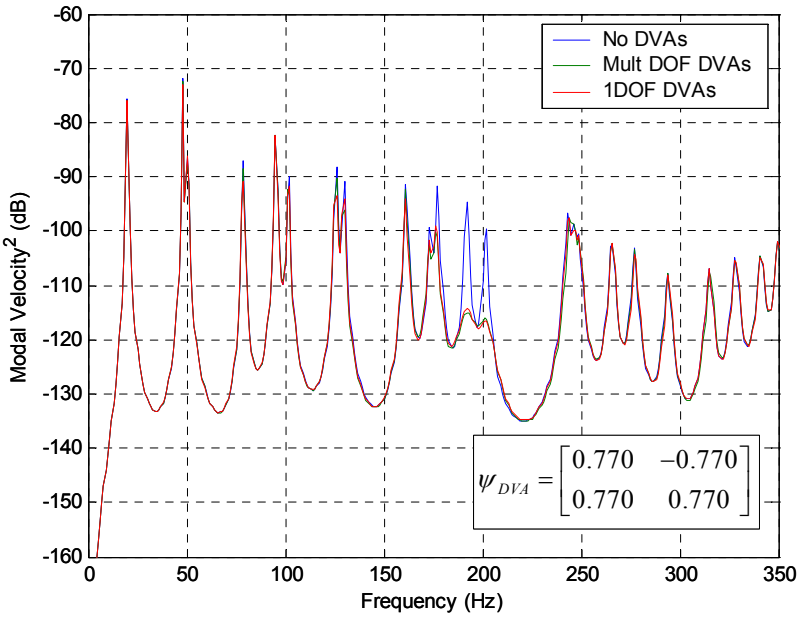

Figure 3.23 Kinetic energy of pinned-pinned plate for (2,4) and (4,2) targeted modes. The resulting *MR* of 7.3% is due to the poor coupling.

In example "C" in Figure 3.20 and Figure 3.21, the targeted modes are (1,3) and (1,4), which have large coupling coefficients; refer to Figure 3.4. The resulting coupling coefficients, shown in Figure 3.24, prove too that these modes are very compatible.

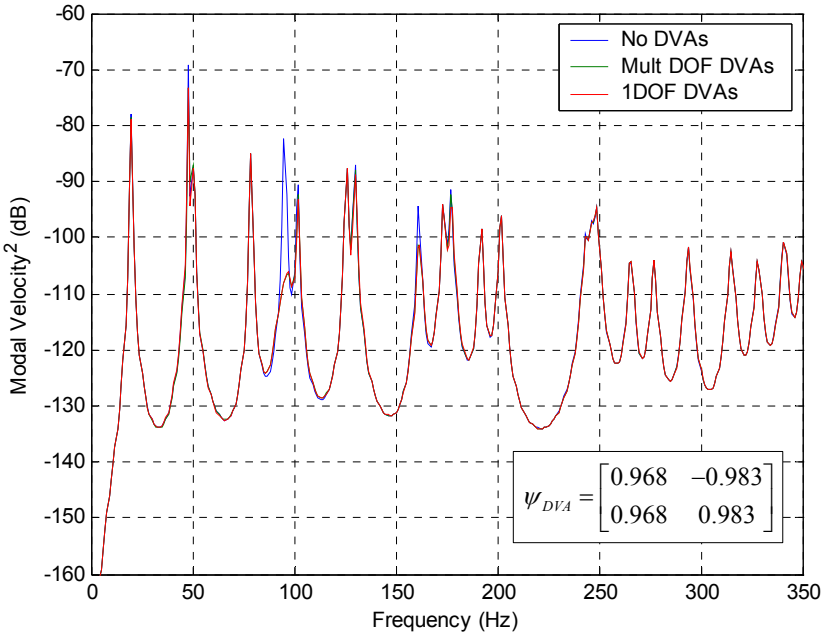

Figure 3.24 Kinetic energy of plate for (1,3) and (1,4) targeted modes. The poor *MR* of 5.2% is due to the high frequency separation, σ, of 0.51.

As seen in the Figure 3.24, the (1,3) mode at 95.2 Hz is attenuated by 22 dB, but the (1,4) mode is hardly affected, resulting in a *MR* of 5.2%. For this case, σ = 0.51, which is too great to generate a favorable advantage from the 2DOF DVA despite the excellent coupling value, *K*, of 7.6.

If sigma is too low, a SDOF DVA can attenuate two modes without the deterioration of the coupling stiffness. A case such as this is labeled "D" in Figure 3.20 and Figure 3.21. The targeted modes are (4,5) and (6,2), which correspond to resonance frequencies of 400 Hz and 407 Hz. Sigma is 0.017, and results in a *MR* of -16.1% where the mass is 172 grams for the SDOF, and 200 grams for the 2DOF DVA. The *K* value for this pair of modes is 6.9; this is equal to the first example, labeled "A". Therefore, it is evident that the problem lies in the frequency separation of the two modes, indicated by the low sigma. The resulting frequency spectrum of this case is shown in Figure 3.25.

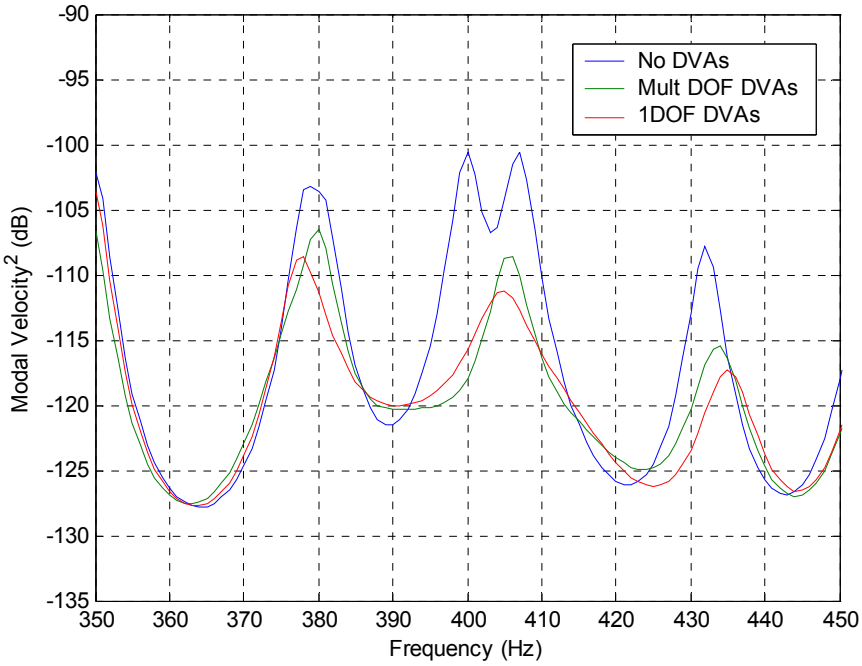

Figure 3.25 Kinetic energy of plate with modes (4,5) and (6,2) treated and untreated. The poor performance, *MR* is negative, is due to the low frequency separation of σ=0.017.

Another factor influencing the *MR*, or DVA performance, is the positioning of the DVA reaction points. This has been mentioned, but not proven with an example. Take case "B", where the *K* value is initially 4.7 due to the poor coupling coefficients of

$$\Lambda_{2DOF} = \begin{bmatrix} 0.770 & -0.769 \\ 0.772 & 0.768 \end{bmatrix} \tag{3.56}$$

To gain perspective on how this coupling coefficient affects the 2DOF DVA performance, the coupling coefficients are set to all unit values:

$$\Lambda_{2DOF} = \begin{bmatrix} 1 & -1 \\ 1 & 1 \end{bmatrix} \tag{3.57}$$

By making this assumption, the *K* value attains a perfect value of 8, and the *MR* is dramatically increased to 45.1%, a difference of over 40 percent. This example proves the importance of optimal coupling.

3.3.6 Mass Ratio as a Function of Number of Degrees of Freedom

The final factor affecting the performance of the MDOF DVAs is the number of degrees of freedom. This factor is difficult to measure because of the many other factors affecting

performance. In theory, the advantage will increase with the number of degrees of freedom as long as the circumstances are optimal. These circumstances include the frequency separation, the choice of targeted modes, and the optimal positioning of each reaction point. However, when the number of DOF increases, the complexity of the DVA resonance characteristics also increases, and therefore limits the opportunity of finding instances where the MDOF DVA would be advantageous. This will therefore lead to instances where the higher DOF DVA is acting less than optimally, and is subsequently less advantageous than the lower DOF DVA. So, while there is an increasing relationship between advantage and number of DOF, there is a more dominant decreasing relationship between the number of DOF and the availability of circumstances where a MDOF DVA is advantageous. This is shown by evaluating the *MR* as the number of DVA DOF is increased for a set of primary system modes. In this section, an evaluation of this relationship will be made. The relationship will be specific to this set of modes, but will illustrate the predominate characteristic.

The response of the primary system used throughout this section is shown in Figure 3.25. Using a 2DOF DVA to target the (2,6) mode at 381 Hz, and the (4,5) mode at 400 Hz results in an *MR* of 20.4. By increasing the number of DOF of the DVA to three, and targeting three modes, an additional 100 grams is added to the MDOF DVA system. The additional targeted mode is the (5,4) mode at 407 Hz. The resulting *MR* is 34.5%, an improvement of 14.1 percent over the advantage of a 2DOF system. The frequency separation between the modes is 26 Hz across the range of 281 Hz to 407 Hz, $\sigma = 0.07$. The targeted modes are such that there are effective reaction points available. This can be seen by the mode shapes of the DVA and the reaction point coupling coefficients.

$$\Psi_{\text{DVA}} = \begin{bmatrix} 0.959 & 0.329 & -0.871 \\ 0.770 & 0.792 & 0.129 \\ 0.906 & -0.645 & 0.937 \end{bmatrix}; \qquad \Lambda_{\text{3DOF}} = \begin{bmatrix} 0.577 & 0.408 & 0.707 \\ 0.577 & -0.817 & 0 \\ 0.577 & 0.408 & -0.707 \end{bmatrix} \tag{3.58}$$

While the mode shapes do not correspond to each other perfectly, the overall advantage gained by the contribution of each mass to every targeted mode outweighs the hindrances of the system's less than unity coupling coefficients.

The next step is to evaluate a 4DOF system targeting the three modes targeted above in addition to the (6,2) mode, which also resonates at 407 Hz. This is convenient because the higher the order of the system, the more sensitive the system is to close frequency separation.

This system results in an *MR* of 28.9%, which is better than the 2DOF system, but worse than the 3DOF system. The coupling problems associated with the 4DOF system start to hinder the system and limit its performance to less than that of the 3DOF DVA. The coupling matrices for the 4DOF system are:

$$\Psi_{DVA} = \begin{bmatrix} 0.918 & 0.592 & 0.939 & -0.333 \\ 0.942 & 0.041 & -0.923 & -0.389 \\ 0.592 & -0.131 & -0.949 & 0.516 \\ 0.933 & -0.014 & 0.930 & 0.430 \end{bmatrix}$$

$$\Lambda_{4DOF} = \begin{bmatrix} 0.500 & 0.188 & -0.500 & 0.682 \\ 0.500 & 0.682 & 0.500 & -0.188 \\ 0.500 & -0.682 & 0.500 & 0.188 \\ 0.500 & -0.188 & -0.500 & -0.682 \end{bmatrix} \tag{3.59}$$

From these matrices, it can be seen that the mode shapes match very well for nearly each mode. The fourth mode doesn't match very well, but the since the fourth mass contributes to the first three modes, an advantage still exists.

This trend continues for a 5DOF system targeting the aforementioned four modes, as well as the (3,6) mode at 432 Hz, with a resulting *MR* of 30.5%. Moving on to a 6DOF system, the MDOF advantage starts to fade away. The sixth targeted mode at 454 Hz is the (6,3) mode. The resulting *MR* for this system is 8.8%. While still an advantage over the SDOF DVAs, the advantage has clearly dropped as a result of the complexity of the system. The opportunity to yield quality coupling coefficients has diminished, and the cumulative negative effect of the DVA coupling stiffness values dominates the system.

Overall, this specific case yields what one might expect. Shown in Figure 3.26, the advantage of MDOF over SDOF DVAs peaks at about three DOF, and then diminishes into ineffectiveness as the complexity is increased. It should be noted that since this performance curve represents a specific system, the optimal order of a MDOF DVA will not always be 3DOF. In fact, it is typical for the optimal MDOF DVA to be 2DOF because it offers the most simplicity with regard to frequency separation, targeted mode shapes, and positioning. But in general, the principle relationship between order of MDOF DVA and *MR* is: as the order increases, the possible advantage increases, while the availability of finding the optimal design circumstances decreases.

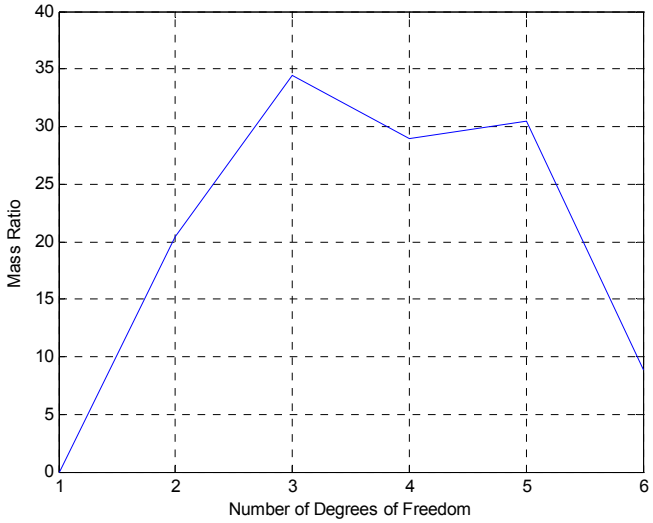

Figure 3.26 Mass ratio as a function of number of DOF for a plate primary system targeting up to six modes.

3.4 MDOF DVAs Acting on a Cylindrical Shell

This section was supported by and includes the work of Simon Estève and Dr. Marty Johnson in the Vibrations and Acoustics Lab (VAL) at Virginia Tech, and explores the use of MDOF DVAs on a cylindrical shell. The principle purpose of this section is not to fully characterize the performance of MDOF DVAs on a cylinder, but to demonstrate how MDOF DVAs can be analytically evaluated on a variety of primary structures. Additional complexity arises when using a cylindrical shell as the primary structure due to its circular cross section. Because of their symmetry, cylinders have two orthogonal circumferential modes of the same order and require a ring of DVAs to effectively target one mode of the system. This will be further explained in the discussion of the equations of motion. Specific examples will be used to analyze the effectiveness of MDOF DVAs acting on a cylinder, despite the fact that the primary structure is less than ideal.

3.4.1 Equations of Motion for MDOF Acting on a Cylindrical Shell

The natural frequencies and mode shapes of a cylindrical shell can be calculated from a five DOF model that considers three displacements and two rotational motions of each element. Assuming simply supported boundary conditions, the radial displacement mode shape can be written as,

$$\Psi_{N(n,m)} = \begin{Bmatrix} \Psi^{C}_{N(n,m)}(z,\theta) = \dfrac{1}{\sqrt{\Lambda_{n,m}}} \sin\left(\dfrac{\pi n z}{L}\right)\cos(m\theta) \\ \Psi^{S}_{N(n,m)}(z,\theta) = \dfrac{1}{\sqrt{\Lambda_{n,m}}} \sin\left(\dfrac{\pi n z}{L}\right)\sin(m\theta) \end{Bmatrix} \tag{3.60}$$

where the mode order, n is 1,2,…., m is 0,1,2,…., L is the length of the cylinder, and $\Lambda_{n,m}$ is a normalization factor for the n, m mode described in reference[29]. Because of its circular symmetry, cylinders have circumferential modes whose orientation depends on the excitation point. To take this into account, the cylinder will be considered to have two orthogonal circumferential modes (one sine, Ψ^{S}_{N} and one cosine, Ψ^{C}_{N}) of the same order, m. For this analysis, each of these modes are considered independent despite the fact that they both exhibit the same resonance frequency.

The out of plane displacement, w, will be described as a modal summation over N modes (including both sine and cosine modes) of the modal amplitudes and

$$w = \sum_{N=1}^{\infty} \Psi_{N}(z,\theta) a_{N}(\omega) \tag{3.61}$$

where z is the longitudinal direction, and θ is the angle from zero degrees. This summation includes both *sine* and *cosine* modes described in equation (3.60). Using physical parameters given in reference[30], the natural frequencies of the cylinder can be calculated and are shown in this reference.

3.4.2 Design: Finding the Optimal Position and Number of DVAs

Due to the symmetry of the cylinder, and its orthogonal circumferential modes, the DVA treatment is applied to the cylinder in rings of DVAs. The number of DVAs in each ring is chosen to be large enough such that unwanted modal interactions are avoided. The supporting data for this can be found in reference [30]. The performance of the DVAs is dependent on the number of DVAs being odd and spaced evenly around the circumference of the cylinder. The positioning of the DVAs, therefore, needs only to be optimized with respect to the location in the longitudinal direction. And this position optimization problem is evaluated again with the genetic algorithm, which accounts for the coupling coefficient with respect to the longitudinal, n, mode, the stiffness and mass matrices, and the mode shapes of the DVA in the form of the variable, R.

$$R = \Psi_D \mathbf{K}_{0D} \mathbf{M}_D^{-1/2} \mathbf{P}_D \tag{3.62}$$

The resulting positioning for DVA rings that target the third and fourth longitudinal modes would be similar to that in Figure 3.27.

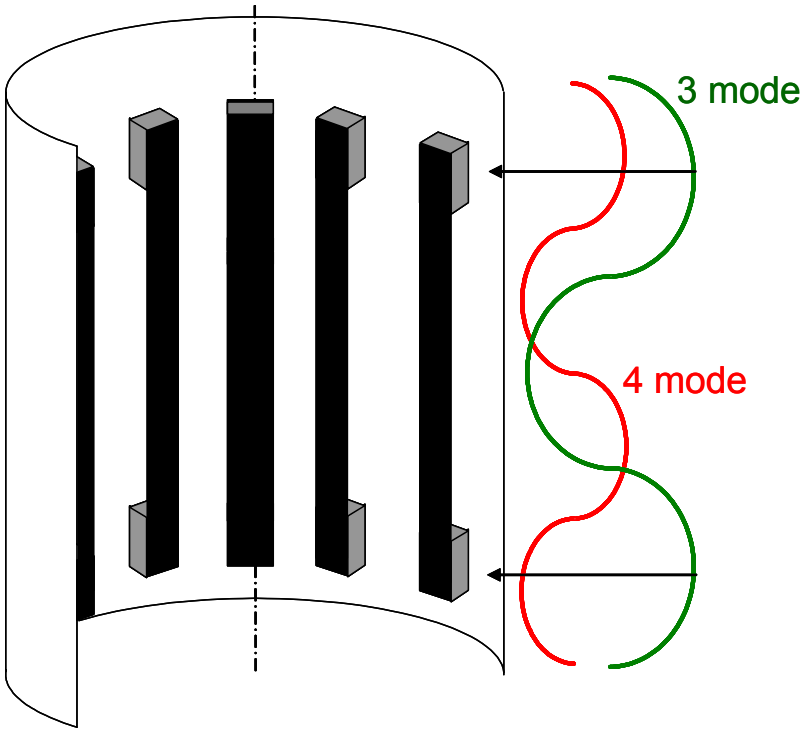

Figure 3.27 2DOF DVA ring applied to cylindrical shell intended to target the third and fourth longitudinal modes.

3.4.3 Performance: Mass Ratio as a Function of Targeted Modes, Positioning, and Degrees of Freedom

The performance of the DVA, measured by the mass ratio *MR*, is again highly dependent on the targeted modes, the positioning of the DVA reaction points, and the number of order of the MDOF DVA. The DVA reaction point positioning has been thoroughly discussed in the preceding section, and affects the DVA performance on the cylinder in a very similar manner. The key difference, in terms of positioning, is the physical feasibility of implementing the device on a cylinder. Because the circumferential dimension is ignored for a cylinder, the remaining longitudinal vibration, behaves very similar to a beam. Therefore, the reaction points in which the MDOF DVA are coupled to the cylinder are limited to locations along the one dimension of longitudinal mode shapes. And in order to effectively attenuate low frequency resonances, the

DVA needs to target the three and four longitudinal modes. This creates the physical difficulty of coupling the DVA masses across a large distance, as shown in Figure 3.27. The implication is that the structure connecting the two DVAs may have to be substantially stiffer than the cylinder itself, which is not very feasible in practice.

Assuming the physical design of the MDOF DVA is feasible, the DVA performance becomes mostly dependant on which resonance frequencies are targeted. Like the plate, the frequency separation, sigma, affects the performance. For a 110" long cylinder with an inner radius of 48", the kinetic energy frequency response is shown in Figure 3.28. Because of the symmetry of the cylinder, the MDOF DVAs are applied in rings of 13 DVAs. So for a 2DOF DVA, there will be 26 masses, two rings of 13. Other than the placement of the DVAs in rings and the inherent difference in the equations of motion that characterize the cylinder vibration, the cylinder analysis is performed in the same fashion as the plate. Each DVA mass in the model is 25 grams and has a damping coefficient of 6%. The stiffness matrix is developed through the 'fgoalattain' command in MATLAB, and the reaction point placement is chosen by the genetic algorithm. From the MDOF DVA performance, an equivalent SDOF DVA system is designed to have the same performance, and the total mass is compared. The *MR* factor is computed in the same way as in previous sections.

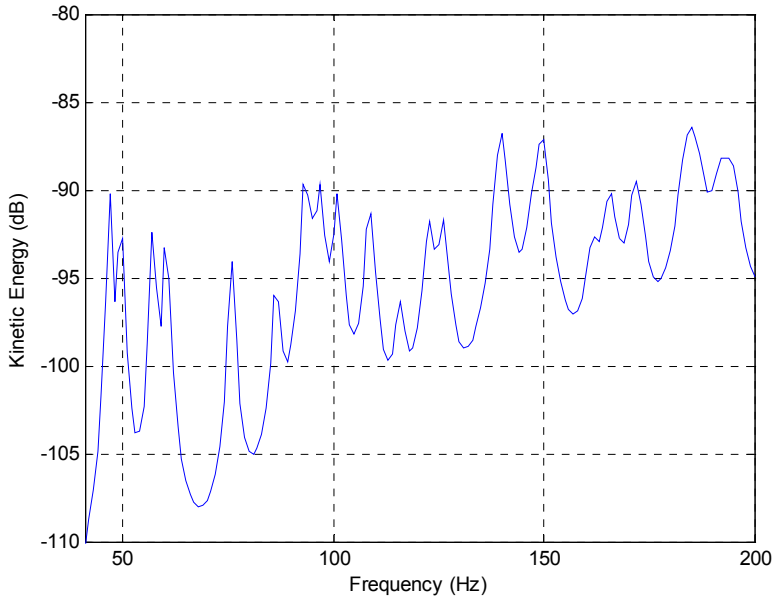

Figure 3.28 Analytical model of the kinetic energy of cylindrical shell in the 50 to 200 Hz frequency band.

To demonstrate the sigma factor, first observe the targeting of the (3,9) and (4,9) modes at 140 and 183 Hz, respectively. Shown in Figure 3.29(a), the 2DOF DVA and 1DOF DVA system are very similar with respect to the targeted frequencies. The sigma value in this case is 0.27, resulting in an *MR* of 11.0%. By decreasing the frequency separation and targeting the (3,11) and (4,9) modes at 166 and 184 Hz, respectively, the *MR* is greatly improved. Shown in Figure 3.29(b), the sigma value is 0.10, and the *MR* is 24.5%. Notice that while the three and four longitudinal modes are targeted for both scenarios, the circumferential mode is nine for both targeted modes in the first scenario, but is nine and eleven for the second. This indicates that it is not critical to target the same circumferential mode. The longitudinal mode, however, is quite critical in that they must be different. Otherwise, the situation arises where the first and second DVA modes are counteractive to one another and performance is deteriorated.

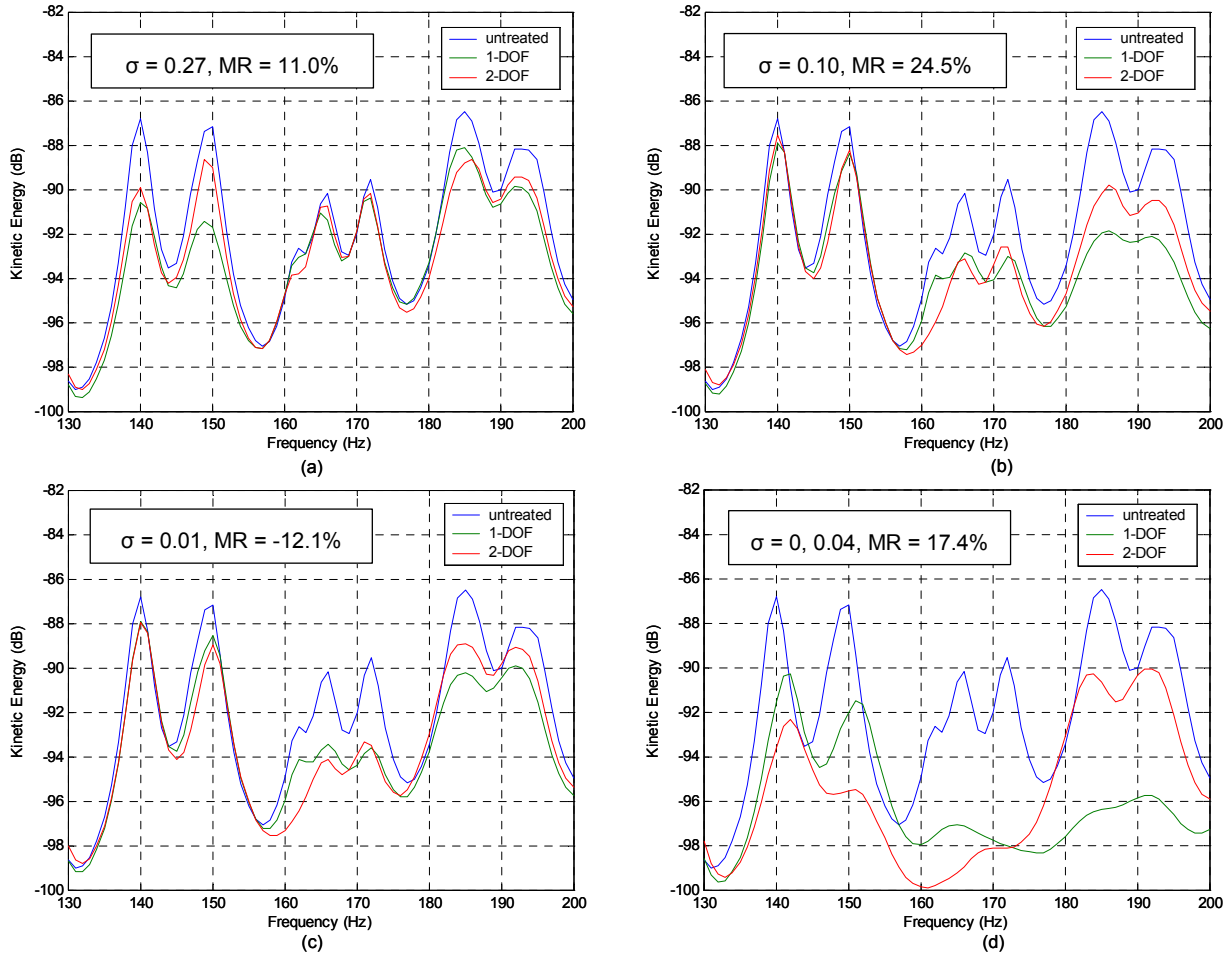

Figure 3.29 (a) Targeted (3,9) and (4,9) modes at 140 and 183 Hz. (b) Targeted (3,11) and (4,9) modes at 166 and 184 Hz. (c) Targeted (3,11) and (3,6) modes at 166 and 171 Hz. (d) Targeted (1,12), (3,11), and (3,6) at 165, 166, and 171 Hz.

Figure 3.29(c) shows the targeting of the (3,11) and (3,6) modes respectively at 165 and 171 Hz. For an favorable sigma value of 0.04, the *MR* of -12.0% indicates no advantage using a MDOF DVA. This is due to the targeting of the same longitudinal mode. Finally, Figure 3.29(d), targeting the (1,12), (3,11), and (3,6) modes at 165, 165, and 171 Hz respectively demonstrates a 3DOF DVA targeting three modes on the cylinder. For the sigma values of 0 and 0.04, the *MR* is a substantial 17.4%. A 4DOF DVA would be near impossible to effectively use on the cylinder, and does not demonstrate any advantage in the analytical model.

3.5 Conclusions

The principle goal of this chapter was to demonstrate that the total absorber mass of a DVA system can be reduced by using MDOF DVAs in place of SDOF DVAs, while maintaining equivalent performance. First, an analytical model was developed to compare the total absorber mass of SDOF and MDOF DVA systems on a lumped parameter system. This simplified system demonstrated the theoretical advantage possible using MDOF DVAs because the mode shapes of the MDOF DVA and the primary system can be matched. A model was then developed for a mass comparison of MDOF and SDOF DVA systems on a pinned-pinned plate. A distributed system introduces the difficulties of matching mode shapes and developing MDOF DVA designs. The effects of parameters such as targeted modes, positioning, and the number of degrees of freedom of MDOF DVAs were investigated and discussed. Finally, the DVA comparison was applied to a cylindrical shell, which again added complexity to the analysis. This demonstrated the application of the modeling techniques to a variety of structures.

It was concluded that there exist circumstances under which MDOF DVAs require less mass than SDOF DVAs. But for optimal performance, the frequency separation of the targeted modes must be considered, the MDOF DVA must be designed with regard to the targeted resonance frequencies and mode shapes, the DVA reaction points must be optimal, and the physical design must be feasible.

Chapters four and five will now transition to active control of structural modes with a two degree of freedom dynamic active vibration absorber (DAVA). The design, optimization, and application of the device is presented.

Chapter 4: DAVA: Two Degree of Freedom Dynamic Active Vibration Absorber Theory and Design

The next two chapters of this thesis detail the design of an electromagnetic 2DOF DAVA that is designed to attenuate the low frequency structural vibration of an ELV payload fairing. The dual mass design, shown in Figure 1.1, couples the magnet mass of the actuator to the mass of a stiff honeycomb plate through elastic spider plates in the actuator. An active force is generated in between the masses by the motion of the magnet when the actuator coil is supplied with alternating current (AC). This force is transmitted to the honeycomb plate, and then coupled to the fairing with a block of acoustic foam. The electrical and mechanical components of the DAVA are specifically designed to utilize the dual resonance of the device to maximize low frequency attenuation using active control.

First, chapter four will review the original design that inspired the application of a 2DOF DAVA to the cylinder. A description of the experimental techniques used to characterize and optimize the mechanical and electrical parameters of the DAVA follows. An analytical evaluation of different DAVA designs with respect to the targeted frequency band is discussed next. This analysis will be supported by experimental data, and lead to a final design for use in high level testing, which is detailed in chapter five.

4.1 DAVA Theory and Previous Work

As mentioned in chapter one, the design used in this experiment is based on an existing design patented by R. A. Burdisso and J. D. Heilmann[23]. This design consists an active element positioned in between two reaction masses, which are attached to a primary structure through elastic elements. This design was applied to a cantilevered beam, and compared to traditional SDOF DAVAS. It was found that the 2DOF DAVA was able to "achieve the same level of vibration reduction using only half the control effort required by the single reaction-mass actuator."[24]

4.2 2DOF DAVA Characterization

This section will detail the methods used to measure the parameters that characterize the resonance and forcing characteristics of the DAVA. The DAVA, shown in Figure 1.1, is comprised of two components: an electro-magnetic actuator and a foam block with a honeycomb

plate glued to one surface. The influence on performance of these mechanical and electrical components is discussed further in following sections.

4.2.1 Mechanical Characterization of 2DOF DAVA

The actuator shown in Figure 4.1 (a) contains a Nickel-Iron-Boron (NdFeB) magnetic mass that is held in place by a bolt running vertically through the actuator. The elastic elements in the actuator are referred to as spider plates and provide a stiffness that allows motion of the mass in the vertical direction while keeping the magnet accurately centered in the housing. The spider plates are machined fiberglass discs in which the stiffness is a function of the pattern of removed material and thickness.

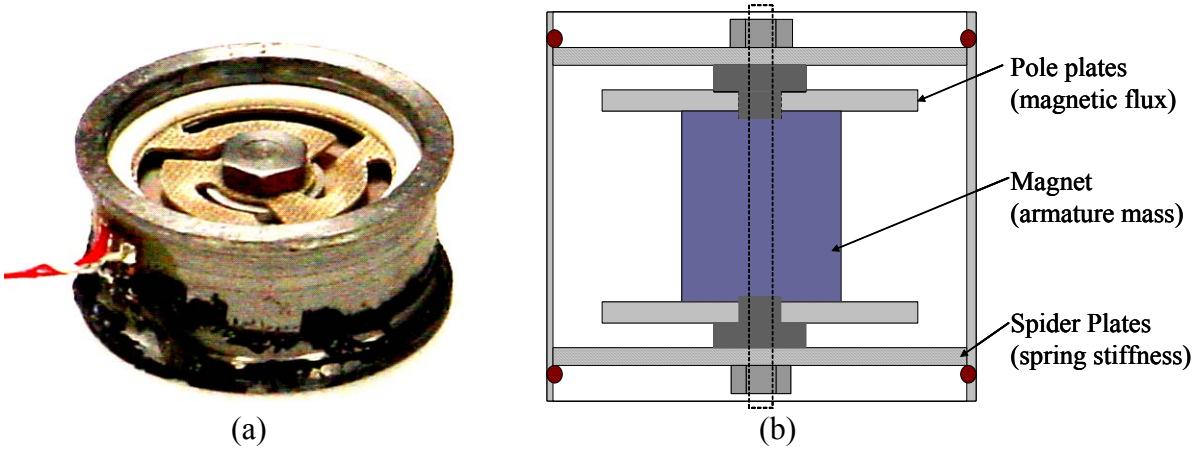

Figure 4.1 (a) Photograph of magnetic actuator. (b) Schematic of magnetic actuator showing key mechanical components.

The goal of the final DAVA design is to have a device that exhibits a large output across a frequency span of 50 to 200 Hz, while attaining the greatest force output per voltage/current input as possible. Due to the actuator's one DOF, it has one resonance frequency, which is dependent on the magnet mass and spider stiffness, and slightly dependent on the level of damping in the spider plate. In order to accomplish the 50 to 200 Hz resonance band goal, both moving masses of the DAVA, the actuator mass and the honeycomb plate, must resonate within this range. The goal was to find an actuator with a resonance frequency in the 75 to100 Hz band. A Motran actuator, Figure 4.2 (a) was considered; its resonance occurs at approximately 125 Hz and has a peak output force per volt of about 16 Newtons. It was determined that an in-house design would provide more flexibility and allow for design modifications that would improve performance, such as the use of rare earth magnets in order to reduce weight. The design

engineer/machinist of the actuator, Steve Booth, inspired the names 'Booth Shaker 1 or 2', which are the terms used for the successive versions of the in-house designs. The first design, Booth 1, was used to examine the effects of adjusting key parameters such as spider stiffness, actuator mass, pole plate effectiveness (discussed in further sections), and clearance issues when mounting the device.

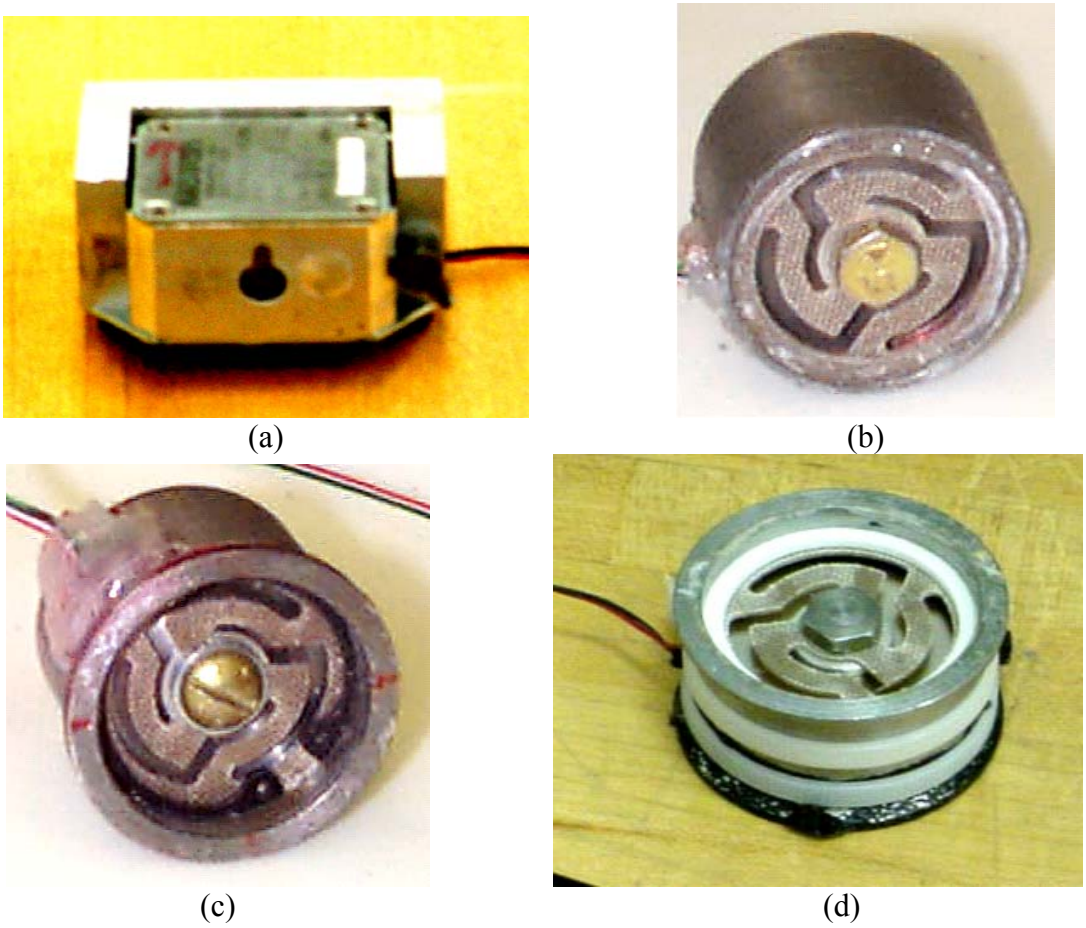

Figure 4.2 (a) Motran actuator shown in a mounting bracket. (b) Booth 1 actuator. (c) Booth 2 actuator. (d) Booth 3 actuator.

The resonance frequencies of the actuators are a function of the magnet mass and the stiffness of the spider plates through the relationship,

$$\omega_n = \sqrt{\frac{k_{\text{spider plates}}}{m_{\text{magnet mass}}}} \tag{4.1}$$

While the magnet mass can be weighed, the spider stiffness is more difficult to determine. The resonance frequency, however, can be determined by observing the frequency response of the magnet acceleration. For random noise input, the peak of the acceleration response is a close

indicator of resonance. The test setup for this experimental data collection is shown in Figure 4.3(a). The actuator is placed in a vice grip while driven with random noise. An accelerometer is placed on one end of the bolt that runs through the actuator. The actuator is blocked on both ends by two wooden slats; one having a hole through the center so the accelerometer has clearance and is not crushed by the vice grip. With the wooden blocks in the vice grip, the transfer function of acceleration per input voltage is collected. The resulting transfer function indicates the resonance frequency of the actuator. The force output generated by the actuator per input voltage is the transfer function multiplied by the magnet mass.

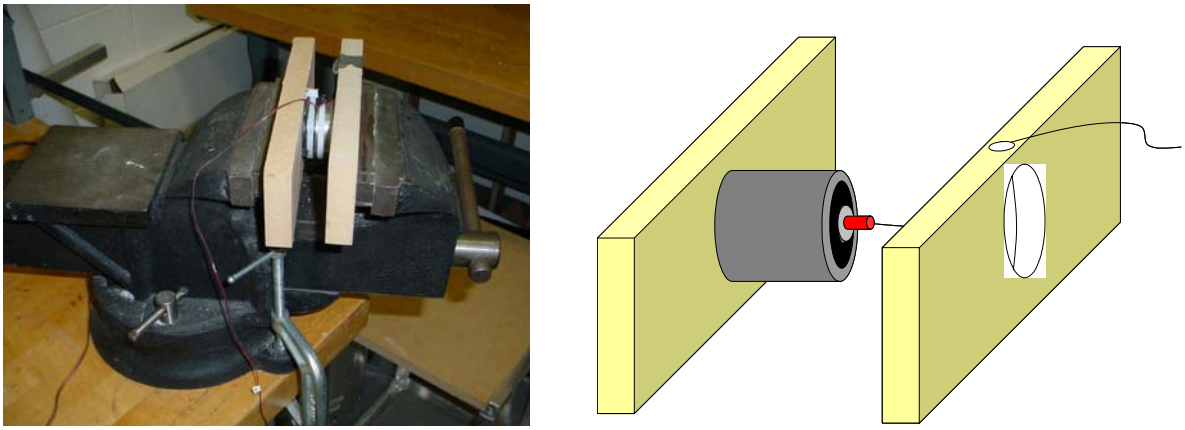

(a) (b)

Figure 4.3 (a) Booth 3 actuator in vice grip used to measure blocked response. (b) Schematic of wooden planks used to hold actuator blocked in the vice grip without damaging the accelerometer.

The response of the Booth 1 actuator is shown in Figure 4.4. It was designed to exhibit the same characteristics as the Motran actuator. The Booth 1 actuator has a resonance at about 175 Hz, which is well above the desired value, but has a force output relatively close to the Motran. The first objective was to lower the resonance frequency of the Booth actuator without drastically changing the design and without adding mass. By using thinner spider plates, the stiffness value of the system is reduced and the natural frequency is lowered to 60 Hz.

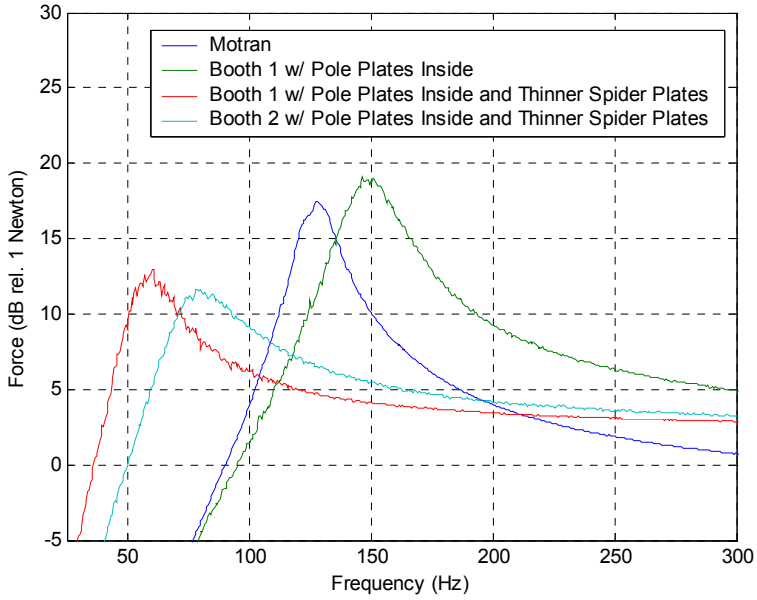

Figure 4.4 Output force per input voltage of Motran and Booth actuators. The resonance frequency decreased with the use of thinner, less stiff, spider plates.

As the target natural frequency was 75 to 100 Hz, it was convenient that the second design, which was supposed to only differ by the shell casing, had a slightly higher natural frequency of 80 Hz. The Booth 2 design is comprised of the same components as the Booth 1 design, but had a flange on the casing to allow for easier mounting. The different natural frequencies can be explained by errors in manufacturing; which is to say the Booth 1 and Booth 2 were made independently and slightly inconsistently. Based on the performance of the first two prototypes, eight actuators, shown in Figure 4.2(d), were then manufactured with the intent of having very consistent characteristics. The transfer functions of these eight Booth 3 actuators are shown in Figure 4.5. All show resonance frequencies within the 85 to 105 Hz frequency band. The new actuators were designed to have a much lower profile, and excluded the pole plate component, which will be described in the following section.

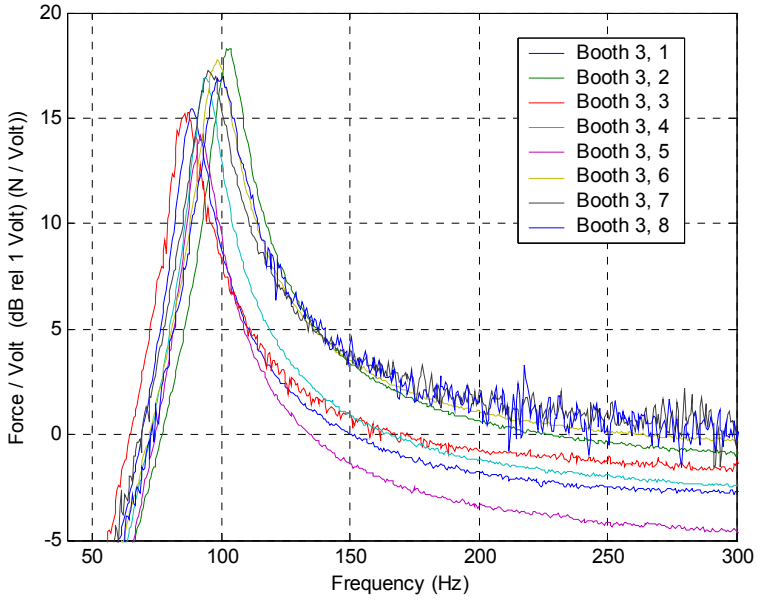

Figure 4.5 Force per voltage transfer functions of eight Booth 3 actuators.

The actuator is the first of two degrees of freedom in the DAVA configuration. The second element is the honeycomb plate and foam block, which allows for compression in the vertical direction, shown in Figure 1.1 and Figure 4.6. The melamine foam used in the design is lightweight (0.14 grams/in^3) acoustic foam that acts as a spring in the DAVA configuration. A honeycomb plate is glued to one surface of the foam forming a spring mass system. This type of honeycomb plate was chosen because it is very stiff and does not show any resonance characteristics within the 50 to 200 Hz bandwidth (i.e. it acts as a rigid mass). The system natural frequency is dependent primarily on the stiffness of the foam and the mass of the plate. The plate density is about 2 grams/in^2, and the stiffness of the foam is dependent on both the cross sectional area and the thickness. Originally produced in 48"x 9 ½"x 2" strips, the stiffness becomes slightly variant with respect to how it is cut, the direction it is cut, and sometimes which strip the block is cut from. The stiffness can be increased by decreasing the thickness of the block, or by increasing the cross-sectional area of the contact surface. When increasing the cross-sectional area, though, the size of the plate is also increased which increases the plate mass. For a 9.5"x 9.5"x 2" block of foam, the stiffness is about 380 kN/m. This stiffness can be decreased to as little as 34 kN/m for a 4" x 4" x 2.5" block, which is about the lower size limit.

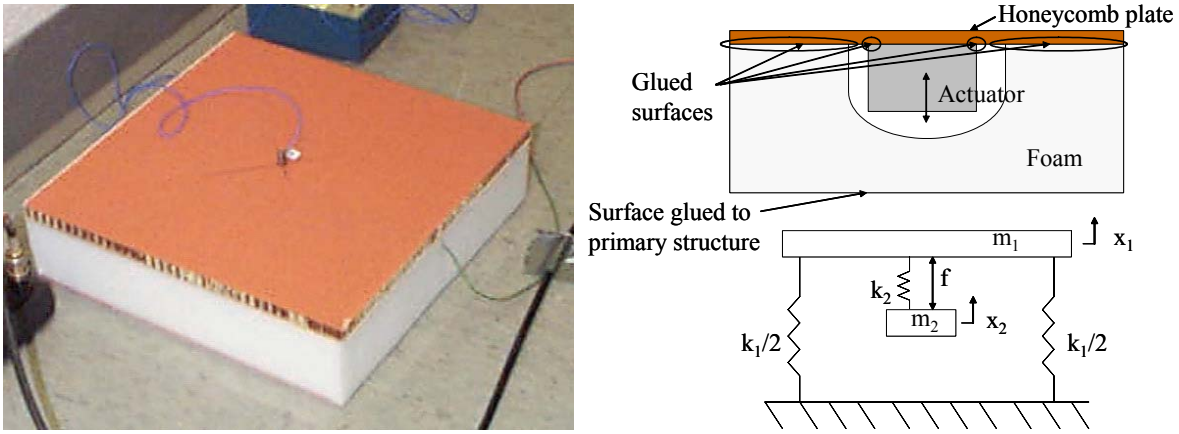

Figure 4.6 (a) Photograph of assembled DAVA glued to floor. (b) Schematic of DAVA configuration (top) and free body diagram of DAVA configuration (bottom).

Assembled, the DAVA appears, from the outside, like the photograph in Figure 1.1 and Figure 4.6 (a). The 2DOF system, depicted in Figure 4.6(b), indicates the dual resonance of the device. Ideally, the dual resonances would create a plateau across the 50 to 200 Hz frequency band as the Booth 2 actuator in a 9.5" x 9.5" x 2" foam block appears to in Figure 4.7.

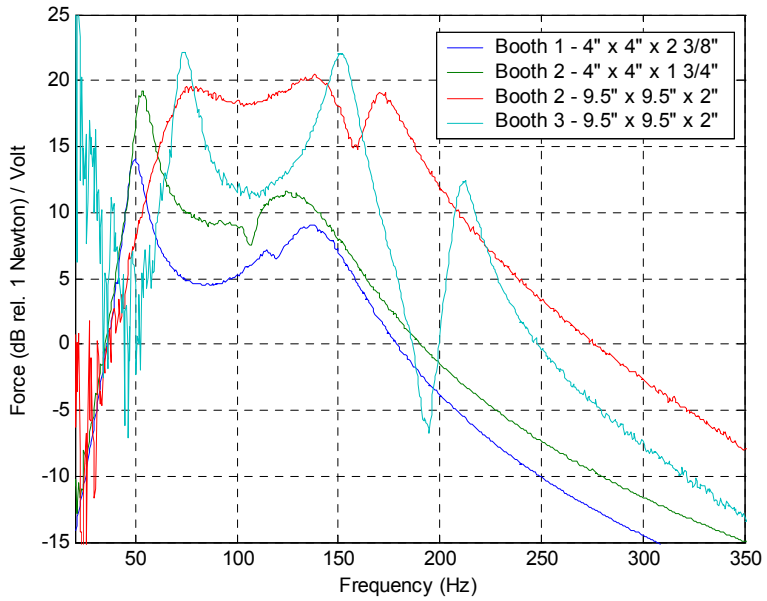

Figure 4.7 Force response for different DAVA configurations and actuators.

Figure 4.7 shows the transfer functions of the force transmitted to the primary structure per volt across the actuator. The force generated by the DAVA is measured by collecting acceleration data on the top plate of the DAVA while the DAVA is taped to the floor with

double sided tape to eliminate base motion. In the frequency domain, the acceleration of the top plate can be divided twice by $i\omega$ to obtain the displacement. The displacement is then multiplied by the stiffness of the foam to obtain the force transmitted into the base. The stiffness of the foam is obtained by disassembling the DAVA and evaluating the plate-foam resonance. First the plate is peeled off of the foam block, and the actuator is removed from the configuration. The plate is then glued back onto the foam block and then placed on a shaker to measure the acceleration of the top plate. An example of this is shown in Figure 4.8 for an 8"x 8" x 2" foam block and 16 in^2 honeycomb plate. With the resonance frequencies obtained from this data, the foam stiffness can be approximated by,

$$k = (2\pi f)^2 m_{plate} \tag{4.2}$$

$$f_1 = 194\,Hz \qquad k_1 = 156\,kN$$
$$f_2 = 179.5\,Hz \qquad k_2 = 158\,kN$$
$$f_3 = 169\,Hz \qquad k_3 = 163\,kN$$

where $m_{plate} \gg m_{foam}$.

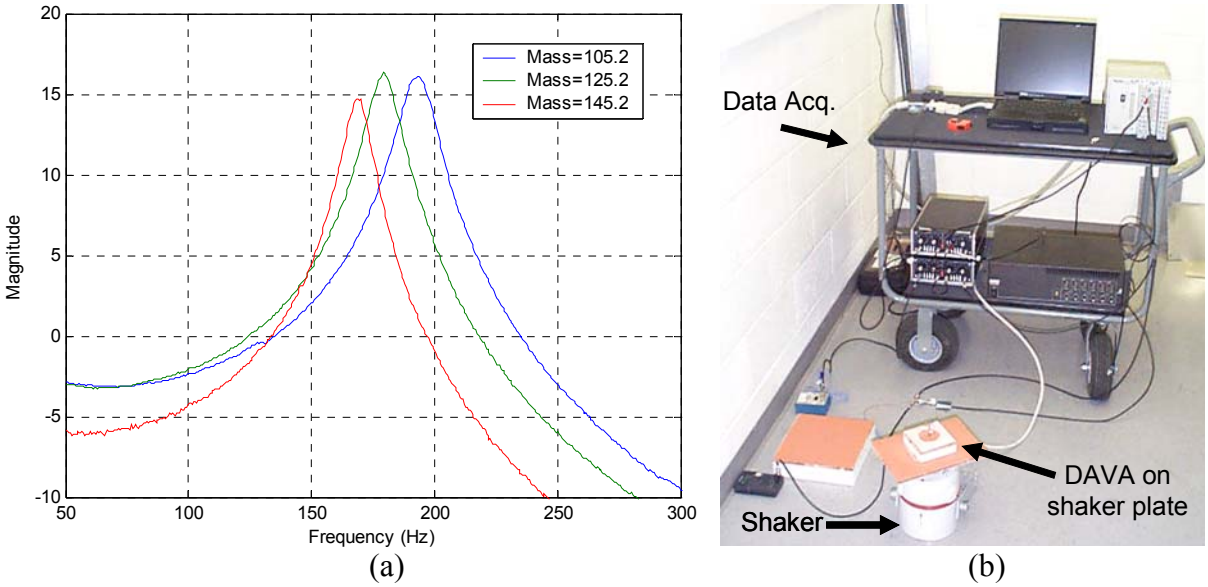

(a) (b)

Figure 4.8 (a) Transfer function of top plate acceleration and shaker acceleration allows the estimation of the foam-plate resonance. (b) Test setup for calculating the DAVA and foam-plate frequency response.

4.2.2 Electrical Characterization of 2DOF DAVA

The electrical characterization was supported by, and includes work done by Arnaud Charpentier and Cory Papenfuss. The electrical components, shown in Figure 4.9, of the

actuators include an electrical coil, a NdFeB magnet held in place by a bolt and spider plates, and two pole plates used in some actuator designs to reduce the magnetic field gap. The coil is glued to the interior of the actuator shell using a high strength glue bond and is the source of the electromagnetic field.

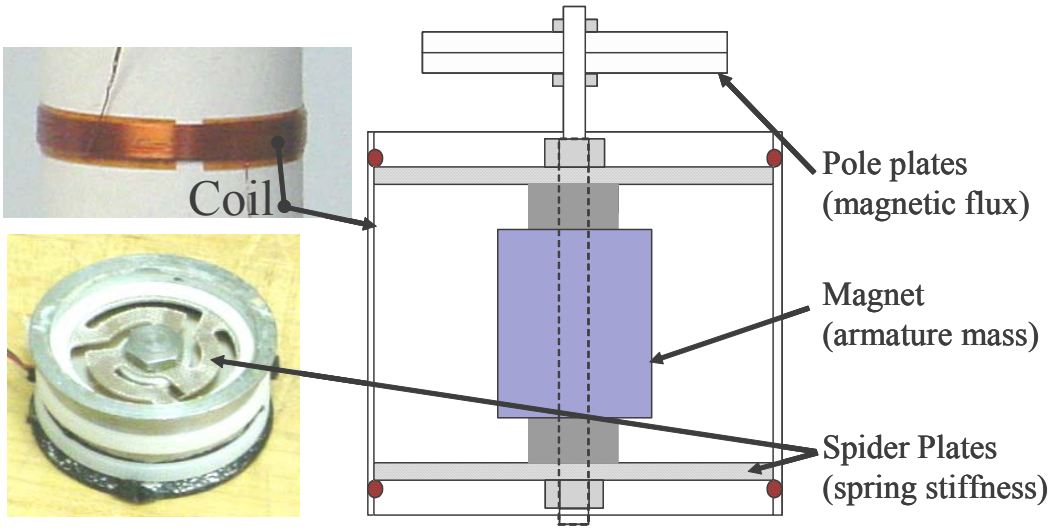

Figure 4.9 Photographs of coil, assembled actuator, and schematic of actuator components. The actuator was assembled and tested with the pole plates outside of the shell to determine their electromagnetic effects without changing their mechanical effects.

The magnetic field generated by the coil is proportional to the number of turns and the length of the coil through the relationship

$$B = \mu_o n I \tag{4.3}$$

where μ_o is a permeability of vacuum constant, n is the number of turns in the coil per total coil length, and I is the current passing through the coil. This is depicted in Figure 4.10. At the time of design, this relationship was not investigated in great detail with regard to maximizing the force exerted onto the magnet. However it was know that the relative magnet permeability and air gap between the coil and magnet were important to obtain good performance. Therefore, the magnet type chosen was NdFeB, which has a very strong magnetic field and results in a higher force exerted onto the primary structure per unit weight.

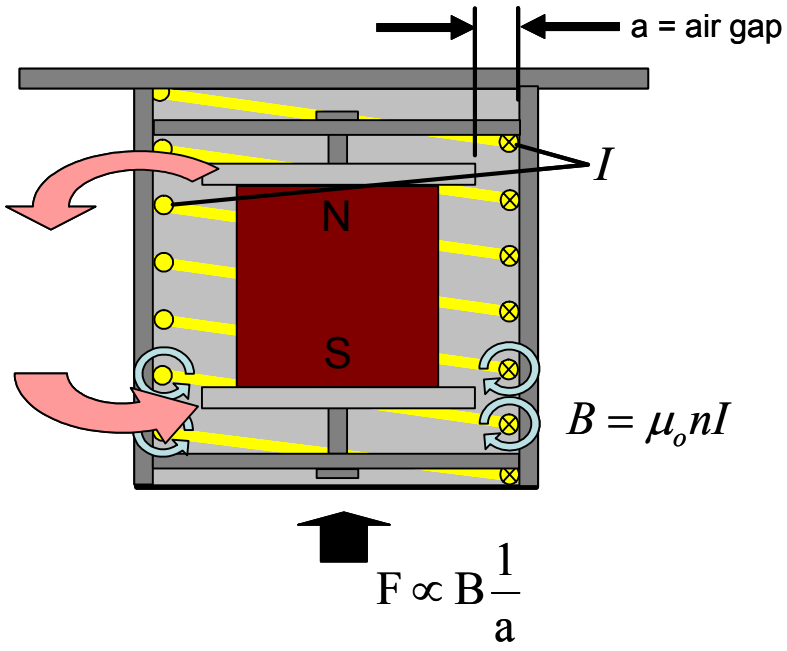

Figure 4.10 Parameters influencing electromagnetic actuator. The pole plates were investigated to evaluate the result of decreasing the air gap, *a*.

The effect of the air gap on performance was investigated. Knowing that the air gap is inversely proportional to the magnetic force, the steel pole plates were used to decrease the air gap and improve actuator performance. The difficulty in evaluating this effect of the pole plates is that the addition of pole plates increases the total armature mass, which would also increase the performance. This was overcome by comparing the generated force of the actuators with the pole plates inside the actuator, as shown in Figure 4.1(b), and with the pole plates outside of the actuator shell, as shown in Figure 4.9. The force output results of these two configurations are shown in Figure 4.11, and indicate that the pole plates do not better the performance of the actuator by a significant amount at resonance, but result in a 4 dB increase above resonance.

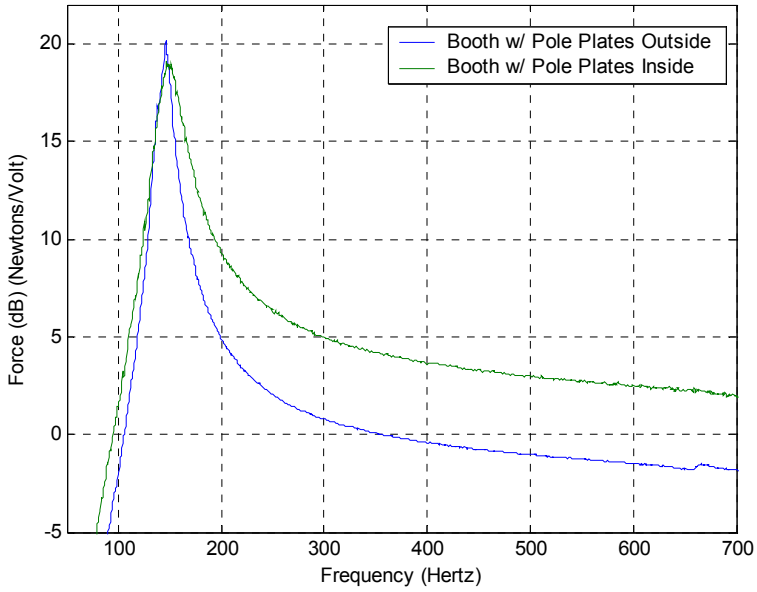

Figure 4.11 Comparison of booth actuators with different pole plate configurations, but equivalent mass.

4.2.3 Electro-Mechanical Characterization of 2DOF DAVA

The actuator can be modeled as an electro-mechanical system[31] as shown in Figure 4.12. The electrical model of the actuator is shown as a R-L (resistance and inductor) circuit, where $\Gamma = Bl$.

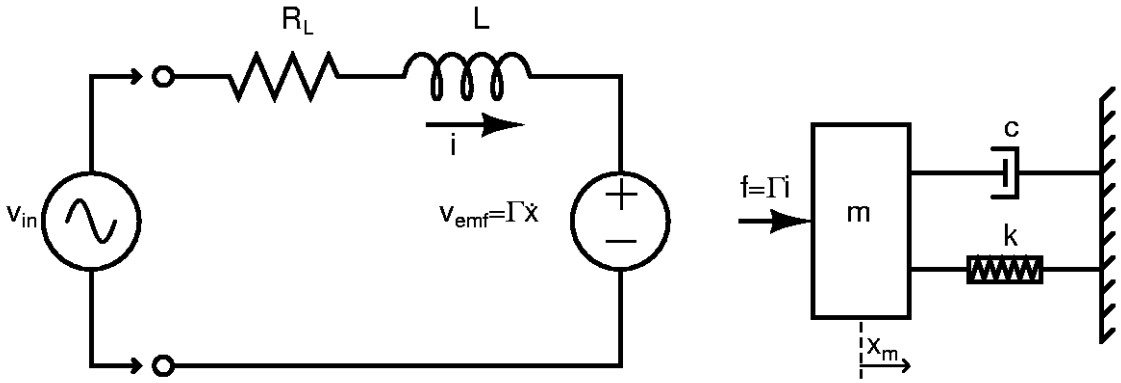

Figure 4.12 Electro-mechanical model of actuator.

The electrical resistance of the actuator, determined using a voltmeter and verified through analytical validation, was found to be 4.7 Ohms. In order to extract the inductance, the motor is rigidly mounted in a vice, as shown in Figure 4.3, and the acceleration of the armature

mass is the measured output per input voltage. The resulting bode plot is shown in Figure 4.13. The electrical admittance is represented by the equation,

$$Y = \frac{1}{Z} = \frac{1}{U} = \frac{1 + \beta l \cdot i\omega \cdot X_m}{R + i\omega \cdot L} \tag{4.4}$$

where βl is the force factor, R is the electrical resistance found to be 4.7 Ohms, L is the coil inductance found from the high-frequency asymptote, and X_m is the measured displacement of the armature mass. At low frequencies, the admittance is mostly the inverse of the resistance. Therefore, the resistance is verified experimentally. However, at high frequencies, the admittance is dominated by the inductance, and the inductance is found to be 0.16 mH.

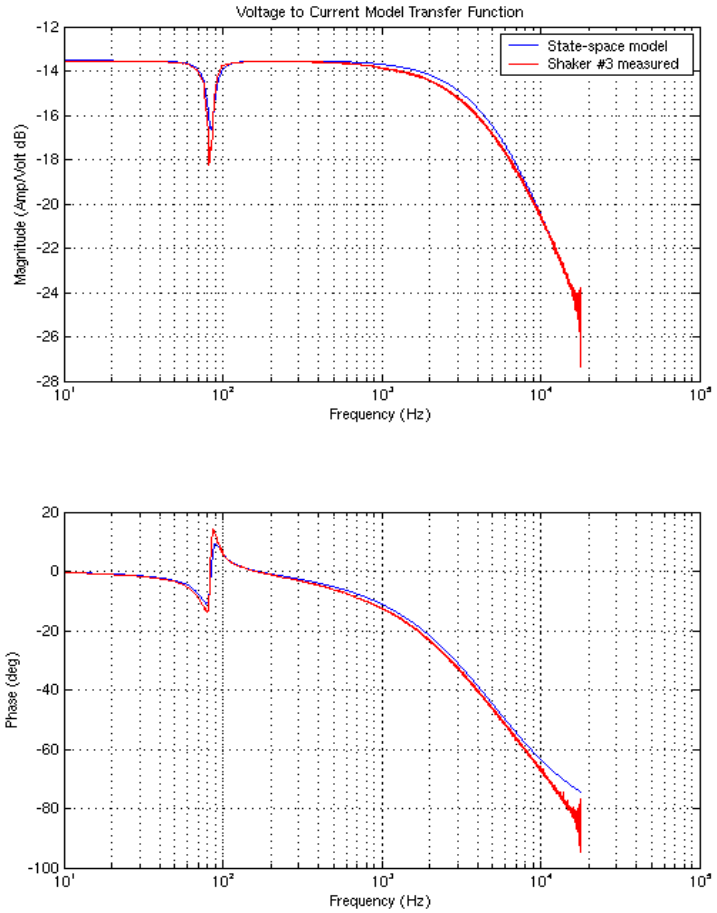

Figure 4.13 Bode plot of actuator clamped to a rigid bench compared to an analytical model[31].

4.2.4 Linearity of DAVA

A critical parameter of the DAVA is the power consumed by the actuator during operation. Particularly relevant in the case of orbit bound systems, the weight of the DAVA

system, including power sources, is to be minimized as much as possible. To determine the power requirements of the current DAVA system, two tests were conducted to determine the power consumption versus performance. The effectiveness is measured as the integration of the force autospectrum in the 50 to 300 Hz frequency band.

The first test evaluated the actuator in a blocked configuration, and measured the acceleration of the armature mass, input voltage, and input current. Shown in Figure 4.14 is the magnitude, phase, and coherence of the acceleration of the armature mass with respect to the input voltage. The legend on the graph indicates the average power consumption in Watts. The average power is defined as the mean product of the instantaneous voltage across the actuator and the instantaneous current across the actuator. Figure 4.14 indicates that as the input power is increased, the natural frequency decreases. This is due to variations in the spider plate stiffness with respect to the increased output. The magnitude of the transfer function is affected slightly as the power is increased, but it is mainly the overheating of the coil that deteriorates its performance. It is important to note the coherence between the acceleration and the voltage across the actuator, that starts to break down at 17.7 and 38.0 Watts, where the actuator was starting to overheat.

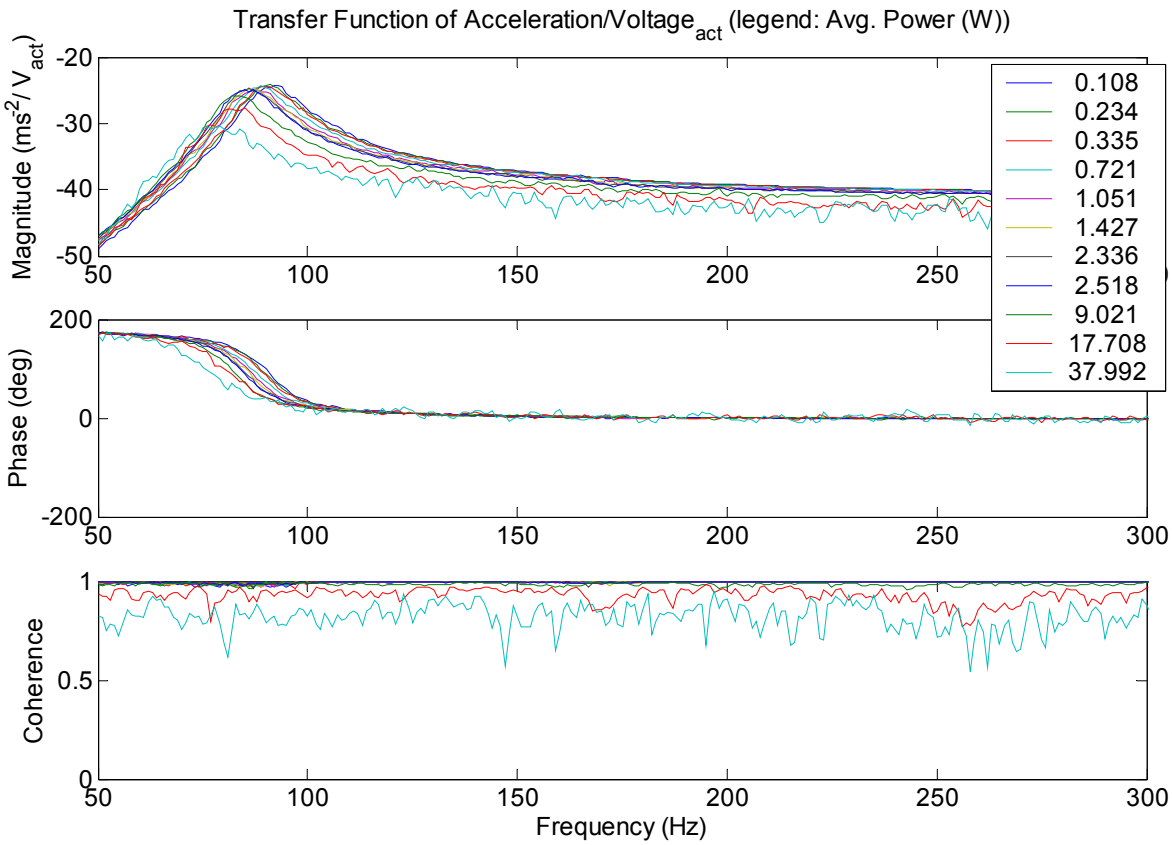

Figure 4.14 Magnitude, phase, and coherence of actuator in blocked configuration as input power was increased.

In order to obtain a true measure of performance, the autospectrum of the force generated by the actuator was computed. This was accomplished by computing the force through the relationship of magnet mass multiplied by the magnet acceleration. This autospectrum is shown in Figure 4.15, and indicates that the force generated by the actuator increases as the power increases. The natural frequency shift is also observable in this figure.

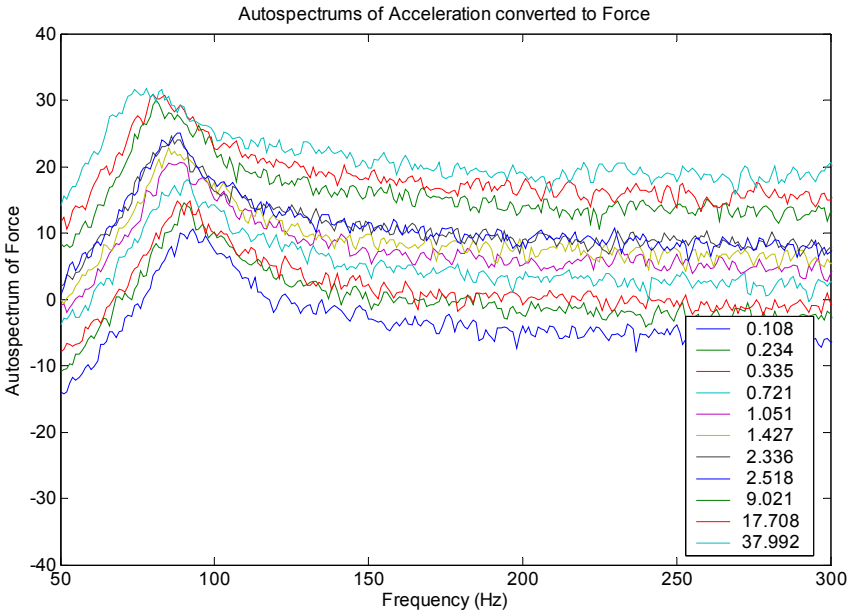

Figure 4.15 Autospectrum of force exerted by clamped actuator. Legend indicates power inputted in to the actuator in Watts.

Figure 4.16 shows the "effectiveness" as a function of input power. The effectiveness seems to be linear at low power levels, but then leads to a lower order relationship as the coil heats up and actuator becomes non-linear. This nonlinearity can be caused by the high displacements of the magnet stretching the spider plate stiffness into nonlinearity. Another possibility could be that the magnet is traveling out of the magnetic field generated by the coil into regions of nonlinearity. This nonlinearity is bad for active control because it produces "spillover" into higher frequencies.

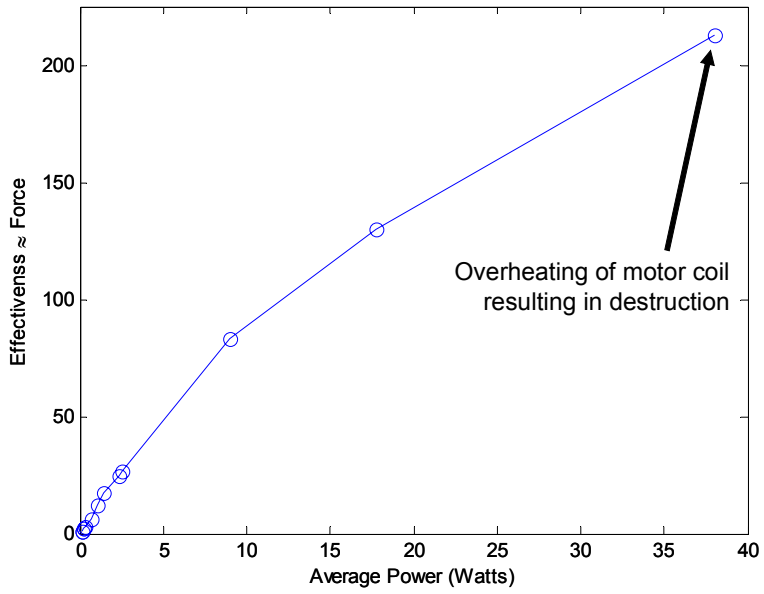

Figure 4.16 Integration of force autospectrum from 50 to 300 Hz versus average power supplied to actuator in clamped configuration.

The DAVA was also tested in its 2DOF configuration glued to the floor. An accelerometer measured the acceleration of the top plate, while input voltage and input current were also measured. Data collection was conducted in the same way as the actuator test, and all of the same data was collected. Figure 4.17 shows the transfer function magnitude, phase, and coherence of the top plate acceleration per input voltage. The DAVA configuration demonstrated a similar trend of decreasing natural frequencies for an increase in supplied power.

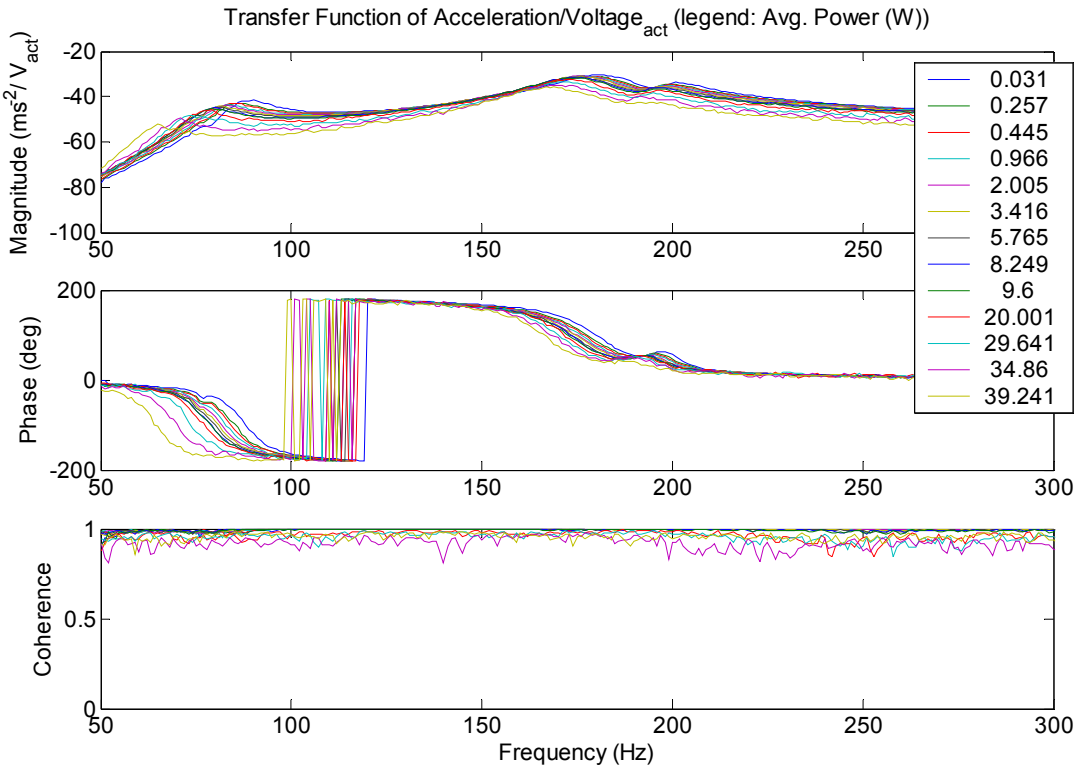

Figure 4.17 Magnitude, phase, and coherence of DAVA configuration as input power was increased.

The autospectrum was also computed for the DAVA configuration using the top plate acceleration data. The acceleration was integrated twice to find the top plate displacement, which was multiplied by the foam stiffness as a measure of the force exerted into the primary system, or in this case the ground. The force autospectrum is shown in Figure 4.18 and shows that the design requirements of the DAVA have been satisfied. As the supplied power is increased, the "effectiveness" increases steadily until it reaches its maximum performance. At which point, the actuator coil overheats and deteriorates the "effectiveness".

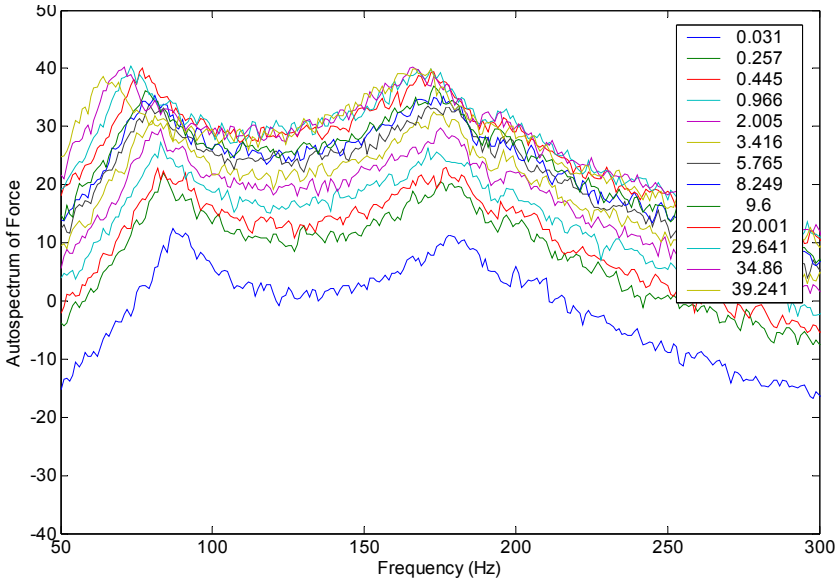

Figure 4.18 Autospectrum of force exerted DAVA glued to floor. Legend indicates power inputted in to the actuator in Watts.

The DAVA linearity can be seen in Figure 4.19. As in the clamped configuration, the DAVA "effectiveness" increases as a function of input power linearly until it reaches a peak performance at about 30 Watts. At this point, the coil either overheats or the glue bond overheats and breaks the bond between the actuator and the DAVA plate. The same nonlinearity is exhibited in the DAVA. This implies that the nonlinearity is due to the actuator.

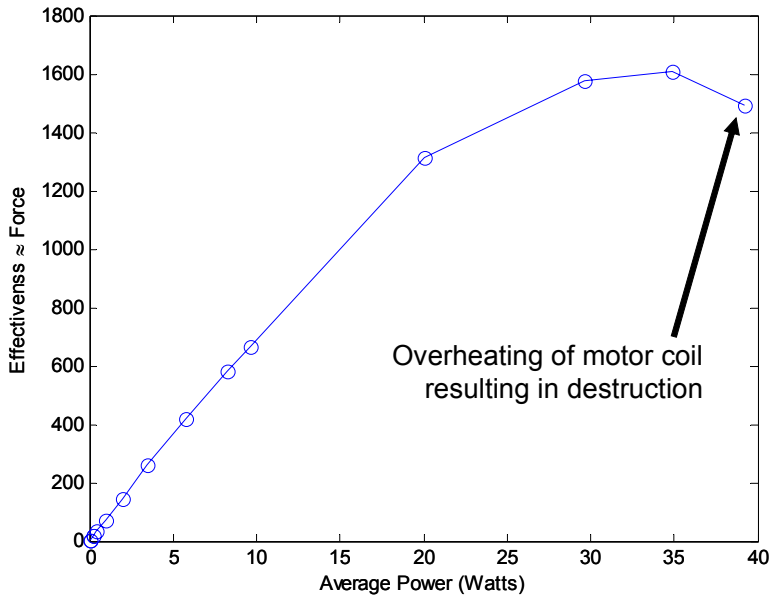

Figure 4.19 Integration of force autospectrum from 50 to 300 Hz versus average power supplied to actuator in clamped configuration.

4.3 Analytical Model of DAVA

The first objective in the DAVA design process was to develop methods to measure each of the DAVA parameters. Next, the actuator components were modified to optimize its performance. Lastly, the DAVA plate and foam sizes were optimized using a model of the DAVA and its performance. An analytical model developed in MATLAB was used to evaluate the DAVA performance as a function of the DAVA plate mass and foam stiffness. This section will detail the modeling of the DAVA, experimental validation of the model, and the optimization of the DAVA design with respect to foam size and stiffness and plate mass.

4.3.1 Analytical Modeling of DAVA

First the dynamics of the DAVA were described as a 2DOF system as shown in Figure 4.20. The force generated by the DAVA and exerted into the primary structure per unit of force generated by the actuator is written as

$$\frac{F_{DAVA}}{F_{act}} = \left(k_1 + i\omega c_1\right)\frac{X_1}{F_{act}} \tag{4.5}$$

where the term X_1/F_{act} is written as

$$\frac{X_1}{F_{act}} = \frac{1}{K + i\omega C - \omega^2 M}\begin{bmatrix} 1 \\ -1 \end{bmatrix} \tag{4.6}$$

In this expression, the parameters are defined as

$$M = \begin{bmatrix} m_1 & 0 \\ 0 & m_2 \end{bmatrix}; \qquad K = \begin{bmatrix} k_1 + k_2 & -k_2 \\ -k_2 & k_2 \end{bmatrix}; \quad C = \begin{bmatrix} c_1 + c_2 & -c_2 \\ -c_2 & c_2 \end{bmatrix} \tag{4.7}$$

as shown in Figure 4.20.

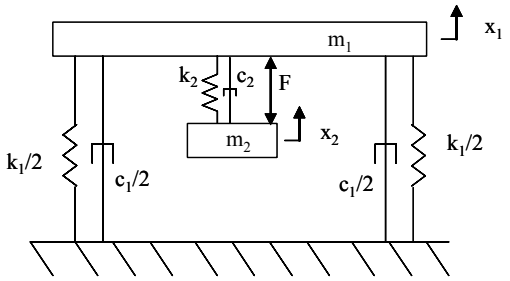

Figure 4.20 Free body diagram of DAVA with reciprocal force acting between masses.

Since the target frequency band is from 50 to 200 Hz, the "effectiveness per unit mass", *E*, is considered the integration of the force exerted over this frequency band divided by the total mass of the system. This is written as

$$E = \frac{\sqrt{\int_{50\,Hz}^{200\,Hz} \left(\frac{F_{DAVA}(f)}{F_{act}(f)} \right)^2 df}}{\alpha m_2 + m_1} \tag{4.8}$$

where F_{DAVA} is the force exerted by the DAVA, F_{act} is the force exerted between the two masses, m_1 and m_2 are the plate and magnet masses respectively, and α is a weighting factor that accounts for the mass of the electronics necessary to drive the actuator. There is currently no cost associated with this detriment; therefore the variable, α, is used to estimate various levels of consequence. This detriment is not factored into m_1 because there is no additional mass associated with increasing the plate mass. The RMS of the force ratio is integrated over a frequency band of 50 to 200 Hz, as shown in Figure 4.21. The square root of this value is then divided by the sum of the plate mass and weighted magnet mass.

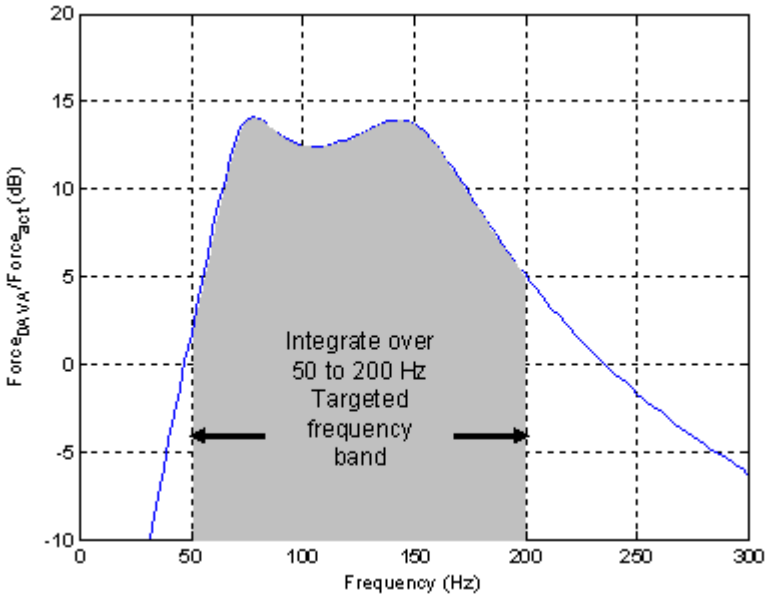

Figure 4.21 Integration of force transfer function to estimate effectiveness of DAVA, equation (4.8).

Using the effectiveness per unit mass, *E*, as the performance criterion or cost function, the model was run with varying plate mass and foam stiffness. Figure 4.22 shows the three dimensional results of the model evaluating variation in foam stiffness and plate mass for the Booth 2 actuator with a mass weighting factor α equal to one. The optimal foam stiffness and plate mass will dictate the design of the DAVA. Notice the high performance associated with very low plate mass. When the mass is very low, the effectiveness is greatly increased due to the division of the effectiveness by the total mass. However, this effect does not bias the optimization because the minimum weight of the plate is constrained to 100 grams: the weight of the 70 gram actuator shell plus about 30 grams for the smallest size plate, about 4" x 4", necessary to mount the actuator. The actuator shell is included in the plate mass because it is rigidly glued to the plate.

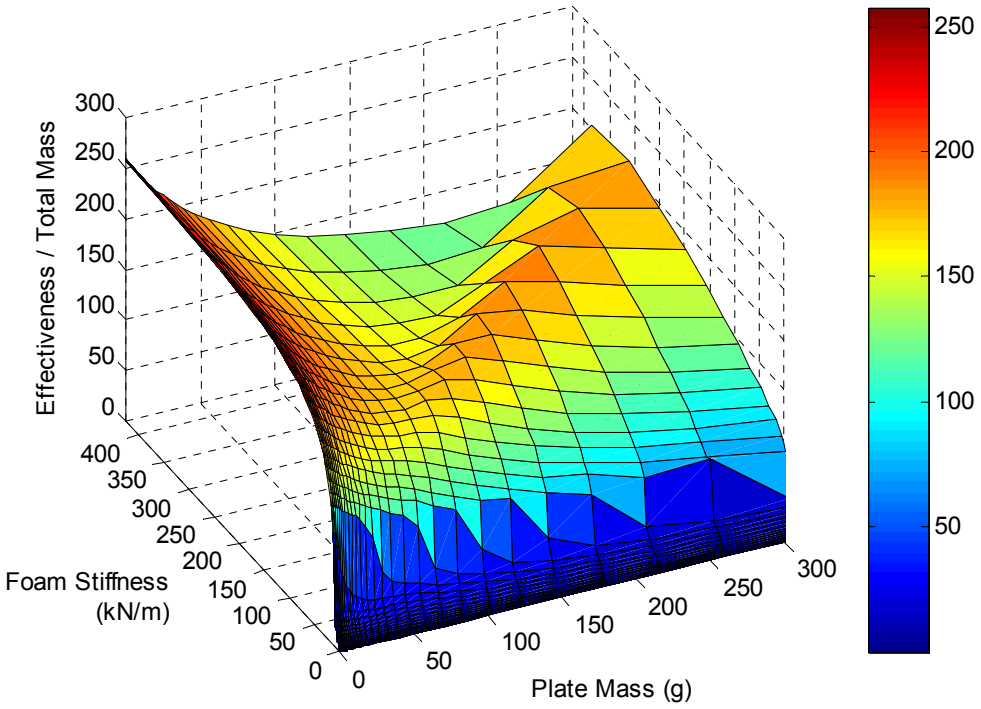

Figure 4.22 Analytical model of DAVA with varying plate mass and foam stiffness. DAVA "effectiveness", *E*, is the performance measure that accounts for force exerted over targeted frequency band.

Taking into account the 100 gram plate mass limit, it can be seen that there is a ridge along the three dimensional plot, shown in Figure 4.23. The optimal DAVA is along this ridge, but the data does not indicate a clear dominate peak.

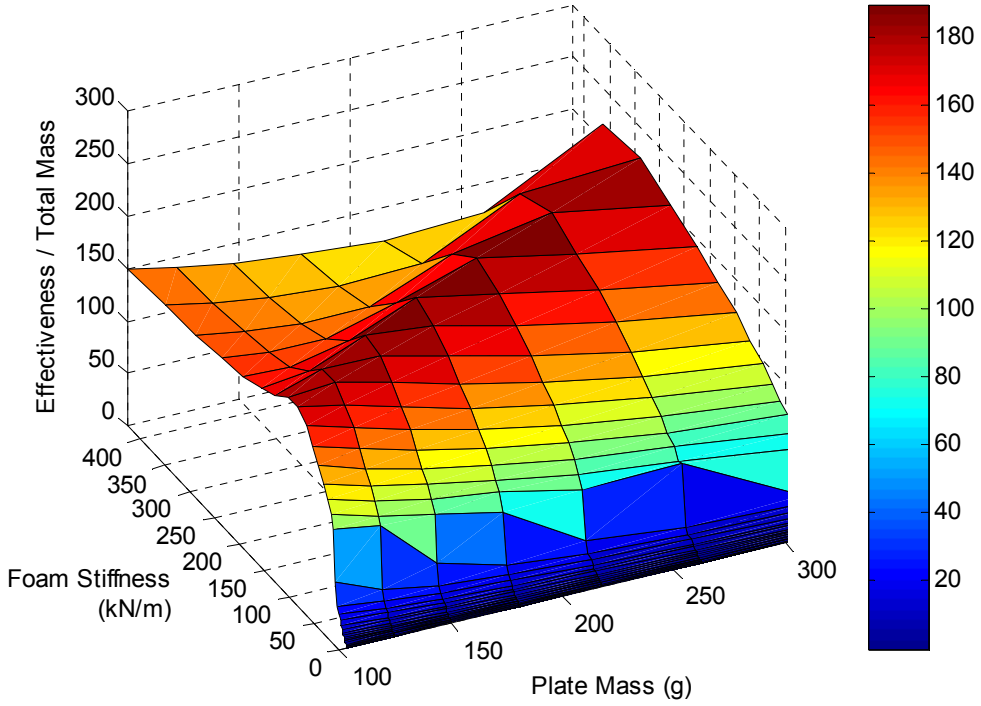

Figure 4.23 Analytical model of DAVA with varying plate mass and foam stiffness. The plate mass is limited to values over 100 grams because of the weight of the actuator shell.

To gain a better perspective on the optimal plate mass and foam values, a contour plot is shown in Figure 4.24. In this figure, it can be seen that there is a minimum foam stiffness of about 125 kN/m required to attain an optimal level of performance. For optimal performance, as the design is enlarged, the plate mass should be increased proportionally with an increased foam stiffness.

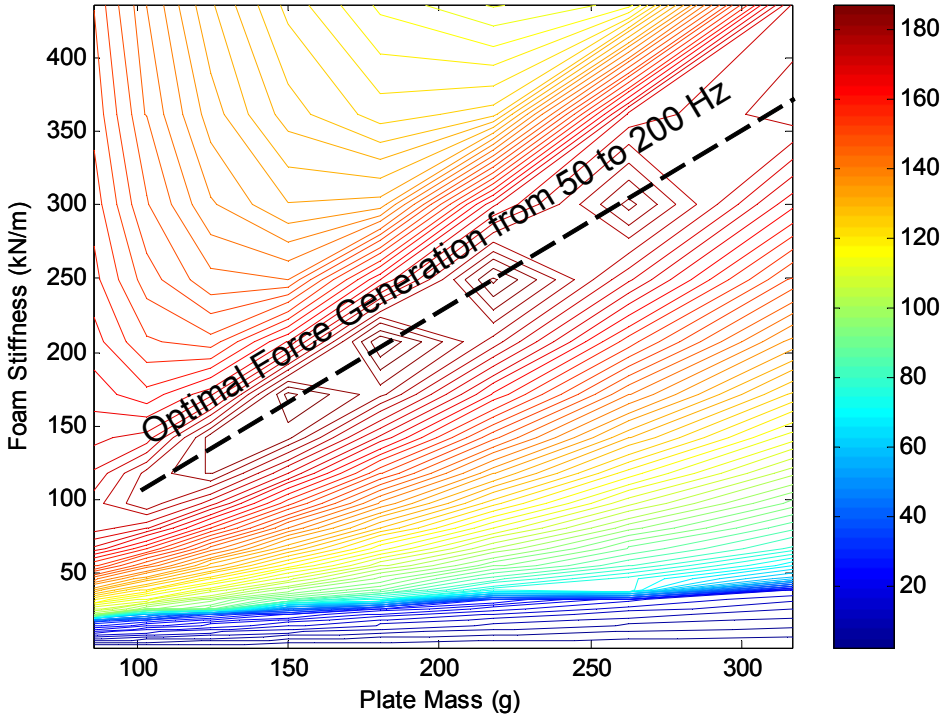

Figure 4.24 Contour plot of analytical model indicating optimal designs for DAVA parameters.

4.3.2 Experimental Validation of DAVA Model

Before the analytical model of the DAVA can be utilized to choose a design, it must be validated through experimental results. This validation is performed by producing several different sizes of DAVAs, evaluating the effectiveness per unit mass, *E*, of each design, and then comparing the experimental results to the results of the analytical model. Several examples of the force generated by the DAVA are shown in Figure 4.25.

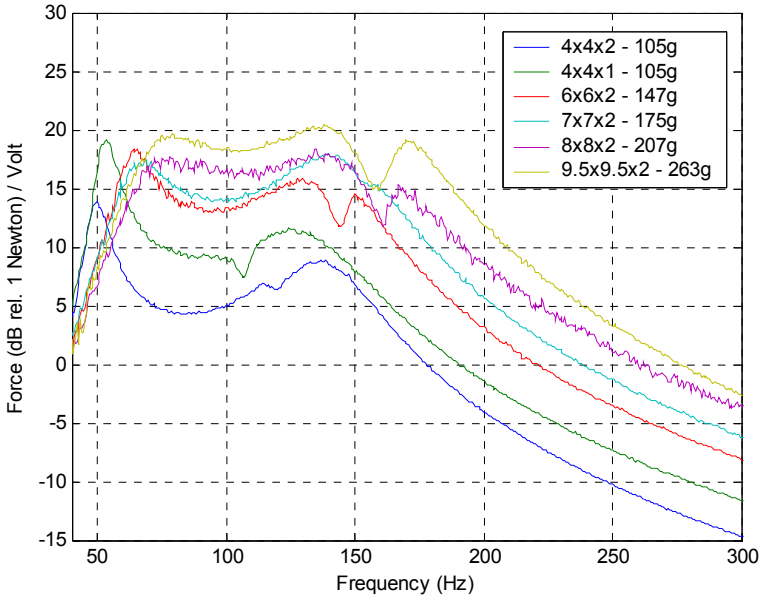

Figure 4.25 Experimental results of different DAVA sizes and masses, used to validate analytical model.

Shown in Figure 4.26 is the overlay of experimental results, marked as X's and scaled as a measure of effectiveness, over the analytical model results for varying plate mass and foam stiffness. The x-axis represents the total passive lumped mass, which includes the actuator shell (70 grams), the honeycomb plate, and ½ of the weight of the foam. The passive lumped mass is mainly influenced by the varying size of the honeycomb plate, which is about two grams per square inch. A lighter and less rigid plate was used for a 7" x 7" x 2" size DAVA to evaluate the effects of a lighter plate mass. The lighter board allowed the for a lighter plate mass while still using a large cross section of foam and thus a large foam stiffness. While the large foam stiffness helps the force output, the reduction of plate mass negatively influenced the results. Use of the lighter plate and metal washers glued to the plate, created more data points on the graph.

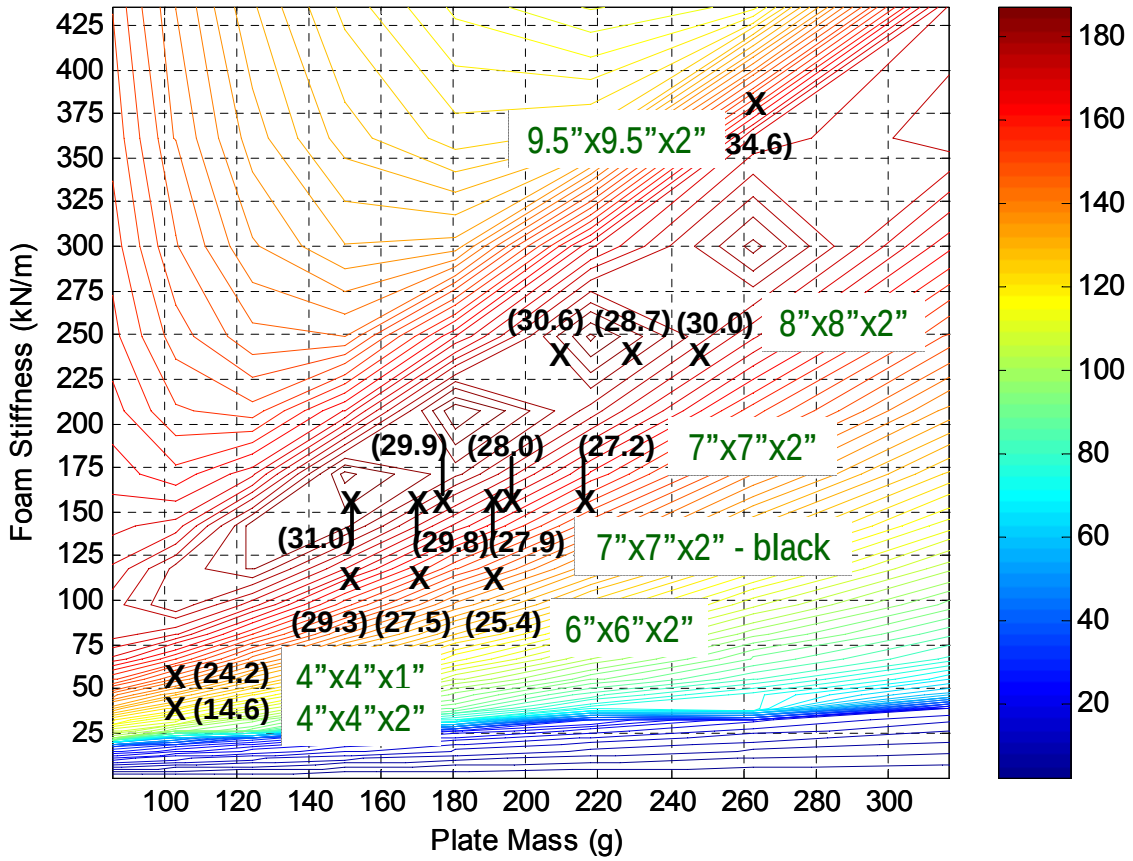

Figure 4.26 Experimental validation of analytical model, which shows effectiveness as a function of varying plate mass and foam stiffness.

Overlaid on the analytical contour plot, the experimental data points indicate that the model trends are consistent with the data obtained through experimentation. The initial DAVA prototype designs were of the sizes 4” x 4” x 2” and 4” x 4” x 1”, which produced poor experimental results compared to future designs. The analytical model was then developed, and these early designs fell on regions of poor effectiveness. Later designs were constructed that fell much closer to the optimum effectiveness line in the analytical model. These models were shown to have a much higher value of effectiveness per unit mass in the experimental results.

Along with performance, the designs of the DAVA were also influenced by the ease of production. One factor was that the foam was provided in 9.5” wide by 48” long strips. Since the design was always limited to a square, in order to simplify the dynamics of the device, the size was limited to a cross section of 9.5” x 9.5”. These foam strips were supplied with a thickness of 2”. As mentioned, the foam stiffness can be increased by decreasing the thickness.

However it is necessary to make accurate cuts as an uneven foam surface can have a large effect on the stiffness.

Upon evaluation of the model and experimental data, the 9.5" x 9.5" x 2" DAVA design was chosen to be used on the cylinder. This design allowed for fast, easy production, provided the largest possible DAVA given the supplies of foam available, and was the most "effective". To estimate the advantage gained by using a DAVA in place of a point actuator, the "effectiveness" was computed for both devices using equation (4.8). The result is 32% greater effectiveness for the DAVA.

4.4 Conclusions

This chapter presented the analytical and experimental design and characterization of a DAVA to be used to attenuate structural vibration on a scale model of a payload cylinder. The effect of each of the DAVA mechanical and electrical components on its "effectiveness" was described. Testing methods were then established and used to optimize actuator parameters such as the spider plate stiffness, magnet mass, and magnetic air gap. An analytical model of the DAVA was also developed to measure the effectiveness per unit mass as a function of these parameters. This was validated by experiment for several data points on the performance plot. Using the optimal design, eight prototype DAVAs were built, and their electro-mechanical properties and power consumption were tested. Compared to the point actuator, it was shown to be 32% more "effective".

Chapter 5: Experimental Results of DAVA on Cylinder

This chapter will present the results of applying the final DAVA design developed in chapter four to the scale Boeing fairing. To reduce the interior sound pressure level of the fairing, the DAVA actuators were used in a feed-forward control system designed at Virginia Tech and operated by Arnaud Charpentier of Vibro-Acoustic Sciences, Inc. (VASci) and Virginia Tech professor Dr. Marty Johnson. The control architecture that was used was multiple-input multiple-output (MIMO) adaptive feed-forward active structural acoustic control (ASAC). This work and the results presented in this chapter are based on and include figures from a VASci project report[32]. It is included in this thesis in order to demonstrate the successful implementation of DAVAs with a multi-channel control system.

5.1 Cylinder Background and Test Goals

The cylinder provided by Boeing is made of a honeycomb core and a graphite epoxy skin; and it measures 2.8 meters long and 2.46 meters in diameter. This prototype is a reduced scale of the cylindrical portion of the Delta IV payload-fairing model, shown in Figure 5.1[33]. The cylinder ends are capped by 5.7 cm thick-layered plywood stiffened by aluminum I-beams. In order to create a sealed and continuous boundary condition, the cylinder is slotted in the end cap. The structural characteristics of the test cylinder were obtained experimentally in October 2001.[33]

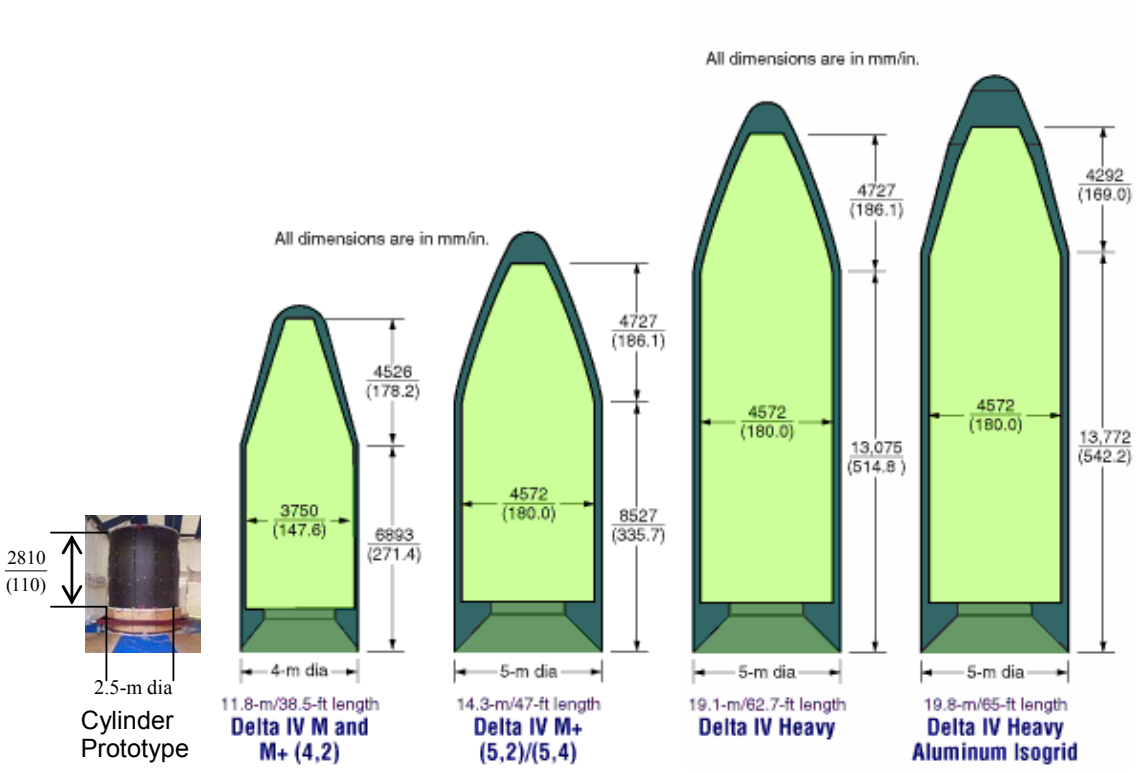

Figure 5.1 Size comparison between the prototype and the Boeing Delta IV payload fairing family.[33]

Of the experiments discussed throughout this chapter, the goals are to: (1) determine the acoustic response that can be generated by the eight DAVAs glued to the interior wall of the cylinder; (2) determine the control performance of the DAVAs within the targeted frequency bandwidth; (3) determine the response/efficiency of the DAVAs under different levels of primary field sound pressure levels (SPL)s; and (4) examine the relationship between power consumption of the DAVAs and performance to establish whether the DAVAs can provide sufficient control to actual launch environments.

5.2 Test Setup

The location of the test site was chosen to be the Virginia Tech Airport, in Blacksburg, Virginia. This location was chosen because it provided the space and isolation necessary to conduct such a loud and large-scale experiment. A 30’ x 30’ x 16’ tent was used to shelter the cylinder, speakers, and sensors; and an 8’ x 20’ trailer was used to house and secure the data acquisition equipment for the duration of the test. Powering all of this equipment was a 60 kW

generator positioned 100 feet away from the test setup. This test site and layout is shown in Figure 5.2 and Figure 5.3.

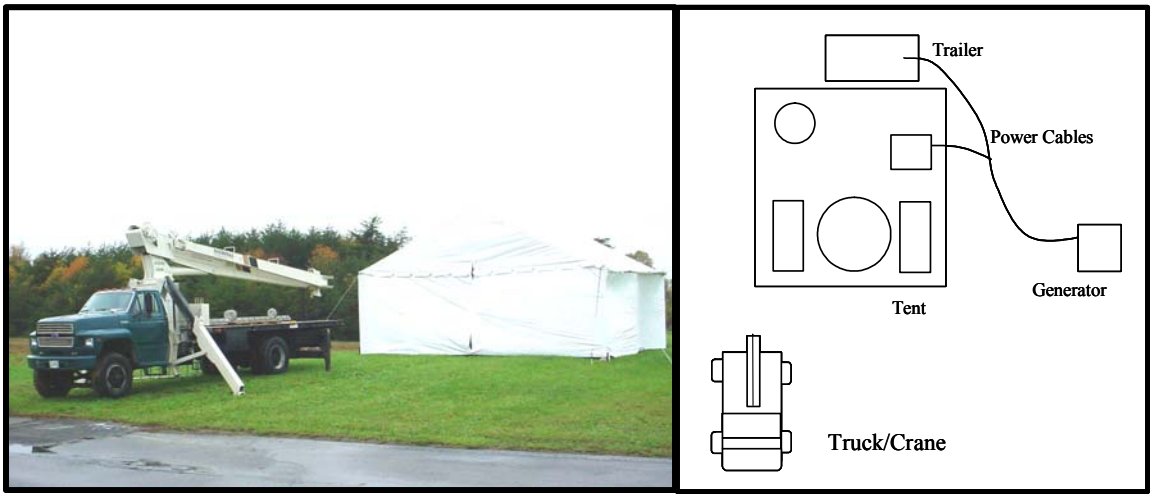

(a) (b)

Figure 5.2 (a) Photograph of crane and tent at test site. (b) Diagram of test site layout.

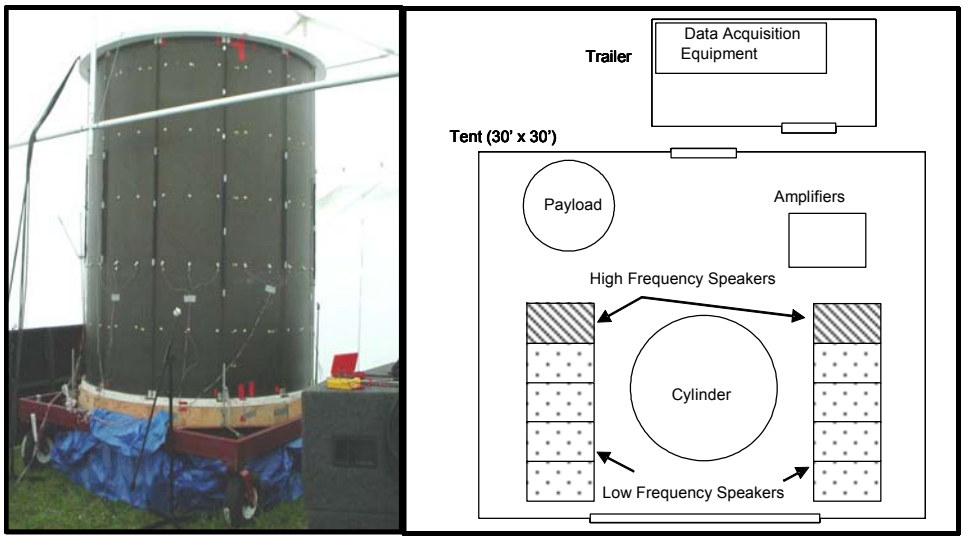

(a) (b)

Figure 5.3(a) Photograph of cylinder inside tent. (b) Diagram of test site layout.

5.2.1 Acoustic Disturbance

External acoustic disturbances of up to about 130 dB were generated with two walls of eight speakers, one on each side of the cylinder, as shown in Figure 5.4a. The Nexo B-1 speakers are equipped with 15" drivers and have frequency band ranging from 38-600 Hz. This speaker system was driven by a digital controller (to avoid speaker overload) and four 5000 Watt

Crown MA 5002vz amplifiers as shown in Figure 5.4b. For the tests requiring higher frequencies, four Nexo M-3 Mid frequency speaker cabinets were used. Two high frequency speakers stacked on each side of the cylinder, a second digital controller, and two extra Crown amplifiers were necessary to complete the sound generating system. Two independent noise generators fed each speaker bank in order to maintain two uncorrelated sources.

This test configuration was intended to simulate the launch environment experienced by the actual Boeing payload fairing. "The sound produced tends to be broadband in nature and propagates up the side of the launch vehicle fairing as a plane wave at a reasonably sharp oblique angle of incidence."[32]

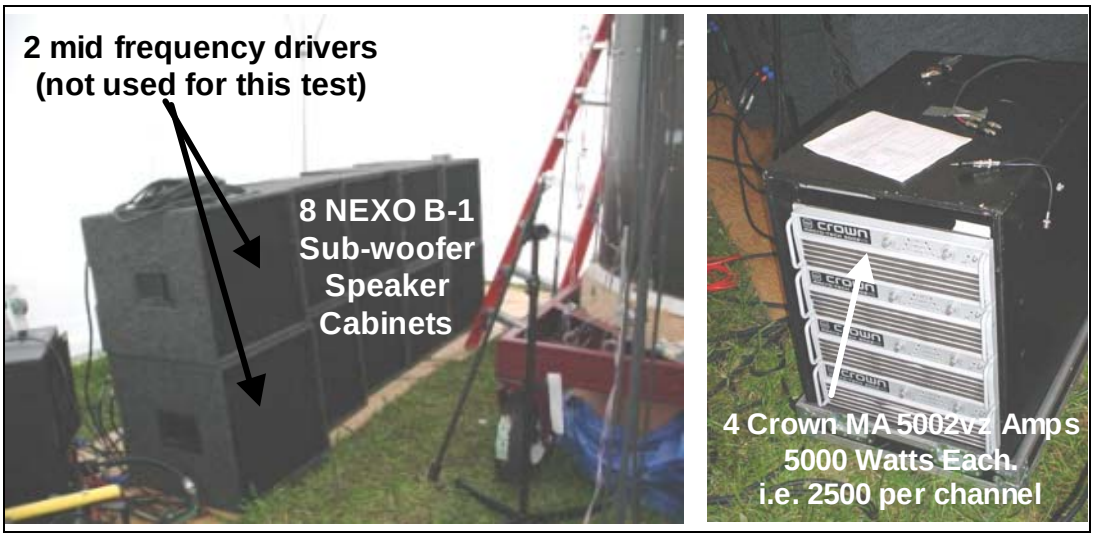

(a) (b)

Figure 5.4(a) Photograph of ten Nexo speakers equipped with 15" drivers. (b) Photograph of four 5 kW Crown amplifiers, which were used to power the speakers.

5.2.2 Data Acquisition

All data acquisition (DAQ) was performed using Lab View software specifically developed by Jamie Carneal and Rick Wright of Virginia Tech to record a maximum of 96 channels simultaneously. Nearly all tests were recorded once in the frequency domain, and once in the time domain to provide a level of redundancy. The frequency measurement records the auto-spectrums of each channel, and the real and imaginary cross-spectrum elements of each channel with a specified reference channel (typically the input to one of the walls of speakers). About 25 to 30 seconds of time data was recorded to validate the frequency response function (FRF) computations and serve as backup data. Often, low level testing was also performed to

validate the accelerometer measurements that might have clipped the dynamic range of the DAQ during high level excitation.

5.2.3 Reference Sensors

Four external microphones, type 4135/4136 B&K ¼", were used to characterize the disturbance signal applied to the cylinder. "Two of the four microphones were used as reference sensors. No more than two reference sensors were required because the most complex disturbance case was two uncorrelated sound sources, each with a strong spatial correlation (incident and diffracted plane wave)."[32] These microphones are shown in Figure 5.5[32].

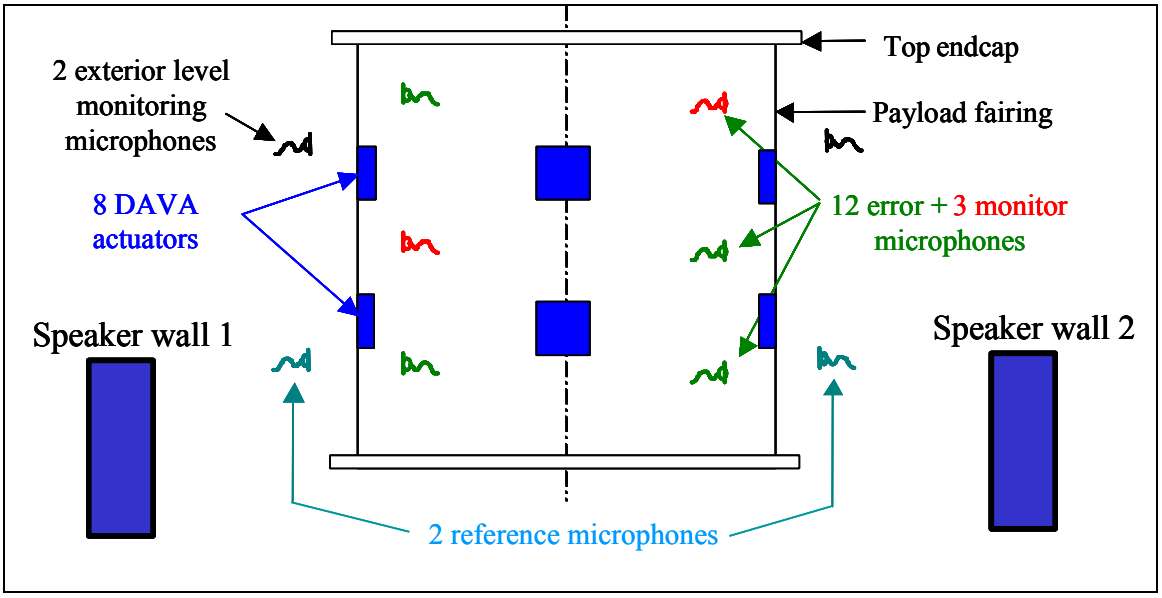

Figure 5.5 Reference sensors and DAVA positions on cylinder.[32]

5.2.4 Error and Monitoring Sensors

Fifteen 40PR ¼" G.R.A.S. microphones were used to measure the SPL inside the cylinder. "Twelve of these microphones were used for the ASAC controller as error sensors. The other three were monitoring sensors (for global control performance evaluation)."[32] The fifteen microphones were equally spaced 72° apart around the cylinder in three rings of five (top, middle, and bottom). These microphones have a dynamic range of 146 dB to accommodate the high sound pressure levels generated during testing. Figure 5.6 indicates the internal and exterior microphone positions.

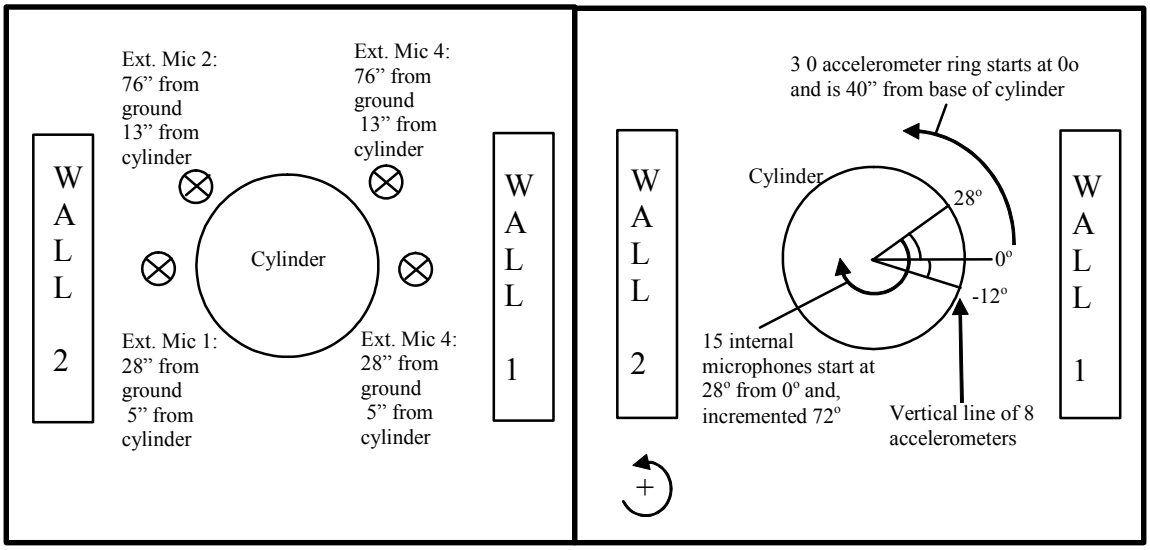

Figure 5.6 Repeated diagram of test setup to show microphone and accelerometer sensor locations.

A ring of 30 accelerometers was fixed with wax to the exterior at a height of 40” from the bottom end-cap of the cylinder, seen in Figure 5.7. Also, a vertical line of 7 accelerometers located at minus 12^{o} from the zero axis was attached in order to capture the axial modes indicated in Figure 5.6 and seen in Figure 5.8.

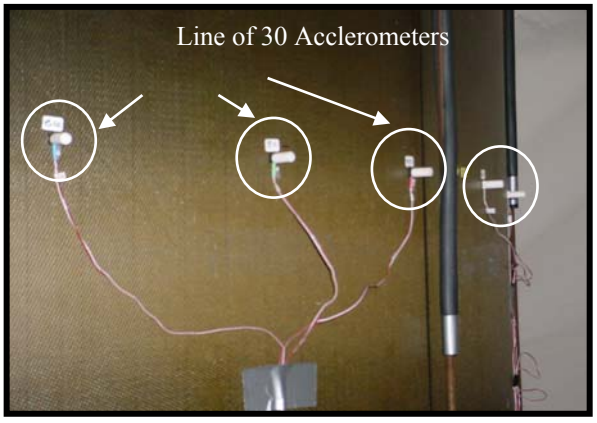

Figure 5.7: Ring of accelerometer waxed on the cylinder.

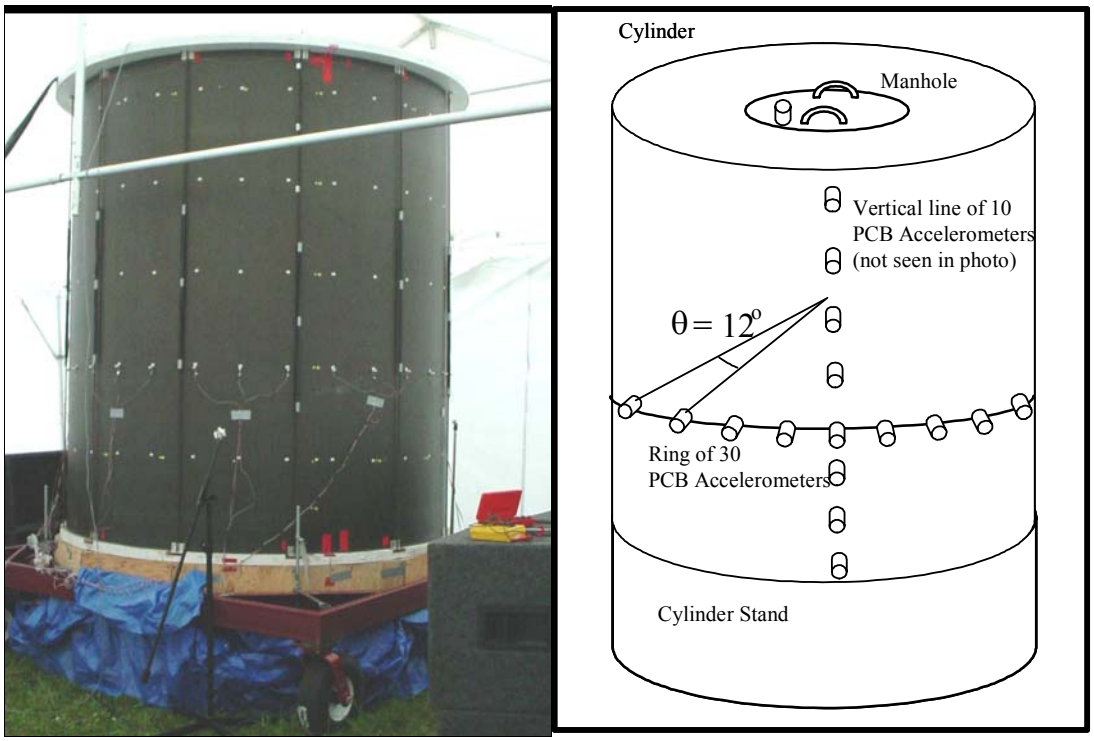

Figure 5.8 Photograph of cylinder with diagram indicating accelerometer positions.

5.2.5 DAVA Positioning

The 9.5" x 9.5"x 2" DAVAs were taped to the interior of the cylinder with double sided tape. Because of the curvature of the cylinder, square edges of the on the DAVA's foam block needed to be slightly curved to fit against the cylinder wall. This was done by taping sheets of sandpaper onto the interior cylinder wall, and rubbing the foam blocks on the sandpaper. The foam was shaved into a shape matching the curvature cylinder wall.

A total of eight DAVAs were used in the testing. They were positioned in two rings of four actuators, separated by 90^{o} and located a third of the distance from the top of the cylinder and a third of the distance from the bottom of the cylinder. This is shown in Figure 5.5.

5.3 Test Results

This section presents the experimental results collected in order to accomplish the goals stated earlier in this chapter. The experiments conducted include: (1) the measurement of the acoustic response generated independently by each of the eight DAVAs; (2) an analysis of the global attenuation attained by the DAVAs within the targeted frequency bandwidth; (3) a study of the effect different primary field levels have on the DAVAs control performance; and (4) the

measurement of voltage across and current through one of the DAVA actuators for varying primary field levels.

The tests were performed with a multiple coupled channel controller in outdoor, free field conditions at various primary filed levels ranging from 100 to 130 dB. The attenuation results are presented in integrated one-third octave frequency bands; a commonly used benchmark for evaluating fairing noise reduction.

5.3.1 Acoustic Response of the DAVAs

The acoustic response of each DAVA actuator was measured to first establish each DAVA as a properly functioning actuator, performing similarly to each other, and second to verify that their control authority is sufficient for quality active control. Knowing the SPL generated by the DAVAs is also useful as a baseline for future DAVA designs. The SPL measurements for each DAVA were space-averaged at the 15 interior microphone locations. The one-third octave bands for each actuator are shown in Figure 5.9. The DAVAs show similar control authority with respect to each other, and indicate an efficient actuation range over the 80 to 160 Hz frequency band.

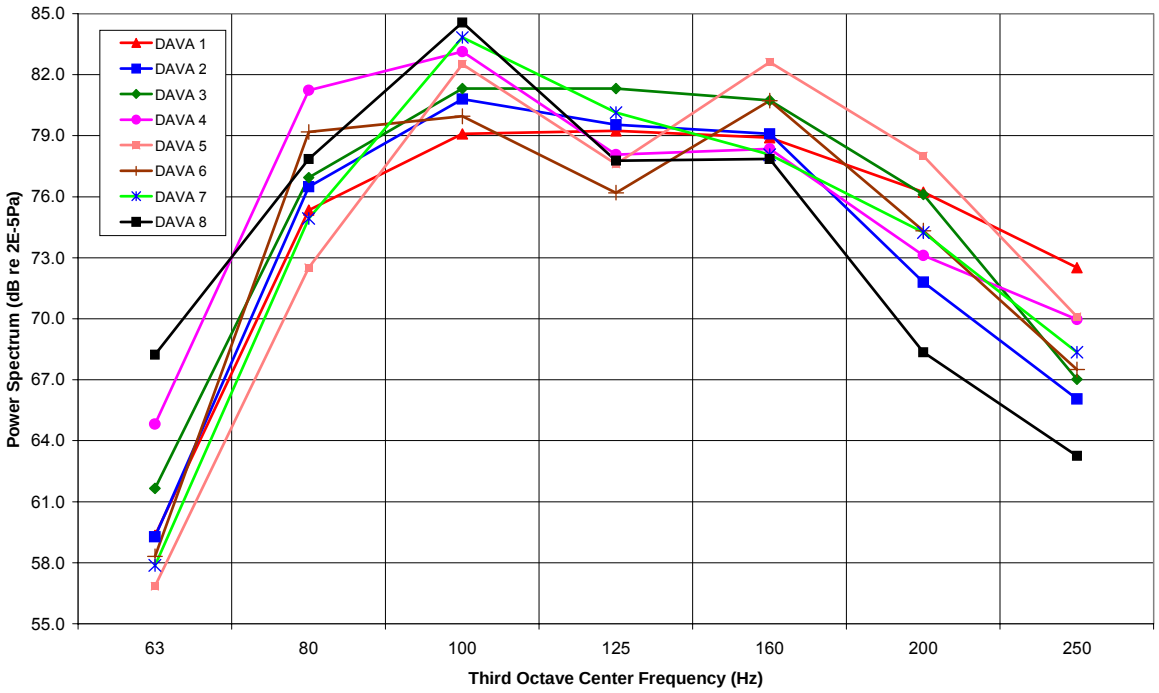

Figure 5.9 Mean square pressure level inside the fairing per unit input voltage to the DAVA[32].

5.3.2 DAVA Performance for Low Level Excitation

The first measurement of the DAVA performance was conducted with two independent primary sources running at low level (100 dB), using two reference microphones near the disturbance. Note that a measurement of the coherence between the disturbance signal (referred to as the ideal reference) and the non-ideal microphone sensors showed a coherence of over 0.985, confirming that the excitation system can be assumed linear. Therefore, using different reference sources does not significantly affect the results. Figure 5.10 shows the performance of the DAVAs at the error microphones with the control on (red) and control off (blue). The attenuation at the error microphones over the 70 to 200 Hz frequency band is 4.9 dB, with peak attenuations of 9 dB at resonance frequencies at 78 and 140 Hz. The results are the space-averaged control performance for the 12 error sensors located inside the fairing. This test is summarized as test 1 in **Error! Reference source not found.**.

Table 5.1 Summarization of experimental results of DAVA control testing[32].

Test ID		1	2	3	4	5
Number of disturbances		2	2	2	2	2
Disturbance level		low	low	moderate	large	high
Exterior level (in dB [40-250] Hz)		101	100	117	125	130
Number of references		2	2	2	2	2
Reference type		mic near disturbance	ideal	ideal	ideal	ideal
Broadband attenuation (in dB [70-200] Hz)	Error mics	4.9	9.3	7.9	6.6	5.7
	Monitor mics	4.7	7.7	7.2	6.8	6.1
	Coherent limit	14	13	13	12	13
DAVA Power consumption (in W [40-300] Hz)		0.03	0.04	1.7	16	25
Convergence time (min)		> 5	> 5	> 5	> 5	< 1

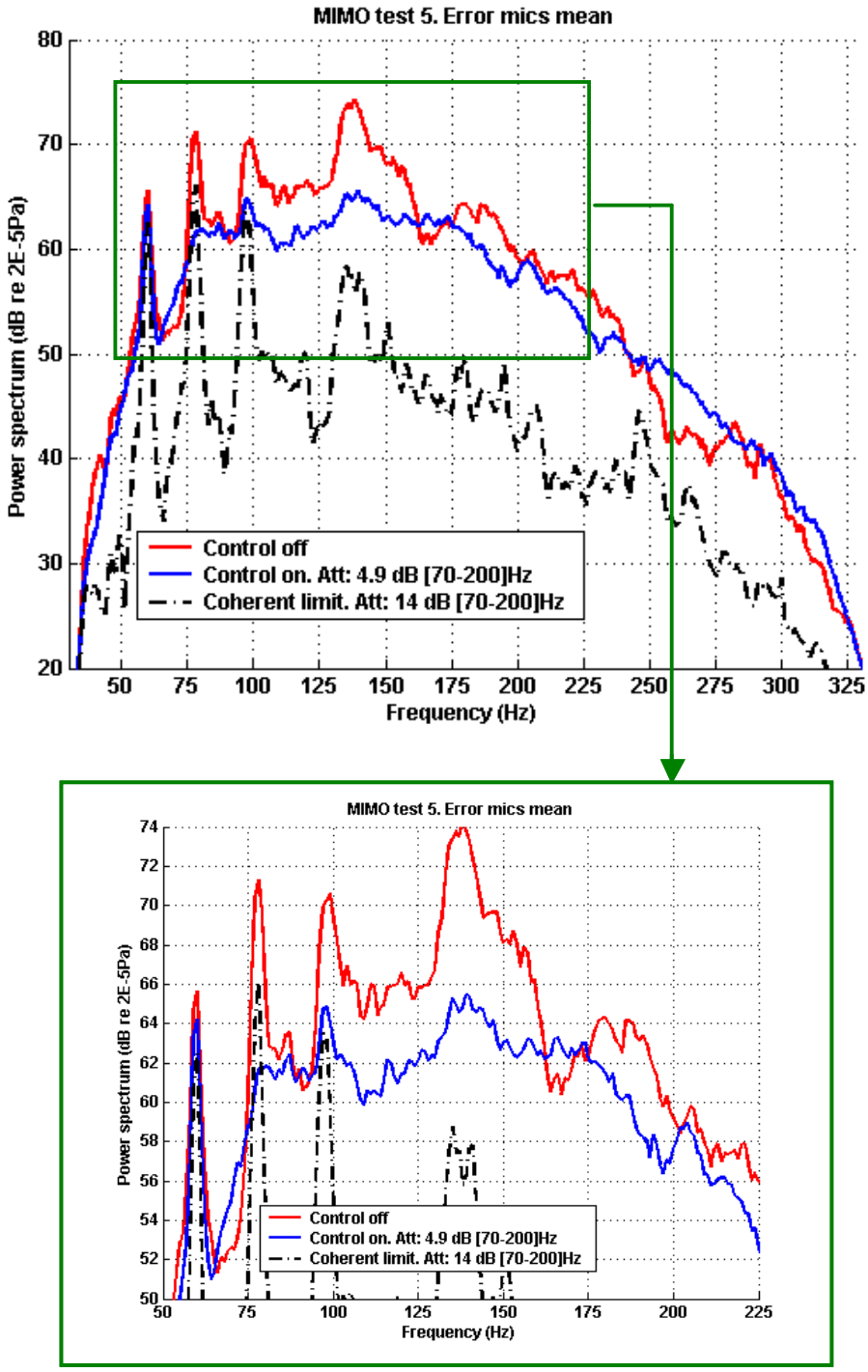

Figure 5.10 DAVA performance at low excitation level, 100 dB[32].

5.3.3 DAVA Performance for Increased Primary Field Levels

Another goal of the experimentation was to evaluate how high of an external primary field level the actuators could control. This was explored by performing four experiments of

increasing levels of the primary field, as shown as Test IDs two through four in **Error! Reference source not found.**. Each test used both speaker banks as independent disturbances, and each disturbance signal was used as an ideal reference for control. The exterior primary field levels were varied, producing levels of 100, 117, 125, and 130 dB. Figure 5.11 shows the mean one-third octave band attenuation of the 12 error microphones inside the fairing. The figure shows that the attenuation is significant, over 7 dB, across the 80 to 200 Hz octave bands for low level excitation. And while the performance deteriorates as the exterior primary field is increased, attenuation of over 3 dB is achieved for even the highest excitation level across a significantly broad band of frequencies. It should also be noted that only eight actuators were used in this experiment, whereas a greater number of actuators could significantly improve performance.

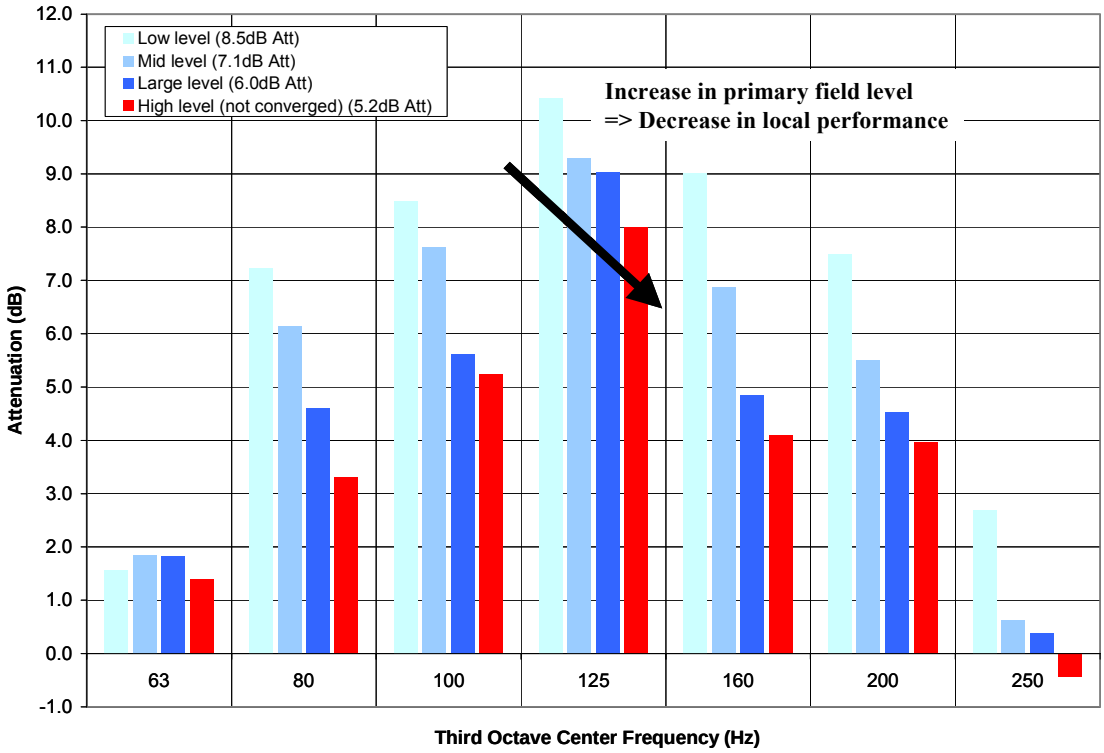

Figure 5.11 Affect of primary field level on the DAVA control performance[32].

5.3.4 DAVA Power Consumption

The previous section indicates a decrease in DAVA performance as a function of increasing primary field. When the primary field is increased to high levels, the DAVA is supplied with greater power, which is necessary to achieve control over the enhanced vibrations.

And it seems as though the DAVA can not handle the increased load supplied during the high level excitation. But by looking at the voltage across and current through one of the DAVAs, the problem may not lie within the DAVA, but rather the amplifier powering the DAVA. Power data from section 4.2.4 shows that the DAVAs can handle an average power of about 35 Watts of average power before their performance starts to deteriorate. During the high level testing, the DAVAs were supplied with a control voltage ranging from 10 to 12 VRMS, producing about 20 Watts of average power. This leads to the examination of the power amplifier used during testing. Figure 5.12 shows the time history of the DAVA voltage, current, and top plate acceleration. The top plot shows how the voltage across the actuator is flat, and appears to be a clipped signal. Likewise, the spikes in the current plot could indicate a clipping amplifier. If the problem did lie within the amplifier, and not the DAVA, there is reason to suggest that the DAVA could perform even better at high excitation levels. Future high level testing should again include the monitoring of the DAVA voltage and current, as well as the monitoring of the amplifier clipping.

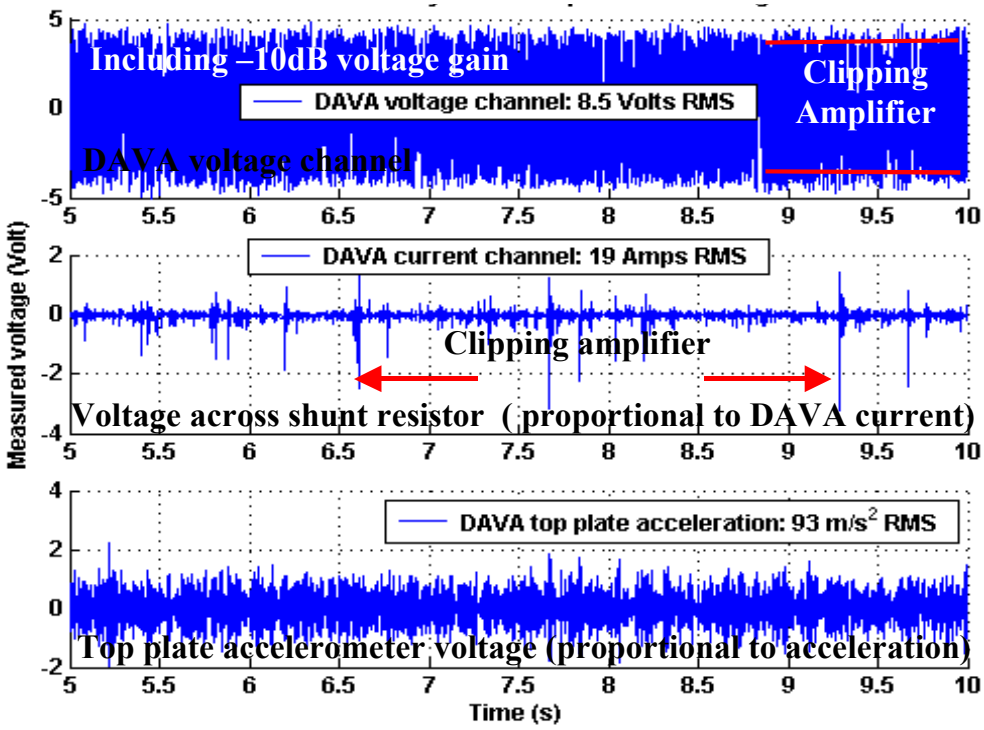

Figure 5.12 Time history of the voltage, current, and top plate acceleration of DAVA#5 during high level control testing[32].

5.4 DAVA Test Conclusions

Based on the work conducted by VASci and Virginia Tech, the goals of the DAVA testing have been met. The acoustic response of the DAVAs was characterized and indicates a band of resonance over the desired frequency band. This performance was demonstrated on the cylinder by the attenuation within the targeted bandwidth of about 5 dB, including peak reductions as high as 9 dB. The DAVA performance was also observed as a function of external SPL excitation and demonstrated good capability in the targeted bandwidth for even the highest tested level of excitation. Also, the power consumption was explored and discussed with respect to existing tests. Overall, the testing accomplished the experimental goals, and provides quality support of the DAVA design process.

Chapter 6: Conclusions and Future Work

This chapter will restate the goals set out at the beginning of this research, review the results and conclusions that can be made from the work performed, and suggest future work that will aid in the development of these concepts.

6.1 Conclusions

This thesis presents an investigation of the use of passive MDOF DVAs and active DAVAs for the control of structural vibration of distributed systems. Chapters two and three focused on the use of passive MDOF DVAs in comparison to multiple SDOF DVA systems. The goal was to determine if MDOF DVAs could provide the same performance using less total absorber mass. This goal was achieved through experimental testing and analytical modeling of DVA systems on various primary systems.

The second half of this thesis was dedicated to the design and application of a 2DOF DAVA for use in an active control system on the Boeing payload fairing. By optimally designing the electro-magnetic actuator, foam, and plate mass, the DAVA shown in Figure 1.1 was intended to generate the greatest force possible across the 50 to 200 Hz bandwidth. Several prototypes were produced and applied to the payload cylinder for use in a feed-forward control system.

A detailed account of the MDOF DVA and 2DOF DAVA goals, results, and conclusions are presented.

6.1.1 MDOF DVA Conclusions

The goals of the research investigating MDOF passive DVAs were to: (1) establish experimental data supporting the assertion that 2DOF DVAs can attenuate multiple modes of a distributed system, (2) develop a method for comparing MDOF DVAs to 1DOF DVAs, (3) establish if there is a potential advantage in using MDOF DVAs on particular systems, and (4) investigate the characteristics that dictate where the MDOF DVAs are most advantageous; all within the realm of broadband excitation of a resonant system.

The principle behind using MDOF DVAs is that they can utilize the multiple mode shapes that correspond to their multiple resonance frequencies to couple into the modes of the primary system to improve the attenuation of structural resonance frequencies. This is done by matching the mode shapes of the DVA with the mode shapes of the primary system at the resonance frequencies of interest. By utilizing all of their mass at each resonance, this can result in MDOF absorbers providing attenuation equivalent to a set of 1DOF absorbers while using less mass.

First, it needed to be established that MDOF DVAs are able to attenuate multiple modes of a distributed system. To accomplish this, a 2DOF stacked DVA was modeled, optimized, produced, and implemented on the model Boeing payload fairing. Analytical models aided the design of 15 2DOF stacked DVAs that were intended to have two resonance frequencies matching the target resonance frequencies of the cylinder. The DVAs were applied to the cylinder and tested under structural excitation. The results showed attenuations of 5.6 and 4.3 dB in the 40 to 70 Hz, and 120 to 160 Hz frequency bands respectively, with peak reductions of 19 dB. This demonstrates that multiple resonances of a MDOF DVA can be used to target multiple resonance frequencies of a distributed system. The analytical modeling of the stacked 2DOF DVAs was also used to validate the principle that there is never an advantage in using the stacked 2DOF DVAs in place of a set of 1DOF DVAs.

The next step was to develop an analytical model for comparing the total absorber mass of MDOF and SDOF DVA systems for a given level of performance. First, the analysis technique that was developed generates an ‘n’ DOF DVA by finding a stiffness matrix that results in DVA resonance frequencies matching the targeted frequencies. It then generates a set of SDOF DVAs that perform equally to the MDOF DVA. This is done by breaking down the MDOF DVA equations of motion and creating SDOF DVAs that match the MDOF DVA modal

forces. The measure of performance is evaluated in terms of kinetic energy within a frequency band about the targeted frequencies, and the mass savings is represented by *MR*, the mass ratio of the mass difference divided by the mass of the SDOF system.

This technique was used to compare MDOF DVAs to SDOF DVA systems for three primary systems: a lumped mass system, a pinned-pinned plate, and a cylindrical shell. The resulting mass ratios, *MR*, for the best MDOF DVA designs found in this analysis are shown in Table 3.1. The lumped mass system provided a good measure of the ideal performance because it can be matched exactly by a MDOF DVA by simply scaling the parameters of the primary system. Figure 3.11 shows the performance as a function of frequency separation, the primary parameter influencing performance. The optimal MDOF DVA for a lumped mass system was a 2DOF system, resulting in an *MR* of 33%. The limiting factors in performance are that the SDOF DVAs are very effective for low targeted frequency σ values, and that the MDOF DVAs decrease in performance for high σ values.

Table 6.1 Comparison of the optimal MDOF DVA for each primary system evaluated.

Primary System	**# DOF**	**Frequency Separation, σ**	**Absorber Mass (grams)**		***MR* (%)**
			SDOF	MDOF	
Stacked (1 Reaction Point) Lumped Mass	2	All cases	Equal	Equal	0
Multi-Reaction Point Lumped Mass	2	0.17	3	2	33
Pinned-Pinned Plate	2	0.04	320	200	38
Cylindrical Shell	2	0.10	265	200	25

For a pinned-pinned plate, the coupling at the DVA reaction points must be accounted for because the primary system mode shapes can not be exactly matched by the DVA mode shapes. Under ideal circumstances, mass savings of greater than 30% can be attained by using a MDOF DVA in place of a SDOF system on a plate. The advantage in the plate primary system is that the SDOF DVA effectiveness at low σ frequency separation can be nullified in some cases because of poor coupling into the multiple primary system mode shapes that are targeted. This results in cases where the *MR* can reach 38%, shown in Table 6.1. To optimize this potential, the coupling position of the DVA reaction points must be taken into account. There is an optimal

coupling position for every set of targeted modes that influence the *MR* performance by as much as 35%.

The MDOF DVA performance is also a function of the order of MDOF DVA. The principle relationship between order of MDOF DVA and *MR* is: as the order increases, the possible advantage increases, while the probability of matching the DVA mode shapes to the primary system decreases. Therefore, the optimal number of DOF is dependent on the primary system and the targeted modes. But the principle of this relationship defining an optimal order is valid for all cases.

To physically implement these MDOF DVAs onto a plate as modeled, the DVA design and positioning would need to be very stable. Small variations in the DVA design (i.e. mass, coupling stiffness, and coupling position) could result in the loss of advantage over the more stable SDOF DVAs.

The use of MDOF DVAs on a cylindrical shell was also investigated, and it was found that there are instances that indicate MDOF DVAs could be used advantageously to save as much as 25% of the mass used in a set of SDOF DVAs. The modeling also showed the performance was a function of the same factors as in the plate primary system. Physical implementation of attaching the DVAs at the optimal coupling positions on a cylinder, however, poses a problem. Because the axial modes are targeted, the minimum spatial separation is one-half the length of the axial wavelength. This implies that the structure connecting the DVA masses may have to be substantially stiffer than the cylinder itself, which is not very feasible in practice.

6.1.2 2DOF DAVA Conclusions

The primary goal of the 2DOF DAVA research was to design and implement an actuator exhibiting a band of resonance in the low frequency band of 50 to 200 Hz. Its performance was to be tested in an active control system reducing the structural vibration of the BOEING payload fairing. Iterative experimentation and testing was first used to optimize the spider plate stiffness, magnet mass, and magnetic air gap of the electro-magnetic actuator. Then, an analytical model of the DAVA was developed to measure the effectiveness per unit mass of the DAVA as a function of foam stiffness and plate mass, the remaining design parameters. This model was validated through experimental testing of several data points on the performance plot and then

used to choose the final DAVA design. Prototype DAVAs were then constructed and characterized with respect to their electro-mechanical properties and power consumption. They were then compared to the point actuators and shown to be more than 30% more "effective" under the definition of equation (4.8).

The DAVA performed linearly at low power levels, but exhibited nonlinearity when driven with over 30 Watts. When driven at high levels, the magnet displacement stretches the spider plate stiffness to nonlinearity. Also, the large magnet displacements take the it farther from the magnetic field generated by the coil, and into the region of nonlinearity. Either of these effects could be contributing to this nonlinearity at high levels.

The DAVAs were then applied to the BOEING payload fairing and tested in an active control system conducted by VASci and Virginia Tech. The acoustic response of the DAVAs was characterized and indicates an efficient actuation range over the 80 to 160 Hz bandwidth. Under active control, the cylinder SPL levels were attenuated by about 5 dB in the targeted bandwidth, including peak reductions as high as 9 dB. The performance and power consumption of the DAVA were also measured for increasing external SPL levels; and while the performance declined as the SPL levels increased, significant attenuation was attained.

6.2 Future Work

Little existing research was found on the investigation of MDOF DVA performance in comparison to SDOF DVA systems. Therefore, that research was mostly analytical, leaving a lot of experimental work to be done. The 2DOF DAVA research, however, was mainly design and experimental testing. But the design aspect of this research leaves room for improvement. This section will suggest work that will continue the development of both aspects of the research.

6.2.1 MDOF DVA Future Work

The research performed on the use of MDOF DVAs was mostly analytical. Therefore, the future work should focus on developing physical experimentation to validate the analyses performed. Experimentation could start with a primary system simplified to represent a lumped mass system. Using the honeycomb plates and foam blocks used in the DAVA design as the primary spring-mass system, a scaled 2DOF multi-reaction point DVA could be easily produced to have equivalent mode shapes and resonance frequencies. This primary system and 2DOF DVA could be tested for various coupling stiffness values to obtain a range of separation lengths

between resonance frequencies. SDOF DVA systems could be tested as well, and the *MR* values would then supplement the analytical data developed in the research. One of the difficulties that lie ahead is the physical design of the 2DOF, and eventually the more difficult 'n' DOF DVAs. The most difficult aspect of the design will most likely be the development of accurate coupling stiffness values from the foam blocks.

The next step should follow the analytical models and test MDOF DVAs on a pinned-pinned plate. This would be more difficult than the lumped mass system due to the complexities associated with accurately positioning the DVAs, providing accurate coupling across greater distances, and producing precise foam stiffness values and plate masses. An accurate model of the plate used in the testing should be developed and utilized in the design of the DVA. Again, a comparison of MDOF DVAs to SDOF DVAs would support the principles discussed throughout the research. Lastly, applying the MDOF DVA concept to a cylinder could be examined.

6.2.2 2DOF DAVA Future Work

Because much of the work conducted on the DAVA was design, implementation, and testing, there are a number of areas that could be improved upon with further research. One area would be the improvement of force output per power of the electro-magnetic actuator. Further investigation of the pole plates and their affect on the performance should be conducted. Similarly, the magnet mass and spider plate stiffness could be investigated to determine if there is a better combination resulting in greater output while still remaining resonant in the objective resonance bandwidth of 75 to 100 Hz. An increased output would improve the overall DAVA performance.

The DAVA design could also be investigated for improvement. A lower profile design could reduce the size and volume wasted by the many DAVAs applied to the payload walls. Also, designs that have an outer layer of acoustic foam could help improve high frequency absorption within the payload fairing. Similar design alterations could be made to improve ventilation. This would subsequently increase the life of the actuator under high power loads since the failure is thought to have been associated with overheating.

Lastly, the analysis for designing the DAVA foam and plate values was dependent on an α value that weighs the associated detriment of supplying power to the DAVA. Determining the

value of this detriment and factoring it into the design would provide a more accurate analysis of the optimal DAVA design.

Bibliography

[1] Frahm, Hermann, "Device for Damping Vibrating Bodies," German Patent Serial Number 525,455, 1909, U.S. Patent Serial Number 989,958, (1911).

[2] J. D. Heilmann , "*A Dual Reaction-Mass Dynamic Vibration Absorber for Active Vibration Control*" Master's Thesis, Virginia Polytechnic Institute and Sate University, (1996).

[3]Andreas H. von Flowtow, Andrew Beard, and Don Bailey, "Adaptive Tuned Vibration Absorbers: Tuning Laws, Tracking Agility, Sizing, and Physical Implementations," Proceedings of NOISE-CON 94 (Ft. Lauderdale, Florida), pp 437-454 (May 1994).

[4] M. R. Jolly and J. Q. Sun, "Passive Tuned Vibration Absorbers for Sound Radiation Reduction from Vibrating Panels," Journal of Sound and Vibration, 191(4), pp 577-583 (1996).

[5] J.Q. Sun, M.R. Jolly, and M. A. Norris, "Passive, Adaptive and Active Tuned Vibration Absorbers – A Survey," Transactions of the ASME Vol. 117, pp 234-242 (June 1995).

[6] J. P. den Hartog, *Mechanical Vibrations*, General Publishing Company, Toronto, Ontario (1985).

[7] B. G. Korenev and L. M. Reznikov, *Dynamic Vibration Absorbers*, Wiley, (1993).

[8] G. Maidanik and K. J. Becker, "Characterization of Multiple-Sprung Masses for Wideband Noise Control," Journal of the Acoustical Society of America, 106 (6), pp 3109-3118 (Dec 1999).

[9] K. W. Wang, J. Lamancusa, and L. Mianzo, "An Adaptive Vibration Absorber to Minimize Steady State and Transient Vibrations," Technical Report to Lord Corporation, Pennsylvania State University, (1992).

[10] M. W. Ryan, "Control of an Adaptive Passive Vibration Absorber," Proceedings of the ASME Winter Annual Meeting, (1993).

[11] M. A. Franchek, M. W. Ryan and R. J. Bernhard, "Adaptive Passive Vibration Control," Journal of Sound and Vibration, 189 (5), pp 565-585, (1995).

[12] R. J. Bernhard, "The State of the Art of Active-Passive Noise Control," Proceedings of NOISE-CON 94 (Ft. Lauderdale, Florida), pp. 421-428 (May 1994).

[13] D. Karnopp, "Active and Semi-Active Vibration Isolation," Transactions of the ASME, Vol 117, pp 177-185, (June 1995).

[14] J-H Koo and M. Ahmadian, "A Qualitative Analysis of Groundhook Tuned Vibration Absorbers for Controlling Structural Vibrations," Proceedings of the Institution of Mechanical Engineers, Vol 216 Part K: Multi-body Dynamics, pp 351-359, (2002).

[15] J. P. Maillard and C. R. Fuller, "Active Control of Sound Radiation from Cylinders with Piezoelectric Actuators and Structural Acoustic Sensing," Journal of Sound and Vibration, 222(3), pp 363-388, (1999).

[16] M. E. Johnson and S. J. Elliot, "Active Control of Sound Radiation from Vibrating Surfaces using Arrays of Discrete Actuators," Journal of Sound and Vibration, 207(5), pp 743-759, (1997).

[17] K. Nagaya and L. Li, "Control of Sound Noise Radiated from a Plate Using Dynamic Absorbers under the Optimization by Neural Network," Journal of Sound and Vibration, 208(2), pp 289-298, (1997).

[18] J. Yuan, "Multi-point Hybrid Vibration Absorption in Flexible Structures," Journal of Sound and Vibration, 241(5), pp 797-807, (2001).

[19] K. Nonami, H. Nishimura, and C. Weimin, "Disturbance Cancellation Control for Vibration of Multi-Degree-of-Freedom Systems (Case of Using Active Vibration Absorber and Active Dynamic Vibration Absorber)," Japan Society of Mechanical Engineers, Series C, Vol. 37, No. 1, pp 86-93, (1994).

[20] T. Watanabe and K. Yoshida, "Evaluation and Optimization of Parallel Hybrid Active Dynamic Vibration Absorbers," Japan Society of Mechanical Engineers, Series C, Vol. 37, No. 3, pp 471-476, (1994).

[21] Y. Okada, and R. Okashita, "Adaptive Control of an Active Mass Damper to Reduce Structural Vibration," Japan Society of Mechanical Engineers, Series C, Vol. 33, No. 3, pp 435-440, (1990).

[22] H. Nishimura, K. Nonami, W. Cui, and A. Shiba, "H-infinity Control of Multi-Degree of Freedom Structures by Hybrid Dynamic Vibration Absorber (Experimental Consideration of Rubustness and Control Performances)," Japan Society of Mechanical Engineers, Series C, Vol. 59, pp 714-720, (1993).

[23] R. A. Burdisso and J. D. Heilmann, "Active Dual Reaction Mass Actuator for Vibration Control," U.S. Patent No. 08-825,614, (1997).

[24] R. A. Burdisso and J. D. Heilmann, "A New Dual-Reaction Mass Dynamic Vibration Absorber Actuator for Active Vibration Control," Journal of Sound and Vibration, 214, pp 817-831, (1998).

[25] S. J. Estève and M. E. Johnson, "Reduction of Sound Transmission into a Circular Cylinderical Shell using Distributed Vibration Absorbers and Helmholtz Resonators," Journal of Acoustical Society of America, 112 (6), pp 2840-2848, (December 2002).

[26] S. J. Estève, M. E. Johnson, "Control of Noise Transmission into Cylinder using Helmholtz Resonators and Passive Vibration Absorbers," Submitted to the 11th AIAA/ASME/AHS Adaptive Structures Conference (Norfolk, Virginia), (April 2003).

[27] P. Marcotte, C. R. Fuller, and P. Cambou, "Control of the Noise Radiated by a Plate Using a Distributed Active Vibration Absorber," Proceedings from ACTIVE 99 (Ft. Lauderdale, Florida), pp. 447-456, (1999).

[28] C. R. Houck, J. A. Joines, and M. G. Kay, "A Genetic Algorithm for Function Optimization: A Matlab Implementation," http://www.ie.ncsu.edu/mirage.

[29] E. H. Baker and G. Hermann, "Vibration of orthotropic cylindrical sandwich shells under initial stress," American Institute of Aeronautics and Astronautics Journal 4, pp 1063-1070. (1966)

[30] M. E. Johnson, C.R. Fuller, S. J. Estève, and A. F. Harris, "Contract to the Boeing Company: Investigation of the Use of Helmholtz Resonators and Distributed Vibration Absorbers for the Control of Sound Transmission Through a Composite Cylinder," (February 2003).

[31] C. Papunfuss, "Modeling and Active Vibration Control using Electromagnetic Inertial Actuators," Presented at Signals and Systems Seminar (Blacksburg, Virginia), (March 2003).

[32] A. Charpentier, "Contract Report by Vibro-Acoustic Sciences, Inc.: Payload Fairing Active Noise Cancellation," (February 2003).

[33] M. E. Johnson, C. R. Fuller, S. J. Estève and P. Marcotte, "Contract to the Boeing Company: Investigation of the Use of Helmholtz Resonators and Distributed Vibration Absorbers for Control of Sound Transmission Through a Composite Cylinder," (October 2001).

Vita

Anthony Frederick Harris was born May 2, 1978 in Washington, D.C. to parents Richard and Michele Harris. He grew up in Pomfret, Maryland and attended Maurice J. McDonough High School. In the fall of 1996 he began his college career at Virginia Tech studying Mechanical Engineering. The following summer he started working at the Naval Surface Warfare Center in Indian Head, Maryland as a co-op student where he worked four semesters over the next five years. Tony graduated in May 2001 with a Bachelor of Science degree in Mechanical Engineering with Summa Cum Laude honors. After a summer of full time work at NSWC Indian Head, he entered graduate school at Virginia Tech in the fall of 2001. He taught two semesters of a Mechanical Engineering lab before receiving a research assistantship in the Vibrations and Acoustic Lab under the supervision of Dr. Marty Johnson. After a year of research, Tony returned to full time work at the Naval Surface Warfare Center but transferred to Dahlgren, Virginia in July 2003. While at Dahlgren, he continued to write his thesis; and in December 2003, Tony defended his thesis and completed his Master of Science in Mechanical Engineering degree requirements.